1979

Melting studies of polyethylene terephthalate.

Patricia Leite-james
University of Massachusetts Amherst

MELTING STUDIES OF POLYETHYLENE TEREPHTHALATE

A Thesis Presented

By

PATRICIA LEITE-JAMES

Submitted to the Graduate School of the
University of Massachusetts in partial fulfillment
of the requirements for the degree of

MASTER OF SCIENCE

September 1979

Polymer Science and Engineering

MELTING STUDIES OF POLYETHYLENE TEREPHTHALATE

A Thesis Presented

By

PATRICIA LEITE-JAMES

Approved as to style and content by:

Richard S. Stein

Richard S. Stein, Chairman of Committee

Shaw Ling Hsu

Shaw L. Hsu, Member

Edwin L. Thomas

Edwin L. Thomas, Member

William J. MacKnight, Head
Polymer Science and Engineering

ACKNOWLEDGMENTS

The author wishes to express her sincere appreciation to Professor Richard S. Stein, Research Advisor, for his support and encouragement throughout the course of this work.

Appreciation is expressed to thesis committee members, Professors Shaw Ling Hsu and Edwin L. Thomas, for their valuable suggestions.

Thanks go to colleagues in the research group for their valuable suggestions and to Jeffrey T. Koberstein, in particular. The friendship and cohesiveness of the group has been most appreciated.

The typing of this thesis was done by Excel Secretarial Services. Thanks go to Mrs. Pat Milne for her personal interest in this work.

Special thanks go to David B. James, without whom this sojourn would not have been complete.

ABSTRACT

The object of this research was to study the melting of isothermally crystallized PET and in particular to quantitatively study the changes that occur to the small angle H_v light scattering pattern from PET spherulites through the temperature range in which PET melts. Thin films of PET, previously crystallized at 200°C, were melted at heating rates of 0.2°C/min and 2.0°C/min. H_v light scattering patterns for these films were measured as a function of temperature, both qualitatively using a photographic technique and quantitatively using an Optical Multichannel Analyzer in conjunction with a Vidicon tube. The quantitative data were corrected for instrumental, multiple scattering and disorder effects.

Results from the 2.0°C/min run indicated that the spherulite radius remained constant through the melting region, but that the absolute intensity of the scattering decreased with increasing temperature. Further, the data showed the disorder within the spherulite increased with increasing temperatures. Similar results were observed at a heating rate of 0.2°C/min but the data were complicated by annealing effects. Annealing was shown to result in an increase in the scattering intensity and also in a

decrease in the disorder within a spherulite. The corrected experimental Rayleigh factors were compared with Rayleigh factors calculated from degrees of crystallinity determined by DSC at similar heating rates. Considerable discrepancies were found between experimental and calculated values and these have been explained in terms of imprecise experimental data and correction factors.

TABLE OF CONTENTS

LIST OF TABLES

LIST OF FIGURES

C H A P T E R I

INTRODUCTION

The object of the research was to study the melting of isothermally crystallized Polyethylene Terephthalate (PET) and in particular to quantitatively study the changes that occur to the small angle light scattering (SALS) pattern from PET spherulites through the range in which PET melts. In the past, SALS has been extensively used to study the size and morphology of polymer spherulites[1-5] which range in size from 0.5 to 50 μm. Several theories[1,6] have been developed to predict the shapes of the H_v and V_v light scattering patterns obtained experimentally[6-8] and, in the case of spherulitic polymers, the deviations between theory and experiment have been analyzed in terms of deviations from the perfect spherulite model assumed theoretically.

These deviations result from both external and internal disorder. The most probable forms of external disorder have been ascribed to a distribution of spherulite sizes,[9,10] interspherulitic interference[11-14] and the truncation of spherulites.[15-18] It has been shown[9,10] that the major effect of a distribution of spherulite sizes is to remove the higher order peaks and the effect

of interspherulitic interference has been shown to be negligible when the scattering volume contains a large number of spherulites.[11-14] The impingement of spherulites during growth from the amorphous phase results in truncated shapes. The effect of truncation on the light scattering pattern decreases the angle of maximum scattering intensity and also increases the H_v scattering intensity at small and large angles. Recently, a theoretical procedure has been developed by Misra, Prud'homme, and Stein[19] to estimate the degree of spherulitic truncation in polymer films.

Internal disorder arises from variation in the optic axis orientation within spherulites.[6,20-23] The Stein-Yoon[22,23] lattice theory of orientational disorder in 2-dimensional spherulites allows the optic axis orientation direction in lattice cells to statistically deviate from its mean value in a manner which is correlated with orientation in neighboring cells. The orientational disorder results in excess intensity at both small and large scattering angles and to lower the intensity at the peak maximum. In the Stein-Yoon theory, two forms of orientational disorder are considered. These are disorder in the tilt angle which the optic axis makes with the radial direction of the spherulitic and a disorder in the twist

angle which the optic axis makes about the radial direction.

Deviations also occur between theoretical and experimental sources due to effects such as reflection, refraction and loss of energy due to secondary scattering. Stein and Keane[24,25] have developed procedures to correct for these effects and more recently Prud'homme, Natarajan and Stein[26,27] have developed multiple scattering theories to correct for the experimentally measured light scattering intensities for both attenuation and gain in the scattered intensity due to secondary as well as higher order scattering processes.

In this work quantitative H_v light scattering patterns were obtained from PET spherulites in the melting region and these data were analyzed using the above light scattering theories to determine changes in morphology, disorder and crystallinity within the melting polymer spherulite. These melting studies will also form the basis for future work on the crystallization kinetics of PET studied by SALS and will be valuable in developing a SALS theory which is a function of the degree of crystallinity.

C H A P T E R I I

THEORY

The Rayleigh factor for the sample may be calculated from the experimentally measured light scattering intensity using Equation (1):

$$R(\theta,\mu) = \frac{I(\theta,\mu)}{I_o} \frac{F_c K}{V} \qquad (1)$$

where $R(\theta,\mu)$ is the Rayleigh factor at the scattering angle θ and azimuthal angle μ, $I(\theta,\mu)$ is the experimentally measured intensity at θ and μ, I_o is the incident beam intensity, F_c is a product of the correction factors and K is the instrument correction factor.

The Rayleigh factor for H_v scattering from three-dimensional, perfect spherulites is given by[28]:

$$R(\theta,\mu) = \frac{144\pi^4}{\lambda_o^4} N_s V_s^2 (\alpha_t-\alpha_r)^2 \cos^4(\tfrac{\theta}{2}) \sin^2\mu\cos^2\mu\cos^2\rho \times \Phi_{H_v}^2(U) \qquad (2)$$

where λ_o is the wavelength of the light in a vacuum (638.2 nm), N_s is the number of spherulites per cm^3, V_s is the volume of the spherulite, α_t and α_t are the tangential and radial polarizabilities per cm^3, respectively, and $\Phi_{H_v}(U)$ is the sphere scattering function for H_v polarization given by:

$$\Phi_{H_V}(U) = (4 \sin U - U \cos U - 3\,SiU)/U^3 \qquad (3)$$

U is given by

$$U = 4\pi(R_{s/\lambda}) \sin(\theta/2) \qquad (4)$$

where R_s is the spherulite radius and λ the wavelength in the medium. SiU is the integral defined as

$$SiU = \int_0^u \frac{\sin x}{x}\, dx \qquad (5)$$

and the angle $\cos^2\rho_2$ is given by

$$\cos^2\rho_2 = \cos^2\theta/(\cos^2\theta + \sin^2\theta \sin^2\mu)^{\frac{1}{2}} \qquad (6)$$

The values of $\cos\rho_2$ and $\cos\theta$ are close to unity at small angles and the $\sin\mu\cos\mu$ term shows that $R(\theta,\mu)$ for H_V scattering has a maximum at $\mu = 45°$ and zero at $\mu = 0°, 90°$. It can be shown from the sphere scattering function[29] that $R(\theta,\mu)$ is a maximum at $U = 4.1$ such that Equation (4) gives the statistical average size of the spherulite radius at θmax

$$R_s = \frac{4.1\lambda}{4\pi}\left[\sin\frac{\theta max}{2}\right]^{-1} \qquad (7)$$

At $\theta = \theta max$ and $\mu = 45°$, Equation (2) reduces to

$$R(\theta max, \mu=45°) = \frac{36\pi^4}{\lambda_o^4} N_s V_s^2 (\alpha_t - \alpha_t)^2 \cos^4\left(\frac{\theta max}{2}\right) \qquad (8)$$

$$\times \cos^2\rho_2(\theta max \text{ at } 45°)\Phi_{H_V}^2 \qquad (4.1)$$

Equation (2) predicts that the H_V scattering pattern will have four-fold symmetry and will give the characteristic

four-leaf clover pattern as typically shown in Figures 8 a, b and 9.

A comparison of the theoretically calculated Rayleigh factor with the experimentally measured value leads to differences which are attributable to internal and external disorder. External disorder arises from the fact that volume filling spherulites are not perfect spheres, but are, in practice, truncated and meet at boundaries. If the spherulites are volume filling, then it may be assumed that $N_s V_s = 1$ and the crystallization changes occur only within the spherulite. For isolated perfect spherulites, the volume, V_s, is given by[18]

$$V_s = 4/3\pi R_s^3 \tag{9}$$

For truncated spherulites, the volume is greater than the value calculated from Equation (9) and depends on the value of the truncation parameter, $\sigma^2/\bar{a}^2$, where σ is the standard deviation of the average size of the spherulite and $\bar{a}$ is defined as the mean value of the distance between the boundary of the spherulite and its center. The Rayleigh factor is a function of V_s as shown in Equation (2) such that the intensity change is proportional to R_s^3. Therefore, changes in spherulite radius during crystallization or melting produces significant changes in the Rayleigh factor.

A further deviation from model theory is caused by multiple scattering.[26-27] When the product of sample turbidity and thickness become significant, the scattering ray for the first layer of the sample acts as an incident beam to the next layer within the sample. This product is given by

$$\tau d = \ln(I_o/I) \tag{10}$$

where τ is the turbidity, d is the sample thickness and I_o and I are the incident and transmitted intensities, respectively.

After first correcting the scattering data for truncation and multiple scattering effects, an estimate of the internal disorder parameter, δ, may be made and a correction factor for disorder within the spherulite determined from the ratio of R_{H_V} at U=4.1 to R_{H_V} at U=x, where x is 8 or 12. Taking all of these corrections into consideration, an overall correction factor, F_c, given in Equation (1), may be calculated, where F_c is the product of corrections due to truncation, multiple scattering and disorder. The difference in radial and tangential polarizabilities is given by Equation (11) such that

$$(\alpha_t-\alpha_r) = \Phi_{cr}\,(\alpha_t-\alpha_r)_{cr} + (1-\Phi_{cr})(\alpha_t-\alpha_r)_{am} + (\Delta\alpha)F \tag{11}$$

where Φ_{cr} is the volume fraction of crystallinity of the spherulite, $(\alpha_t-\alpha_r)_{cr}$ and $(\alpha_t-\alpha_r)_{am}$ are the anisotropies of the crystalline and amorphous regions within the spherulite, respectively, and $(\Delta\alpha)F$ is the form anisotropy of the crystalline-amorphous boundary. It is assumed that $(\Delta\alpha)F$ is negligible and there is no amorphous orientation within the spherulite so that $(\alpha_t-\alpha_r)_{am} = 0$. Thus, Equation (11) reduces to

$$(\alpha_t-\alpha_r) = \Phi_{cr}(\alpha_t-\alpha_r)_{cr} \qquad (12)$$

Spherulite anisotropy is related to the spherulite birefringence, Δ_s, by the differential of the Lorenz-Lorentz equation[30]:

$$\Delta_s = n_t-n_r = \frac{2\pi}{9}\left[\frac{(\bar{n}^2+2)^2}{\bar{n}}\right](\alpha_t-\alpha_r)_{cr} \qquad (13)$$

where n_t and n_r are the tangential and radial refractive indices of the crystal and $\bar{n}$ its average refractive index given by $[(n_r+2n_t)/3]$. n_t and n_r may be calculated from n_a, n_b and n_c which are the refractive indices along the a, b and c axes of the unit cell, respectively.

$(\alpha_t-\alpha_r)_{cr}$ may be obtained by rearranging Equation (13)

$$(\alpha_t-\alpha_r)_{cr} = (n_t-n_r)/\frac{2\pi}{9}\left[\frac{(\bar{n}^2+2)^2}{\bar{n}}\right] \qquad (14)$$

A value of Φ_{cr} may be obtained from Equation (12) using the value of $(\alpha_t-\alpha_r)$ calculated from the scattering data

by Equation (2). It could then be possible to compare the volume fraction of crystallinity obtained from light scattering measurements with values obtained from some other method such as Differential Scanning Calorimetry, Wide Angle X-Ray Scattering or Infrared Spectroscopy.

C H A P T E R I I I

EXPERIMENTAL

A. Characterization

Pellets of PET, obtained from the General Electric Company, were dried at 100°C, under vacuum, for 24 hours and stored in a moisture-free environment prior to use. The PET was characterized using intrinsic viscosity and gel permeation chromatography[31] as:

Number average molecular weight, $\bar{M}_n = 1.97 \times 10^5$

Weight average molecular weight, $\bar{M}_w = 5.14 \times 10^5$

Viscosity average molecular weight, $\bar{M}_v = 2.66 \times 10^5$

Molecular weight dispersity, $\bar{M}_w / \bar{M}_n = 2.59$

B. Sample Preparation

The pellets were initially pressed into thin films between sheets of Teflon coated aluminum foil sandwiched between two metal plattens using a Carver Laboratory Press at 290°C. This thin film was used to prepare final samples for light scattering. These samples were molded at 280-290°C between a microscope slide and cover slip separated by a 2 mil thick aluminum shim. This arrangement was sandwiched between Teflon coated aluminum foil

and was positioned between two small metal plattens and allowed to remain in the press for a total of five minutes. During this period, pressure was applied gradually and released with care taken to avoid breakage of the microscope slide. The samples were allowed to cool slowly to room temperature and stored in a desiccator.

Samples as prepared above were isothermally crystallized using the following procedure. The microscope slide-cover glass assembly was doubly wrapped with aluminum foil and clips secured to the package. These thin films were melted on a hot plate at approximately 280°C for ninety seconds. The temperature of the hot plate was measured by a digital thermometer in order to determine temperature variations on the hot plate surface. At the end of the melting period, the packaged samples were secured by clips and immersed in a sand bath which was kept at an equilibrium temperature of 200°C. The samples remained in the sand bath, which retained a temperature of 200±2°C, for a period of two hours and were removed and allowed to cool gradually to room temperature.

C. Differential Scanning Calorimetry

Small samples of isothermally crystallized PET weighing about 5 mg. were melted in a Perkin Elmer Differential Scanning Calorimeter (DSC2) at heating rates

of 10, 2.5 and 0.31°C/min. The DSC was calibrated using an Indium standard of known weight and heat of fusion. Each melting curve was normalized to correct for effects due to different chart speeds, heating rates and sensitivities.

D. Photographic Light Scattering

Qualitative light scattering measurements were obtained photographically using the apparatus shown in Figure (1).[32-33] The light source was a He-Ne laser with a wavelength of 632.8 nm. The sample was inserted between a polarizer and analyzer with polarization directions mutually perpendicular. The depolarized H_v scattering pattern was allowed to fall on a photographic film and a four-leaf clover pattern characteristic of spherulitic polymers was obtained. Thin films of isothermally crystallized PET prepared as previously discussed were melted in a Mettler Hot Stage (Model #FP2) at heating rates of 2.0 and 0.2°C/min and photographs were taken of the H_v scattering pattern as a function of temperature through the melting region using Polaroid type 52 film. A constant sample to film distance of 31 cm was used for all measurements.

E. Quantitative Light Scattering

Description of Apparatus. Qualitative light scattering measurements to complement the photographic data

were obtained using an Optical Multichannel Analyzer (OMA, Model #1205A, supplied by Princeton Applied Research) in conjunction with a Vidicon tube. A He-Ne laser was again used as the light source and a diagram of the apparatus is shown in Figure (2).[34] The apparatus included a series of neutral density filters because of the high sensitivity of the Vidicon tube, although for two out of the three runs, the scattering was too weak to require filters. In comparison, the main incident beam, measured without a sample, required minimally a #3 filter due to the high intensity of the laser. The sample was placed between a polarizer and analyzer such that their polarization directions were perpendicular with respect to each other. One lobe of the H_v scattering pattern, corresponding to $\mu=45°$, fell through a slit onto a ground glass plate and this image was detected by the Vidicon tube focused on this plate. The signal of the image was stored in the OMA and could be either printed using an X-Y plotter or stored on magnetic tape for use in the computer. The image from the Vidicon tube was also displayed on a cathode ray tube (CRT) for instant visual observation of the scattering pattern and a typical intensity scan is shown in Figure (3). The OMA has a total of 500 channels such that each channel corresponds to a specific scattering angle.

Calibration of the Optical Multichannel Analyser with Diffraction Grating. A diffraction grating having 2400 lines/inch was used to calibrate the OMA. The grating was placed in the sample position and measurements were taken with the anlyzer removed. The channel numbers corresponding to the maxima of zero and first order peaks were determined directly from the display on the CRT. In addition, the distance, in inches, between the zero and first order maxima was measured directly from their images along the slit using vernier calipers. This information was later used to convert channel number into absolute scattering angle.

Collection of Data. Thin films of PET isothermally crystallized as described above, were melted in the Mettler Hot Stage, again at heating rates of 0.2 and 2.0°C/min and quantitative H_v SALS patterns were obtained through the melting region. The background intensity was determined by blocking off the incident laser beam, but with the Vidicon tube uncovered. Both sample and background were accumulated over 100 counting cycles and the OMA automatically subtracted the background data from the sample scattering curves. The background corrected data were stored on magnetic tape using a Datacassette Recorder (Model #8400) in conjunction with a Tektronix

Terminal (Model #4006-1). Sample scans could be recorded approximately every 1-2 minutes through the melting region. For one sample, PETC, the annealing effect was assessed by heating the sample from 240 to 265°C at 0.2°C/min, cooling to 250°C and then reheating at 0.2°C/min to above the melting temperature. H_v light scattering patterns were recorded at frequent temperature intervals throughout the experiment.

Treatment of Data. After the melting experiments were complete, the data stored on magnetic tape were fed into the computer for more permanent storage. Considerable problems were frequently encountered at this point due to erratic signals appearing on the tape, some of which seemingly originated from the computer itself. Some of the spurious effects could be minimized by analyzing the data as soon after the experiment as possible and by removing the WRITE tab on the magnetic tape cartridge. Further, it is important to note that it is only possible to write on one side of the tape.

Once the data files were stored in the computer, they were edited to remove spurious information and errors and to get them into the correct format for further analysis. The scattering data at each temperature were corrected for channel sensitivity using a file en-

titled SENSD and the results were calculated using a program entitled BOMA which is the binary form of OMA.[35] A copy of OMA is given in the Appendix. The information required to calculate results included:

a. Channel numbers of zero and first order maxima, in inches; filter factor.

b. Width of slit, in inches; attenuation factor; wavelength of incident light.

c. Diffraction grating, in lines/inch; number of scanning cycles for main beam and for sample; refractive index of sample; and sample thickness, in inches.

d. Constant values to be added to the sensitivity scan; main beam scan; sample scan; and U, the value for each being zero.

Further, the sample scan was smoothed once and main beam intensity was integrated.

Computer calculated results included theta; the scattering vector H (nm^{-1}); the scattering vector H, squared (H^2) and also to the fourth power (H^4); the Rayleigh factor R ($(Sr\text{-}cm)^{-1}$); and the Rayleigh factor as a function of scattering vector H to the fourth power [$R(H^4)$]. The results considered in this work were theta, the scattering vector H and the Rayleigh factor.

Further computer analysis included the use of the program GRAFCAL.[35] This is a plotting program which converted the results into plots of Rayleigh factor as a function of both scattering vector H and scattering vector U at each temperature under consideration.

Determination of Sample Thickness. For quantitative light scattering, it is important to know the thickness of the polymer film very accurately. In this work, the film thicknesses were determined by slicing the sample in half using a glass knife after the melting experiment was complete. The cross section of the sample was then examined using an optical microscope which had been calibrated using a reticle graduated in 0.01 mm divisions. Although this method of determining film thickness was destructive, it allowed a direct measure of the sample thickness to be made. In all cases, the sample thickness was 2.0 mil.

Determination of Sample Turbidity as a Function of Temperature. Sample turbidity is another extremely important parameter since it governs the multiple scattering correction factor which is often a considerable correction as will be seen later. It is extremely difficult to obtain very accurate turbidity factors because of the difficulties in measuring the incident and

transmitted beam intensities and because it is found that the turbidity is also a function of the sample to detector distance. In this work, this distance was kept constant and the turbidities were determined at the same sample to detector distances that were used in the quantitative SALS experiment described above. The incident and transmitted beam intensities were determined by scanning through the main beam and integrating the area under the peak. The product of turbidity and sample thickness could then be determined by Equation (10).

C H A P T E R I V

RESULTS AND DISCUSSION

A. Differential Scanning Calorimetry

The melting of PET by DSC as a function of heating rate is shown in Figure (4). It was found that the total area under the curve increased with decreasing heating rate and that the position of the peak maximum occurred at higher temperatures with decreasing heating rate. Further, at the lowest heating rate, a shoulder appeared on the melting curve. These observations indicate that the lower the heating rate, the greater the annealing effects which occur with increasing temperature. The degree of crystallinity, X_c, of PET was determined from the total area under the curve using a value of 125.4 Jg^{-1} for the heat of fusion of PET.[37] The values of X_c and the melting temperature as a function of heating rate are shown in Table 1. The differences in the initial values of X_c are due to annealing effects which occurred between room temperature and 245°C. The change in X_c through the melting region can be followed by integration of the curves in Figure (4) such that the degree of crystallinity, $X_c(T)$, at a temperature T is related to the area under the curve between T and the temperature at

which the last polymer crystallite melts (that is, the temperature at which a flat baseline resumed). The values of X_c as a function of temperature and heating rate are shown in Figure (5). From these values of X_c from DSC, the Rayleigh factor was calculated and will be compared later in this chapter with the corrected values of the Rayleigh factor from light scattering measurements.

B. Turbidity Measurements

Values of τd as a function of temperature at heating rates of 0.2°C/min and 2.0°C/min have been plotted in Figures (6) and (7), respectively. In Figure (6), it can be seen that τd increases in the region of 245-250°C and then decreases at higher temperatures as melting occurs. The peak in Figure (6) is probably due to extensive annealing effects occurring at this heating rate. Although no peak was observed in Figure (7), a shoulder occurred at about 245°C and this may be due to some slight annealing. This conclusion would be consistent with the DSC data reported in section A of this chapter, which indicated that more annealing occurred at the lower heating rates. These turbidity data will be used in a later section of this chapter to correct the quantitative light scattering data for multiple scattering effects.

C. Photographic Light Scattering

H_v SALS patterns of PET were recorded as a function of increasing temperature at heating rates of 0.2°C/min and 2.0°C/min through the melting region. These photographs are shown in Figure (8) a, b and Figure (9), respectively. The photographs for the heating rate of 0.2°C/min clearly show effects due to annealing. At the lowest temperatures recorded, there was considerable background speckle surrounding the four-leaf clover pattern and this disappeared at higher temperatures. This speckle probably arose from interspherulitic interference and diminished at higher temperatures. At temperatures near the melting point, the intensity of the pattern decreased with increasing temperature but, within experimental error, the size of the scattering pattern remained constant. This indicated that the spherulite size did not significantly change with melting but rather that the spherulites melted uniformly and not from the edges inward. A value of 16 μm was obtained from the photographs as the value of the spherulite radius. The photographs for 2.0°C/min shown in Figure (9) do not indicate any significant annealing effects. The intensity of the four-leaf clover pattern again decreased with increasing temperature as the melting temperature was approached and, within experimental error,

the spherulite radius remained constant through the temperature range studied. No attempt was made to further analyze the intensity data recorded in the photographs since these data were qualitative rather than quantitative. More quantitative data have been obtained using the Optical Multichannel Analyzer and these are described in the next section.

D. Quantitative Light Scattering

Quantitative light scattering data were obtained for four different samples of PET and these data have been designated PET-X, PET-A, PET-B and PET-C, respectively. In runs PET-X and PET-A, the temperature was increased uniformly at a heating rate of 0.2°C/min and in run PET-B, the temperature was increased uniformly at a heating rate of 2.0°C/min. Run PET-C was also carried out using a heating rate of 0.2°C/min but this run differed from PET-X and PET-A in that the temperature was increased, decreased and then increased again. This cycle was done to assess the effect of annealing on the light scattering pattern.

Run PET-X. Figure (10) shows the H_v scattering curves of PET melted at 0.2°C/min through the temperature range in which melting occurred. In this figure, the

intensity is plotted in arbitrary units against channel number and the data have been neither corrected for channel sensitivity nor smoothed. Difficulties were encountered in analyzing these data using the computer since the magnetic tape contained numerous spurious signals which prevented the computer from accepting the data. Therefore, no further analysis of these data were possible. However, although the data shown in Figure (10) are not absolute, the trends observed are correct. It can be clearly seen that the position of the H_v peak maximum remained constant during melting and that the scattered intensity decreased with increasing temperature in this range.

The H_v scattering peak maxima have been plotted as a function of temperature in Figure (11). The intensity initially increased and then decreased rapidly as melting occurred. This increase indicates that annealing occurred in the temperature range of 245 to 265°C. Unfortunately, no further analysis of these data were possible because of the difficulties mentioned above.

Run PET-A. These data were again measured using a heating rate of 0.2°C/min and this run was essentially a repeat of Run PET-X. Figures (12) and (13) show the H_v scattering curves as a function of H and U, respectively

for the temperature range 40 to 245°C. It can be seen that in this region, the scattering intensity increased considerably but the position of the peak maximum remained constant. These results indicate that considerable annealing was probably occurring over this temperature range. At temperatures between approximately 245 and 265°C, the scattered intensity remained almost constant within experimental error as seen in Figure (14). However, Figure (14) also shows that above 265°C, the intensity rapidly decreased as melting occurred. The scattering curves for the melting region are shown in Figures (15) and (16) as functions of H and U, respectively and it can be seen that the position of the maximum again remained constant during melting. The spherulite radius as a function of temperature was calculated from the position of the peak maximum using Equation (7) and Figure (17) clearly indicates that within experimental error, the spherulite radius was constant through the temperature range studied.

Although samples of PET-X and PET-A were crystallized under the same conditions and melted at the same heating rate, the scattering data indicated differences. These may be observed by comparing Figures (11) and (14). It can be seen that in Figure (11), the intensity in-

creased between 245 and 265°C, whereas for sample PET-A, the intensity was almost constant in this temperature range. As mentioned above, this increase in intensity was probably due to annealing effects. Although sample PET-A did not show any annealing in the region 245 to 265°C, Figures (12) and (13) did indicate annealing effects in the range 40 to 245°C. Therefore, annealing was probably occurring in both samples but in different temperature regions or possibly more annealing was taking place in sample PET-X than in sample PET-A. This could be a consequence of the crystallization procedure, since melting on a hot plate and crystallizing in a sand bath are both somewhat unprecise methods. Slight differences in crystallization conditions could have resulted in PET-A being a better crystallized sample than PET-X and, hence, more annealing might therefore be expected with PET-X. Furthermore, annealing effects are both time and temperature dependent so small differences in the thermal histories of the two samples could produce the differences seen in Figures (11) and (14).

Run PET-B. In this experiment, the sample of PET was melted at 2.0°C/min and this run has been designated PET-B. From Figure (18), it can be seen that the value of the scattered intensity remained constant, within

experimental error, over the temperature range 200 to 245°C. This observation indicates that very little annealing occurred between these temperatures and this result is consistent with the DSC and photographic light scattering data reported earlier. Above 245°C, the intensity diminished rapidly as melting occurred and some typical curves are shown in Figures (19) and (20) as a function of H and U, respectively. Throughout the temperature range 200 to 265°C, the position of the peak maximum and hence the spherulite radius remained constant, within experimental error, as may be observed in Figure (21). This observation is consistent with the photographic light scattering data reported in section C.

Run PET-C. This experiment was designed to assess the annealing effects that occur to PET when a heating rate of 0.2°C/min was used. The sample was heated to 265°C at 0.2°C.min and then cooled to 250°C. After cooling to this temperature, the sample was reheated at 0.2°C/min until melting occurred. The data for the initial heating run were designated PET-C1 and the data for the second heating run were designated PET-C2.

Figures (22) and (23) show the effect of temperature on the H_v scattering pattern of PET during the initial heating run, up to 265°C, as a function of H and U, res-

pectively. It can be clearly seen that the intensity of the scattering increased considerably during this experiment and that the peak moved to larger angles with increasing temperature. The increase in the scattering as a function of temperature is shown more clearly in Figure (24). Since the scattering angle is inversely related to the spherulite radius, these results indicate that the spherulite radius decreased with increasing temperature and this is shown in Figure (25). In Figure (23), the H_v scattering curves have been plotted against U so that the peak maximum always occurs at U=4.1. From this figure, it is apparent that not only did the intensity of the scattering change, but the shape of the scattering curve was also affected by the temperature. As the temperature increased, the curve became much less broad and the peak became more well defined. These effects indicate annealing occurring in this temperature range and the data for PET-Cl is in agreement with the earlier data for PET-X.

When the sample was cooled and reheated at 0.2°C/min through the temperature range 250 to 265°C, it was found that the spherulite radius and the intensity of the scattering remained constant, within experimental error. These effects are shown in Figures (25) and (24), respectively. Furthermore, the shape of the scattering curve

remained constant over this temperature range. These results indicate that upon reheating, no further changes occurred to the sample and this observation is consistent with the previous conclusion that annealing was responsible for the changes observed in the scattering curves of run PET-C1.

Above 265°C, the scattering intensity decreased rapidly as has been previously observed with the other samples. This decrease is shown in Figure (24) and the scattering curves themselves are shown in Figures (26) and (27), respectively. The position of the peak maximum again remained constant and the resulting constancy of the spherulite radius, within experimental error, as a function of temperature through the melting region is shown in Figure 25.

Finally, as a comparison, Figure (28) shows the H_v scattering curves for PET-C at 250°C obtained during the initial run and then after cooling and rerunning. It is apparent that annealing has significantly altered the morphology of the sample since the scattered intensity, the shape of the curve and the position of the peak maximum have all been affected.

In the following section of this chapter, the data for PET-A, PET-B, and PET-C have been further analyzed after correcting for effects due to multiple scattering and disorder.

E. Multiple Scattering Correction

The earliest corrections for multiple scattering in spherulitic systems were developed by Stein and Keane[24] using a theory which only took into account the attenuation of the primary beam. This led to a correction factor which was angularly independent at small angles for an incident beam normal to the surface of the film. However, more recent work by Stein and coworkers[26,32,36] showed that this theory was inadequate to explain the experimental data since these clearly indicated that multiple scattering effects were strongly angularly dependent. Prud'homme et al.[26] showed that multiple scattering decreases the scattering of the system at the position of the peak maximum and redistributes the intensity at large and small scattering angles where an increase in intensity is observed. Similar effects were observed as a function of the azimuthal angle μ such that the intensity is decreased at $\mu=45°$ but increased at smaller and larger values of μ.

In order to correct the experimental data for the above effects arising from multiple scattering, theoretical equations have been developed[8,26,27] which give multiple scattering corrections in terms of θ,μ, the product of turbidity and sample thickness τd, and a parameter δ defining the internal disorder in the spherulite.

The correction factors were calculated assuming a value of δ=0.2 using the two-dimensional theory of Prud'homme et al.[8] such that the multiple scattering correction factor $\kappa(U,\mu,\tau d)$ may be defined as

$$\kappa(U,\mu,\tau d) = \frac{[R(U,\mu)]_{\tau d=0}}{[R(U,\mu)]_{\tau d=\tau d}} \qquad (15)$$

where $[R(U,\mu)]_{\tau d=0}$ is the Rayleigh factor calculated for zero turbidity determined from the experimentally measured Rayleigh factor, $[R(U,\mu)]_{\tau d=\tau d}$. Figure (29) shows the correction factor calculated for H_v light scattering with μ=45° at U=4, 8 and 12. It can be seen that $\kappa(U=4)$ is greater than unity, whereas $\kappa(U=8)$ and $\kappa(U=12)$ are less than unity. Application of these corrections therefore increases the intensities of the peak maximum but decreases the intensity at higher angles.

Run PET-A. Intensity data for sample PET-A at U=4, 8 and 12 were determined from the results files associated with the data partially shown in Figure (16) and were designated R_4, R_8 and R_{12}, respectively. The corresponding correction factors, κ_4, κ_8 and κ_{12} were obtained from Figure 29 using the turbidity data shown in Figure (6). The corrected values of R_4, R_8 and R_{12} were calculated from κ_4, κ_8 and κ_{12} and these new values have been designated R'_4, R'_8 and R'_{12}, respectively. Values

of τd, R_4, R_8, R_{12}, κ_4, κ_8, κ_{12}, R'_4, R'_8 and R'_{12} are shown in Table 2 as a function of temperature.

Run PET-B. Intensity data for sample PET-B at U=4, 8 and 12 were determined from the results files associated with the data partially shown in Figure (20) and were designated R_4, R_8 and R_{12}, respectively. The corresponding correction factors κ_4, κ_8 and κ_{12} were obtained from Figure (29) using the turbidity data shown in Figure (7). The corrected values of R_4, R_8 and R_{12} were calculated from κ_4, κ_8, κ_{12} and these new values have been designated R'_4, R'_8 and R'_{12}, respectively. Values of τd, R_4, R_8, R_{12}, κ_4, κ_8, κ_{12}, R'_4, R'_8 and R'_{12} are shown in Table 3 as a function of temperature.

Run PET-C. Intensity data for sample PET-C at U=4, 8 and 12 were determined from the results files associated with the data partially shown in Figures (23) and (27) and were designated R_4, R_8 and R_{12}, respectively. The corresponding correction factors κ_4, κ_8 and κ_{12} were obtained from Figure (29) using the turbidity data shown in Figure (6). The corrected values of R_4, R_8 and R_{12} were calculated from κ_4, κ_8 and κ_{12} and these new values have been designated R'_4, R'_8 and R'_{12}, respectively. Values of τd, R_4, R_8, R_{12}, κ_4, κ_8, κ_{12}, R'_4, R'_8 and R'_{12}

are shown in Tables 4 and 5 as a function of temperature for the two parts of the run which have previously been called C1 and C2, respectively.

F. Corrections For Disorder

It is known that[6,23] disorder of crystals within a polymer spherulite gives rise not only to a broadening of the angular distribution of scattering, but also to a reduction of intensity at the angles of maximum scattering as compared with that for a perfect spherulite. This reduction primarily occurs because of the decrease in anisotropy of the spherulite resulting from the imperfect orientation of the constituent crystals. Therefore, it is necessary to introduce a correction factor, F_{dis}, to account for the reduction in intensity arising from disorder.

For a two-dimensional spherulite, F_{dis} may be obtained using the Yoon-Stein theory[18] in terms of a parameter δ defining the degree of internal disorder. This parameter may be determined from the ratios of the Rayleigh factors measured at U=4 and U=8, and from the ratios of the Rayleigh factors measured at U=4 and U=12. These Rayleigh factors have previously been corrected for multiple scattering using the procedure described in the previous section.

The values of the disorder parameter may be determined from Figure (30) which has been theoretically calculated by Prud'homme et al.[8] From this diagram, it was possible to obtain δ_8 and δ_{12} using the ratios $R_{H_V}(U=4)/R_{H_V}(U=8)$ and $R_{H_V}(U=4)/R_{H_V}(U=12)$, respectively. Ideally, δ_8 should be equal to δ_{12}. The curves shown in Figure (30) were calculated assuming that the twist angle, ω, which the optic axis makes about the radial direction of the spherulite was random and that the truncation parameter $<(\sigma^2/\bar{a}^2)>$ was equal to 0.13. σ is the standard deviation of the average size of the spherulite and $\bar{a}$ is defined as the mean value of the distance between the boundary of the spherulite and its center. This value of 0.13 has been theoretically predicted for a randomly nucleated spherulitic system.[19] It has been shown by Prud'homme and Stein[16] that truncation reduces the angle at which maximum scattering occurs by a factor which depends on the severity of the truncation. In addition to this angular shift, spherulite truncation increases the H_V scattering intensity at small and large angles but reduces it at intermediate angles. Corrections due to truncation effects are very difficult to quantitatively make and no attempt was made in this work to account for truncation. However, the effect of truncation on the maximum intensity is much less than that of disorder[18]

and the error due to truncation will be constant for a given sample.

From the values of δ determined from Figure (30), it is possible to calculate a value for the disorder correction factor F_{dis} using Figure (31). This figure has been theoretically calculated by Prud'homme et al.[8] using a procedure based on a two-dimensional theory. However, Equation (2) of Chapter II was developed from three-dimensional theory and appreciable error could result in the use of a two-dimensional correction factor in a three-dimensional calculation. In the case of PET, where the spherulites had radii in the region of 15-20 μm and the film thicknesses were about 50 μm, the assumption that the spherulites were two-dimensional is not good. However, three-dimensional lattice calculations would require excessive computing times and attempts are currently in progress[28] to evaluate the accuracy of the above approximation.

From δ_8 and δ_{12}, it was possible to determine the correction factor $F(8)_{dis}$ and $F(12)_{dis}$ which may be applied to correct the value of the Rayleigh factor at the H_v peak maximum.

Run PET-A. The ratios R'_4/R'_8 and R'_4/R'_{12} were calculated from the data given in Table 2 where R'_4, R'_8 and R'_{12} are the Rayleigh factors corrected for multiple scattering at U=4, 8 and 12, respectively. These ratios are shown in Table 6 as a function of temperature. From these ratios, it should have been possible to calculate the disorder parameter using Figure (30). However, both the ratios R'_4/R'_8 and R'_4/R'_{12} were too large to allow interpolation of δ from this figure. The large values for these ratios suggest that the sample had a low degree of disorder and this conclusion would be consistent with the observation that no annealing effects were observed in this sample. Since no disorder parameters could be obtained, it was not possible to further analyze the data from this run.

Run PET-B. The ratios R'_4/R'_8 and R'_4/R'_{12} were calculated from the data given in Table 3 where R'_4, R'_8 and R'_{12} are the Rayleigh factors corrected for multiple scattering at U=4, 8 and 12, respectively. These ratios are shown in Table 7 as a function of temperature. From these ratios, it was possible to calculate the disorder parameters, δ_8 and δ_{12}, using Figure (30) and these have been plotted as a function of temperature in Figure (32).

Within experimental error, it can be seen that δ_8 was approximately equal to δ_{12}. Although the ratio R'_4/R'_8 could be more precisely determined than the ratio R'_4/R'_{12} (since R'_8 was much greater than R'_{12}), the error in δ_8 is greater than the error in δ_{12} because of the shape of the X=8 curve in Figure (30). This curve is almost horizontal at small values of δ and small variations in R'_4/R'_8 produce large changes in δ_8. From Figure (32), it can be seen that as melting occurred, the disorder parameter increased.

Using these values for the disorder parameter, it was possible to determine the disorder correction factors $F(8)_{dis}$ and $F(12)_{dis}$ from Figure (31).

Ideally, these should be equal to one another and they have been tabulated in Table 7 as a function of temperature. The Rayleigh factor at U=4, R''_4, has been corrected for disorder using these factors and the corrected Rayleigh factors are also given in Table 7.

Run PET-C. The ratios R'_4/R'_8 and R'_4/R'_{12} were calculated from the data in Tables 4 and 5 where R'_4, R'_8 and R'_{12} are the Rayleigh factors corrected for multiple scattering at U=4, 8 and 12, respectively. These ratios are shown in Tables 8 and 9 as a function of temperature. From these ratios, it was possible to calculate

the disorder parameters δ_8 and δ_{12} using Figure (30) and these have been plotted as a function of temperature in Figures (33) and (34), respectively. Within experimental error, it can be seen that δ_8 was again approximately equal to δ_{12} and that both disorder parameters exhibited similar trends with increasing temperature.

From Figures (33) and (34), it can be seen that during the initial heating run, the disorder parameter was initially constant and then decreased rapidly in the temperature range 260 to 265°C. This observation supports the previous conclusion that annealing occurred in this temperature range, since annealing results in increased order within the spherulite and, hence, in a smaller disorder parameter. Upon cooling from 265°C and rerunning it can be seen that the increased order was retained at 250°C, as evidenced by the small value of δ. δ then remained fairly constant within experimental error until melting occurred at above 265°C. Melting was accompanied by a very large increase in the disorder parameter.

Using these values for the disorder parameter, it was possible to determine the disorder correction factor $F(8)_{dis}$ and $F(12)_{dis}$ from Figure (31). These factors have been determined in Tables 8 and 9 as a function of temperature. The Rayleigh factor at U=4, $R"_4$, has been corrected for disorder using these factors and the corrected

Rayleigh factors are also given in Tables 8 and 9.

G. Determination of the Orientation Function

Using a lattice theory of light scattering from disordered spherulites, Stein and Yoon[23] have shown that the spherulite birefringence decreases as the disorder increases. The orientation function, f_c, of the c axis with respect to the radius of the spherulite is given by $(\Delta_c/\Delta^\circ_c)$ where Δ_c is the crystalline contribution to spherulite birefringence and Δ°_c is the intrinsic birefringence of the crystals within the spherulite. From the lattice model, Stein and Yoon have derived a relationship between f_c and the internal disorder parameter δ. This relationship is shown in Figure (35) and f_c may be determined from the known values of δ using this figure.

Run PET-B. From the values of δ shown in Figure (32), corresponding values of f_c could be found using Figure (35). These values of f_c have been plotted in Figure (36) as a function of temperature. It can be seen that f_c decreased with increasing temperature, as the disorder within the spherulite simultaneously increased.

Run PET-C. From the values of δ_8 and δ_{12} shown in Figures (33) and (34), respectively, corresponding values of $f_c(8)$ and $f_c(12)$ could be found using Figure (35). These values of $f_c(8)$ and $f_c(12)$ have been plotted in Figures (37) and (38), respectively as a function of temperature. It can been seen from these figures that $f_c(8)$ and $f_c(12)$ followed similar trends with increasing temperature. During the initial run, f_c increased rapidly in the temperature range 260 to 265°C and this trend is consistent with annealing effects. After cooling and rerunning, the orientation function remained at a high level until melting occurred and then decreased rapidly as melting took place.

H. Calculation of the Rayleigh Factor from the Degree of Crystallinity Determined from DSC

It is possible to calculate the Rayleigh factor corresponding to the H_v peak maximum using Equation (2) of Chapter II, since both V_s and θ have been experimentally determined. From Equation (12), $(\alpha_t-\alpha_r)$ may be replaced by $\phi_{cr}\ (\alpha_t-\alpha_r)$ and $(\alpha_t-\alpha_r)_{cr}$ may be calculated from literature values of n_t, n_r and $\bar{n}$ using Equation (14).

Values of n_a, n_b and n_c have been determined by Bunn and Daubeny[38] such that

n_a=1.398, n_b=1.733 and n_c=1.806

For PET, $n_r=n_b=1.733$ and $n_t=\frac{n_a+n_b}{2}=1.602$

$\bar{n}$ is given by $\bar{n}=\frac{nr+2n_t}{3}=1.646$

Therefore, using these values, it can be shown that $(\alpha_t-\alpha_r)^2_{cr} = 1.94 \times 10^{-4}$. For an azimuthal angle of 45° $\cos^2\mu = \sin^2\mu = 0.5$. Furthermore, for U=4.1 evaluation of Equation (3) gives $\Phi_{H_V}(4.1) = 0.0079$. The volume fraction of crystallinity, Φ_{cr}, may be calculated from the DSC weight fraction degree of crystallinity, X_c, using Equation (16)

$$\Phi_{cr} = \frac{X_c}{X_c + (1-X_c)\rho_{cr}/\rho_{am}} \qquad (16)$$

where ρ_{cr} and ρ_{am} are the densities of the crystalline and amorphous phases, respectively. For PET, these are 1.46 and 1.33 Mgm^{-3}, respectively.[39-41]

Run PET-B. For this sample, the average spherulite radius was 15.4 μm and the value of θ_{max} was 1.536°. Using these parameters and the constants determined above, it was possible to evaluate Equation (2) to give

$$R(U=4.1,\ \mu=45) = 5.12 \times 10^6\ \Phi^2_{cr}\ (cm\text{-}Sr)^{-1} \qquad (17)$$

Values of Φ_{cr} as a function of temperature were determined from the DSC data, at a heating rate of 2.5°C/min, shown in Figure (5) and substituting these values into Equation (17) gave the temperature dependence of the Rayleigh factor.

This has been plotted in Figure (39) and the diagram also contains the experimental scattering data, uncorrected, corrected for multiple scattering and corrected for multiple scattering and disorder. From this diagram, it can be seen that there were considerable discrepancies between the curve calculated from the DSC data and the experimental light scattering data. These discrepancies will be discussed in a later section of the chapter.

Run PET-C2. For this sample, the average spherulite radius was 18.0 μm and the value of θ_{max} was 1.290°. Using these parameters and the constants previously determined, it was possible to evaluate Equation (2) to give

$$R(U=4.1,\ \mu=45°) = 8.17 \times 10^{6}\ \Phi_{cr}^{2}\ (cm\text{-}Sr)^{-1} \quad (18)$$

Values of Φ_{cr} as a function of temperature were determined from the DSC data at a heating rate of 0.31°C/min shown in Figure (5) and substituting these values into Equation (18) gave the temperature dependence of the Rayleigh factor. This has been plotted in Figure (40) and this diagram also contains the experimental scattering data, uncorrected, corrected for multiple scattering and corrected for multiple scattering and disorder. From this diagram, it can be seen that there were again considerable discrepancies between the curve calculated for DSC

data and experimental light scattering data. These discrepancies will be discussed in the next section.

I. Discrepancies between Experimental and Calculated Light Scattering Data

In both Figures (39) and (40), it can be seen that the experimental H_v light scattering Rayleigh factor, even after correction for multiple scattering and disorder, were significantly lower than the values calculated from the DSC data. This discrepancy could have been due to several factors, both experimental and theoretical. The experimental factor arises because there is some doubt[35] about the accuracy of the quantitative light scattering apparatus, especially at the higher scattering angles. This effect is such that the apparatus underestimates the intensities at high angles, which in turn leads to too large values for the ratios R_4/R_8 and R_4/R_{12}. Since these ratios determine the disorder correction further large errors could possibly result. Another experimental problem is the determination of sample turbidity and the problems associated with accurately determining this parameter have been previously discussed. The multiple scattering correction strongly depends on the sample turbidity and even small errors in τd could lead to large errors in the multiple scattering corrections.

Other factors of a more theoretical nature are the validity of applying these particular multiple scattering and disorder corrections to the data, since these correction factors have been derived from a two-dimensional model and light scattering equations such as Equation (2) were developed using three-dimensional theory. At the moment, it is not possible to easily assess the errors involved in using a two-dimensional correction factor. Furthermore, the multiple scattering correction was determined assuming a value for the disorder parameter. If time had permitted, a procedure should have been used in which the multiple scattering correction factors were redetermined using the values of the disorder parameter calculated from the data. Another source of error results from the neglect of truncation corrections. These corrections would have increased the value of the experimental Rayleigh factor at U=4.1 and would have slightly lessened the observed discrepancy. However, corrections due to truncation are much smaller than corrections due to disorder, and truncation errors cannot completely account for the differences between the experimental and calculated data. Finally, errors undoubtedly exist in the values of Φ_{cr} determined from the DSC data and since the Rayleigh factors depend on Φ_{cr}^2, the errors in the Rayleigh factor would be even greater. Also,

the DSC heating rates were 0.31 and 2.5°C/min whereas the light scattering experiments were carried out at heating rates of 0.2 and 2.0°C/min. Therefore, in view of the above discussion, it is not surprising that differences exist between the experimental and calculated data.

C H A P T E R V

CONCLUSIONS

The melting of isothermally crystallized PET has been studied by DSC and by qualitative and quantitative light scattering at heating rates of 0.2°C/min and 2.0°C/min. All three techniques indicated that annealing occurred at the lower heating rate, complicating the melting behavior.

The quantitative data were corrected for instrumental effects and for errors due to multiple scattering and internal disorder. The Rayleigh factor corresponding to the maximum in the H_v scattering curve was compared with the Rayleigh factor calculated from the degree of crystallinity found by DSC and considerable discrepancies were observed. These were interpreted in terms of inadequate multiple scattering and disorder theories, in terms of the neglect of a truncation correction and in terms of experimental errors resulting from both the DSC and light scattering measurements.

Results from the 2.0°C/min run indicated that the spherulite radius as determined by the position of the peak in the H_v scattering pattern remained constant until

melting occurred, but that the absolute intensity of the scattering decreased with increasing temperature. Further, the data showed that the disorder within the spherulite increased with increasing temperature and that the orientation function decreased. The results indicate that during melting, the spherulites melted uniformly and not from the edges inward.

Similar results were observed at a heating rate of 0.2°C/min but the data were complicated by annealing effects. During the initial heating run, the intensity of scattering increased and the disorder within the spherulite decreased as the temperature was increased. Also, somewhat surprisingly, a decrease was observed in the spherulite radius through the region. Tentatively, this could be ascribed to a melting of disordered regions within the spherulite and these would predominantly occur near the edge of the spherulite. On cooling and rerunning, the spherulite radius remained constant at its previous low value as the temperature was increased throug the melting region. The scattering intensity and the disorder parameter remained constant until the onset of melting at which point the scattered intensity decreased rapidly and the disorder increased rapidly with increasing temperature. It was difficult to make quantitative light scattering

measurements at temperatures very near the melting point because disorder effects considerably broadened the scattering curve and destroyed the peak.

C H A P T E R V I

SUGGESTIONS FOR FUTURE WORK

A. That the OMA be improved to increase the range, sensitivity and accuracy of detection, especially at higher scattering angles.

B. That more precise techniques be developed to melt and crystallize the samples.

C. That the light scattering data be complemented by corresponding optical microscope studies of the spherulites as a function of temperature.

D. That better procedures be developed to measure sample turbidity.

E. That the data be analyzed using three-dimensional multiple scattering and disorder corrections.

F. That the data be corrected for truncation effects.

REFERENCES

1. R. S. Stein, in Structure and Properties of Polymer Films, R. W. Lenz and R. S. Stein, eds. Plenum Press, New York, 1973, p. 1.

2. R. S. Stein, Appl. Polymer Symposium, 20, 347 (1973).

3. R. S. Stein and R. S. Finklestein, Annual Review of Physical Chemistry, 24, 207 (1973).

4. R. S. Stein, J. Chem. Ed., 50, 748 (1973).

5. R. J. Samuels, J. Polym. Sci., Polym. Physics Ed., 12, 1417 (1974).

6. R. S. Stein and W. Chu, J. Polymer Sci., A2, 8, 1137 (1970).

7. R. J. Samuels, in Small Angle Scattering from Fibrous and Partially Ordered Systems, (J. Polymer Science, C, 13), R. H. Marchessault, Ed., Interscience, New York, 1966, p. 37.

8. R. J. Natarajan, D. Y. Yoon, R. E. Prud'homme and R. S. Stein, unpublished work.

9. M. Motegi, T. Oda, M. Moritani and H. Kawai, Polymer J. 1, 209 (1970).

10. R. S. Stein, M. B. Rhodes, P. R. Wilson and S. N. Stidham, Pure and Appl. Chem., 4, 219 (1962).

11. R. S. Stein and C. Picot, J. Polymer Sci., A2, 8, 1955 (1970).

12. C. Picot, R. S. Stein, R. H. Marchessault, J. Borch and A. Sarko, Macromolecules, 4, 467 (1971).

13. I. T. Moneva, Y. W. Brestkin, B. M. Ginzburg and S. Y. Frenkel, European Polymer J., 8, 1033 (1972).

14. R. E. Prud'homme and R. S. Stein, J. Polymer Sci., Polymer Physics Ed., 11, 1357 (1973).

15. C. Picot, R. S. Stein, M. Motegi and H. Kawai, J. Polymer Sci., A2, 8, 2115 (1970).

16. R. S. Stein and C. Picot, J. Polymer Sci., A2, 8, 2127 (1970).

17. S. Tatematsu, N. Hayashi, S. Nomuro and H. Kawai, Polymer J., 3, 488 (1972).

18. R. E. Prud'homme and R. S. Stein, J. Polymer Science, Polymer Phys. Ed., 11, 1683 (1973).

19. A. Misra, R. E. Prud'homme and R. S. Stein, J. Polymer Sci., Polymer Phys. Ed., 12, 1235 (1974).

20. R. S. Stein and T. Hashimoto, J. Polymer Sci., A2, 9, 1747 (1971).

21. R. E. Prud'homme, D. Yoon and R. S. Stein, J. Polymer Sci., Polymer Phys. Ed., 11, 1047 (1973).

22. D. Y. Yoon, "Light Scattering and Deformation Studies of Crystalline Polymers," Ph.D. Thesis, Univ. of Mass., Amherst, Mass., 1973.

23. D. Y. Yoon and R. S. Stein, J. Polymer Sci., Polymer Phys. Ed., 12, 763 (1974).

24. R. S. Stein and J. J. Keane, J. Polymer Sci., 17, 21 (1955).

25. J. J. Keane and R. S. Stein, J. Polymer Sci., 20, 327 (1956).

26. R. E. Prud'homme, L. Bourland, R. T. Natarajan and R. S. Stein, J. Polymer Sci., Polymer Phys. Ed., 12, 1955 (1974).

27. R. T. Natarajan, L. Bourland, R. E. Prud'homme and R. S. Stein, J. Polymer Sci., Polymer Phys. Ed., 14, 1541 (1976).

28. R. E. Prud'homme, Ph.D. Thesis, University of Massachusetts, 1973.

29. T. Yuasa, M.S. Thesis, University of Massachusetts, 1975.

30. R. S. Stein, Rubber Chem. and Technology, 49, 459 (1976).

31. M. K. Parpart, Ph.D. Thesis, University of Massachusetts, 1979.

32. R. S. Stein and M. B. Rhodes, J. Appl. Phys., 31, 1873 (1960).

33. A. Misra, Ph.D. Thesis, University of Massachusetts, 1974.

34. T. P. Russell, J. Koberstein, R. Prud'homme, A. Misra, R. S. Stein, J. W. Parsons and R. L. Rowell, J. Polymer Sci., Polymer Phys. Ed., 16, 1879 (1978).

35. J. T. Koberstein, private communication.

36. M. B. Rhodes and R. S. Stein, J. Polymer Sci., A2, 7, 1539 (1969).

37. J. Brandrup and E. H. Immergut, Eds., "Polymer Handbook," 2nd Ed., Wiley, New York, 1975.

38. C. W. Bunn and R. P. Daubeny, Trans. Faraday Soc., 50, 1173 (1954).

39. C. W. Bunn and C. J. Brown, Proc. Royal Soc., 226A, 531 (1954).

40. M. Kokondu, Y. Sakakibara and H. Tadokoro, Macromolecules, 9, 226 (1976).

41. A. Escala, Ph.D. Thesis, University of Massachusetts, 1978.

TABLE 1

X_c AND MELTING TEMPERATURE AS A FUNCTION OF HEATING RATE

Heating Rate (^{deg}/min)	T peak max (°C)	$\dot{X}_c$
0.31	265	0.32
2.5	261	0.30
10.0	258	0.25

TABLE 2

MULTIPLE SCATTERING CORRECTIONS FOR PET-A

T(°C)	τd	$R_4 x10^{-3}$	$R_8 x10^{-3}$	$R_{12} x10^{-2}$	κ_4	κ_8	κ_{12}	$R'_4 x10^{-3}$	$R'_8 x10^{-3}$	$R'_{12} x10^{-2}$
40.0	2.56	4.16	1.12	3.49	3.49	0.99	0.68	14.5	1.11	2.37
200.0	2.04	9.25	2.90	5.13	2.67	0.86	0.66	24.7	2.49	3.39
240.0	1.97	15.6	3.20	3.32	2.59	0.85	0.66	40.5	2.72	2.19
245.0	2.24	17.4	4.50	5.00	3.00	0.91	0.66	52.3	4.10	3.30
250.0	2.30	15.8	3.70	4.63	3.07	0.92	0.67	48.3	3.40	3.10
253.0	2.09	14.6	3.28	4.29	2.75	0.87	0.66	40.2	2.85	2.83
255.0	1.87	14.1	3.10	3.99	2.47	0.84	0.66	34.9	2.60	2.63
265.0	0.40	14.5	2.80	1.85	1.16	0.88	0.85	16.8	2.46	1.57
266.2	0.35	12.6	2.18	1.33	1.13	0.88	0.86	14.2	1.92	1.14
266.5	0.30	11.2	1.90	1.23	1.11	0.90	0.88	12.5	1.67	1.08
266.7	0.25	10.3	1.75	1.21	1.09	0.91	0.90	11.2	1.59	1.09
267.0	0.21	8.86	1.39	1.04	1.07	0.92	0.90	9.48	1.28	0.94
267.2	0.20	7.55	1.15	0.96	1.07	0.93	0.91	8.07	1.07	0.87
267.4	0.19	6.01	0.89	0.78	1.06	0.93	0.91	6.37	0.81	0.71
267.6	0.18	4.76	0.07	0.65	1.06	0.94	0.92	5.04	0.60	0.59
267.8	0.17	3.74	0.06	0.63	1.05	0.94	0.92	3.92	0.53	0.58
268.0	0.16	2.28	0.04	0.55	1.05	0.94	0.92	2.39	0.36	0.51
268.2	0.15	2.05	0.04	0.68	1.05	0.95	0.93	2.15	0.36	0.64
268.4	0.14	1.52	0.03	0.78	1.04	0.95	0.93	1.58	0.32	0.73
268.6	0.13	1.02	0.02	0.70	1.04	0.95	0.94	1.06	0.23	0.66
268.8	0.12	0.26	0.01	0.63	1.04	0.95	0.94	0.27	0.12	0.60
269.0	0.11	0.33	0.01	--	1.03	0.96	0.94	0.34	0.10	--
269.2	0.10	0.17	0.01	0.64	1.03	0.96	0.95	0.17	0.07	0.61
269.5	0.09	0.06	0.01	0.54	1.03	0.96	0.95	0.06	0.05	0.52

TABLE 3

MULTIPLE SCATTERING CORRECTIONS FOR PET-B

T(°C)	τ_d	$R_4 \times 10^{-3}$	$R_8 \times 10^{-3}$	$R_{12} \times 10^{-2}$	κ_4	κ_8	κ_{12}	$R'_4 \times 10^{-3}$	$R'_8 \times 10^{-3}$	$R'_{12} \times 10^{-2}$
40.0	2.30	5.14	1.42	3.68	3.07	0.92	0.67	15.8	1.31	2.47
200.0	1.85	5.03	1.76	5.75	2.44	0.84	0.66	12.3	1.48	3.80
220.0	1.76	4.30	1.59	6.33	2.30	0.83	0.67	9.89	1.32	4.24
227.5	1.70	3.87	1.62	6.99	2.28	0.82	0.67	8.83	1.33	4.68
230.0	1.64	4.08	1.66	7.33	2.20	0.82	0.67	8.97	1.36	4.91
234.0	1.50	4.38	1.75	7.46	2.04	0.81	0.68	8.94	1.42	5.07
237.5	1.29	4.60	1.66	7.50	1.84	0.81	0.69	8.47	1.34	5.18
241.5	1.16	4.48	1.68	7.35	1.69	0.80	0.70	7.57	1.34	5.15
245.0	1.07	4.61	1.70	7.64	1.63	0.80	0.71	7.51	1.36	5.40
249.0	0.90	4.41	1.68	7.82	1.49	0.81	0.74	6.56	1.36	5.80
252.0	0.74	3.95	1.73	7.80	1.38	0.82	0.76	5.45	1.41	5.93
254.2	0.60	3.23	1.48	7.14	1.28	0.84	0.80	4.13	1.24	5.71
256.0	0.46	2.65	1.31	6.89	1.18	0.86	0.83	3.13	1.13	5.72
257.8	0.33	2.10	0.95	5.92	1.12	0.89	0.86	2.36	0.85	5.12
259.6	0.24	2.21	0.79	5.27	1.08	0.91	0.89	2.39	0.73	4.69
261.3	0.18	2.04	0.68	4.92	1.06	0.93	0.91	2.17	0.63	4.48
262.9	0.14	1.00	0.51	4.67	1.05	0.95	0.93	1.05	0.48	4.34
264.4	1.10	0.39	0.44	4.69	1.03	0.96	0.95	0.40	0.42	4.46

TABLE 4

MULTIPLE SCATTERING CORRECTIONS FOR PET-Cl

T(°C)	τd	$R_4 x10^{-3}$	$R_8 x10^{-3}$	$R_{12} x10^{-3}$	κ_4	κ_8	κ_{12}	$R'_4 x10^{-4}$	$R'_8 x10^{-3}$	$R'_{12} x10^{-3}$
40.0	2.56	3.75	1.48	3.86	3.48	0.98	0.68	1.30	1.45	2.62
200.0	2.04	4.09	1.34	3.28	2.68	0.86	0.66	1.10	1.15	2.16
245.0	2.24	4.16	3.45	2.51	3.00	0.91	0.66	1.25	3.14	1.66
250.0	2.30	4.32	3.57	2.63	3.08	0.92	0.66	1.33	3.29	1.74
253.0	2.09	4.74	3.94	2.90	2.76	0.88	0.67	1.31	3.47	1.94
255.1	1.85	4.86	3.86	2.58	2.44	0.84	0.66	1.19	3.24	1.70
257.1	1.60	4.98	3.67	2.42	2.16	0.82	0.67	1.08	3.01	1.62
259.0	1.36	5.43	3.64	2.12	1.90	0.81	0.68	1.03	2.94	1.44
259.9	1.21	5.83	3.62	1.88	1.75	0.80	0.70	1.02	2.90	1.31
260.9	1.06	6.43	3.53	1.54	1.61	0.81	0.72	1.03	2.86	1.11
261.2	1.02	6.75	3.50	1.40	1.50	0.81	0.73	1.01	2.83	1.02
261.4	0.98	6.94	3.50	1.31	1.50	0.81	0.73	1.04	2.84	0.96
262.0	0.90	7.65	3.69	1.20	1.49	0.81	0.74	1.14	2.99	0.89
262.5	0.82	8.12	3.53	1.02	1.42	0.82	0.76	1.15	2.89	0.78
263.0	0.72	8.83	3.44	0.87	1.37	0.82	0.77	1.21	2.82	0.67
263.5	0.66	9.47	3.49	0.81	1.32	0.83	0.78	1.25	2.90	0.63
264.0	0.58	1.02	3.50	0.76	1.28	0.84	0.80	1.30	2.94	0.60
264.5	0.48	1.04	3.42	0.69	1.21	0.86	0.82	1.26	2.94	0.56
265.0	0.40	1.05	3.26	0.63	1.16	0.88	0.84	1.21	2.86	0.53

TABLE 5

MULTIPLE SCATTERING CORRECTIONS FOR PET-C2

T(°C)	τd	$R_4 x10^{-3}$	$R_8 x10^{-3}$	$R_{12} x10^{-2}$	κ_4	κ_8	κ_{12}	$R'_4 x10^{-3}$	$R'_8 x10^{-3}$	$R'_{12} x10^{-2}$
250.0	0.90	18.6	7.41	14.0	1.48	0.82	0.74	27.5	6.08	10.4
255.0	0.90	17.6	7.89	19.0	1.48	0.80	0.73	27.5	6.31	13.9
259.0	0.90	18.5	8.43	19.6	1.48	0.82	0.74	27.4	6.91	14.5
261.0	0.90	18.9	8.39	18.1	1.48	0.82	0.74	28.0	6.88	13.4
263.0	0.90	18.9	8.04	15.9	1.48	0.82	0.74	28.0	6.59	11.8
265.0	0.75	17.8	6.71	12.4	1.38	0.82	0.76	24.5	5.50	9.2
266.0	0.70	16.9	6.03	11.0	1.34	0.82	0.77	22.7	4.94	8.5
266.8	0.50	15.9	5.40	9.49	1.22	0.86	0.82	19.4	4.64	7.8
267.6	0.18	14.5	3.86	6.38	1.07	0.93	0.91	15.5	3.59	5.9
268.0	0.16	13.3	3.12	5.06	1.05	0.94	0.92	13.9	2.93	4.7
268.5	0.13	11.4	2.48	4.24	1.04	0.96	0.94	11.8	2.38	4.0
268.0	0.12	9.61	2.09	3.65	1.04	0.96	0.94	10.0	2.01	3.9
269.0	0.11	7.72	1.86	3.33	1.04	0.96	0.94	8.03	1.79	3.1
269.2	0.10	5.44	1.47	2.82	1.03	0.96	0.95	5.60	1.41	2.7
269.4	0.09	3.87	1.09	2.48	1.03	0.96	0.95	3.98	1.04	2.4
269.6	0.08	2.71	0.856	2.28	1.03	0.96	0.95	2.78	0.82	2.2
269.7	0.08	1.89	0.602	2.09	1.03	0.96	0.95	1.94	0.58	2.0
269.9	0.08	1.28	0.412	1.85	1.03	0.96	0.95	1.31	0.40	1.8
270.0	0.07	0.817	0.317	1.80	1.03	0.96	0.95	0.84	0.30	1.7
270.2	0.06	0.554	0.233	1.74	1.02	0.98	0.97	0.56	0.23	1.7
270.3	0.06	0.357	0.187	1.79	1.02	0.98	0.97	0.36	0.18	1.7
270.4	0.06	0.244	0.159	--	1.02	0.98	0.97	0.25	0.16	-
270.6	0.06	0.178	0.155	--	1.02	0.98	0.97	0.18	0.15	-

TABLE 6

DISORDER CORRECTIONS FOR PET-A

T(°C)	R'_4/R'_8	R'_4/R'_{12}
40.0	13.1	61.2
200.0	9.92	72.9
240.0	14.9	185
245.0	12.8	158
250.0	14.2	156
253.0	14.1	142
255.0	13.4	133
265.0	6.83	107
266.2	7.40	125
266.5	7.49	116
266.7	7.04	103
267.0	7.40	101
267.2	7.52	92.4
267.4	7.86	89.6
267.6	8.26	84.8
267.8	7.40	67.5
268.0	6.63	46.9
268.2	5.97	33.8
268.4	4.94	21.7
268.6	4.65	16.1
268.8	2.24	4.55
269.0	3.55	--
269.2	2.28	2.82
269.5	1.30	1.18

TABLE 7

DISORDER CORRECTIONS FOR PET-B

T(°C)	R'_4/R'_8	R'_4/R'_{12}	$F(8)_{dis}$	$F(12)_{dis}$	$R''_4(8)\times10^{-4}$	$R''_4(12)\times10^{-4}$
40.0	12.1	63.9	--	--	--	--
200.0	8.31	32.4	--	--	--	--
220.0	7.49	23.3	--	2.9	--	2.87
227.5	6.64	18.9	--	5.0	--	4.42
230.0	6.50	18.3	--	5.2	--	4.66
234.0	6.30	17.6	--	5.6	--	5.01
237.5	6.32	16.4	--	6.4	--	5.42
240.5	5.65	14.7	--	7.5	--	5.68
245.0	5.52	13.9	--	8.6	--	6.46
249.0	4.82	11.3	--	11.5	--	7.54
252.0	3.87	9.2	5.7	14.0	3.11	7.63
254.2	3.32	7.2	10.6	21.0	4.38	8.67
256.0	2.77	5.5	20.0	30.0	6.26	9.39
257.8	2.77	4.6	20.0	43.0	4.72	10.1
259.6	3.29	5.1	11.5	38.0	5.14	9.08
261.3	3.43	4.8	10.0	41.0	4.34	8.90
262.9	2.17	2.4	38.0	--	3.99	--
264.4	0.94	0.9	--	--	--	--

TABLE 8

DISORDER CORRECTIONS FOR PET-Cl

T(°C)	R'_4/R'_8	R'_4/R'_{12}	$F(8)_{dis}$	$F(12)_{dis}$	$R''_4(8)\times10^{-4}$	$R''_4(12)\times10^{-4}$
40.0	8.97	4.96	-	--	-	--
200.0	9.57	5.09	-	--	-	--
245.0	3.98	7.53	5.0	20.1	6.3	25
250.0	4.04	7.64	4.5	20.0	6.0	27
253.0	3.78	6.75	6.6	24.5	8.7	32
255.1	3.67	7.00	7.6	24.0	9.0	29
257.1	3.59	6.67	8.6	25.0	9.3	27
259.0	3.50	7.15	8.8	20.1	9.1	21
259.9	3.52	7.79	8.8	20.1	9.0	21
260.9	3.60	9.28	8.6	20.0	8.9	21
261.2	3.57	9.90	8.7	20.1	8.8	20
261.4	3.66	10.8	7.6	15.3	7.9	16
262.0	3.81	12.8	6.5	8.8	7.4	10
262.5	3.98	14.7	5.0	7.6	5.8	8.7
263.0	4.29	18.1	3.1	5.6	3.8	6.8
263.5	4.31	19.8	3.1	4.5	3.9	5.6
264.0	4.42	21.7	2.6	2.5	3.4	3.3
264.5	4.29	22.5	3.1	3.3	3.9	4.2
265.0	4.23	22.8	3.5	3.4	4.2	4.1

TABLE 9

DISORDER CORRECTIONS FOR PET-C2

T(°C)	R'_4/R'_8	R'_4/R'_{12}	$F(8)_{dis}$	$F(12)_{dis}$	$R''_4(8)\times10^{-4}$	$R''_4(12)\times10^{-4}$
250.0	4.53	26.4	2.3	2.3	6.3	6.3
255.0	4.34	19.8	3.0	4.4	8.3	12
259.0	4.29	20.2	3.0	3.9	8.2	11
261.0	4.41	22.3	2.5	3.2	7.0	9.0
263.0	4.58	25.4	2.3	2.3	6.4	6.4
265.0	4.46	26.6	2.3	2.3	5.6	5.6
266.0	4.40	26.7	2.0	2.6	4.5	5.9
266.8	4.20	24.9	3.5	2.0	6.8	3.9
267.6	4.32	26.3	3.0	--	4.7	--
268.0	4.74	29.6	--	--	-	--
268.5	4.96	29.5	--	--	-	--
268.8	4.98	25.5	--	--	-	--
269.0	4.49	25.9	2.3	--	1.9	--
269.2	3.97	20.7	5.6	4.1	3.1	2.3
269.4	3.83	16.5	6.3	6.2	2.5	2.5
269.6	3.39	12.6	10.1	9.8	2.8	2.7
269.7	3.34	9.70	10.1	10.4	2.0	2.0
269.9	3.28	7.28	10.2	20.1	1.3	2.6
270.0	2.80	4.94	10.8	30.8	0.91	2.6
270.2	2.43	3.29	31.0	--	1.7	--
270.3	2.00	2.12	--	--	-	--
270.4	1.56	--	--	--	-	--
270.6	1.20	--	--	--	-	--

Photographic Light Scattering Apparatus

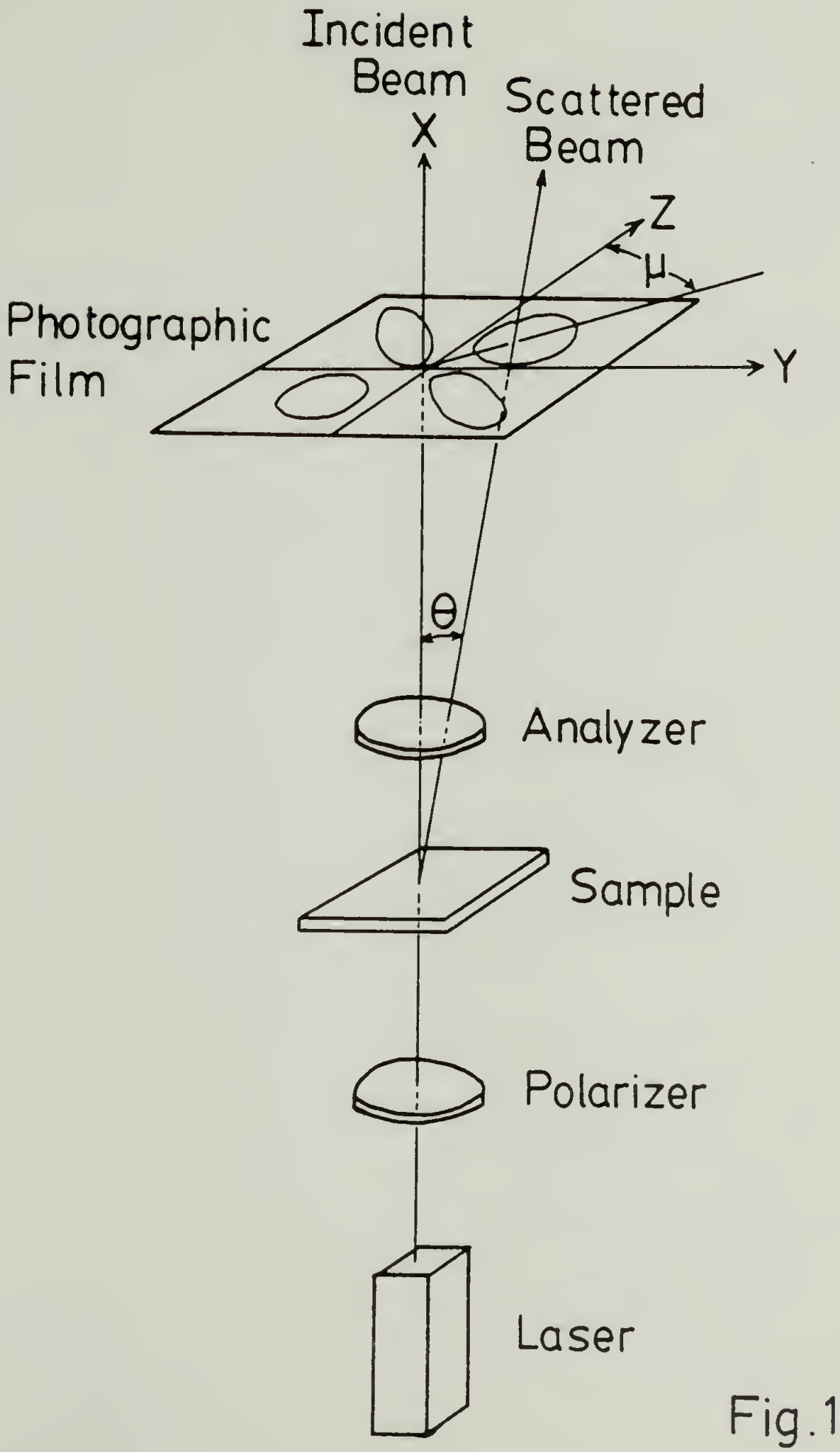

Fig.1

A Schematic Diagram of the Optical Multi-Channel Analyzer

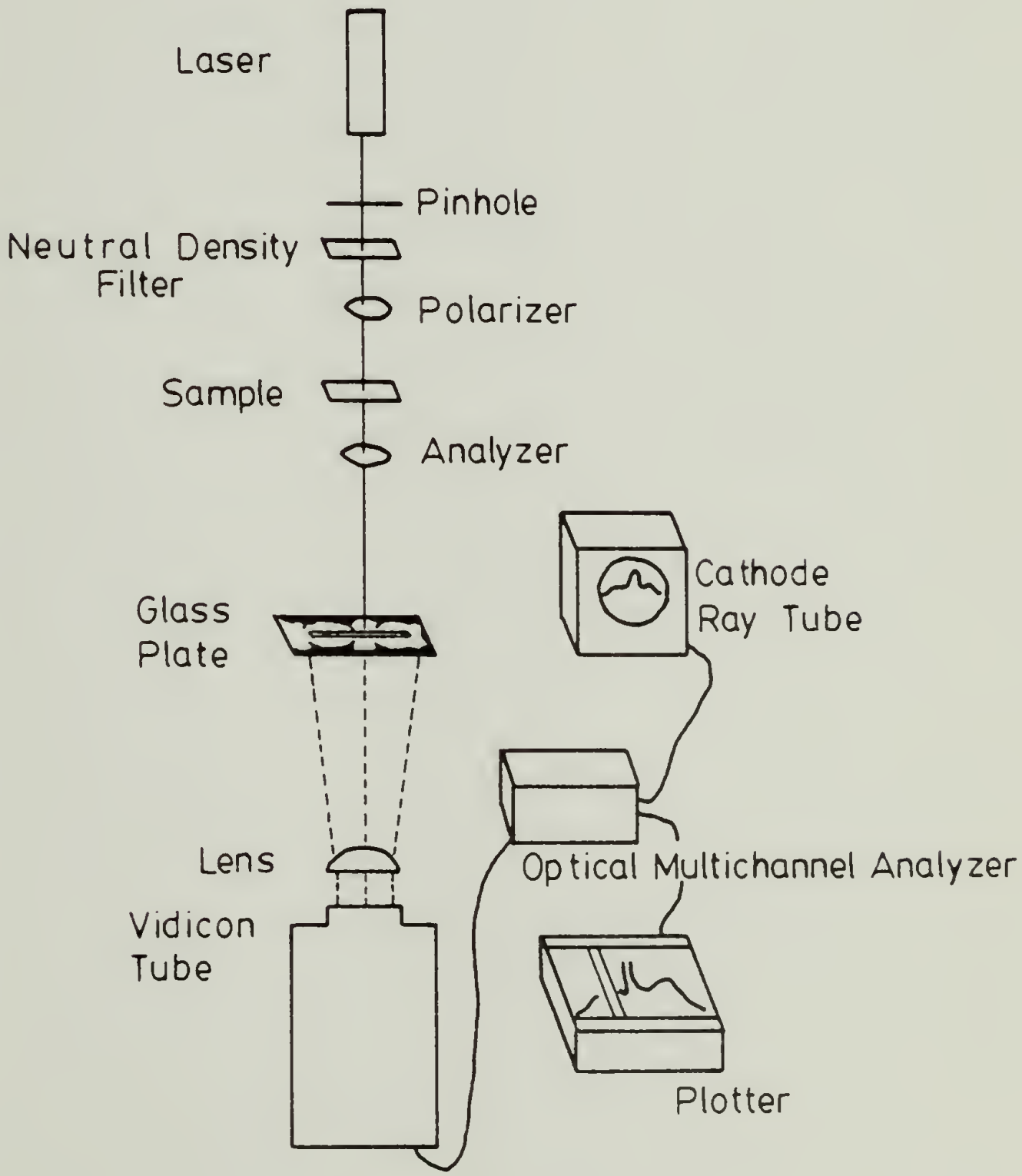

Fig.2

Typical Data from Optical Multichannel Analyzer

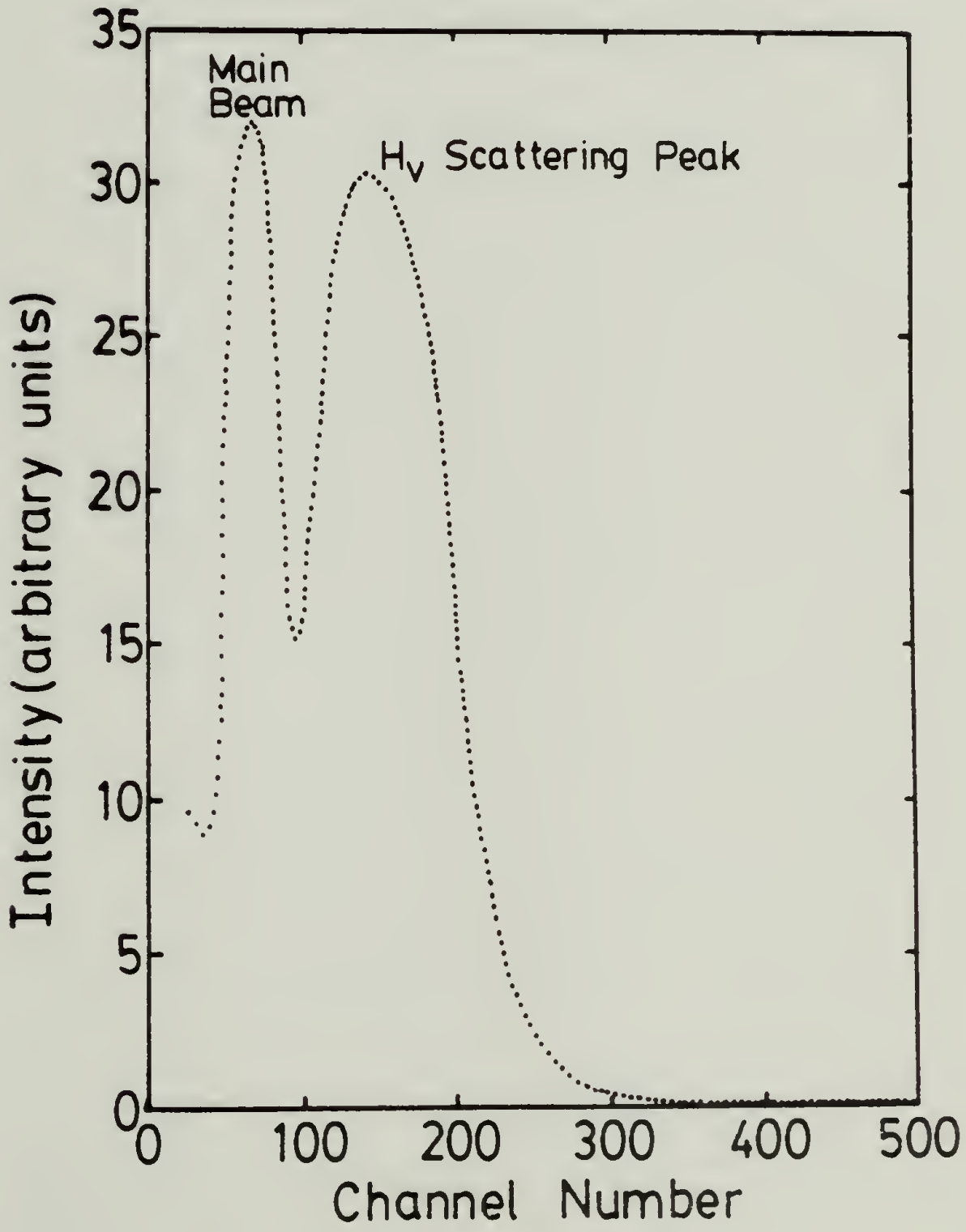

Fig.3

Melting of PET by D.S.C. as a function of Heating Rate

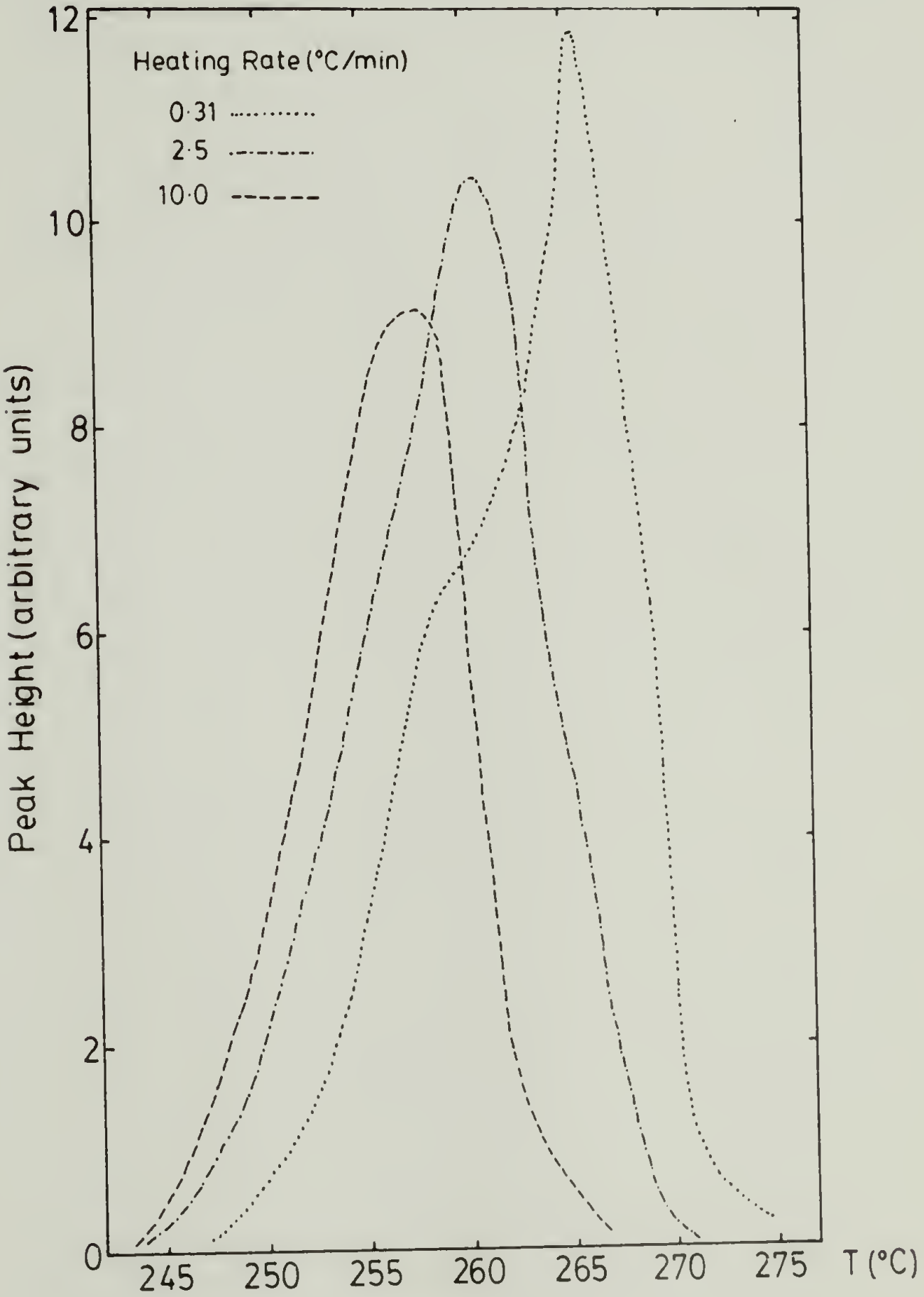

Fig. 4

X_c of Polyethylene Terephthalate by D.S.C. as a function of Temperature and Heating Rate

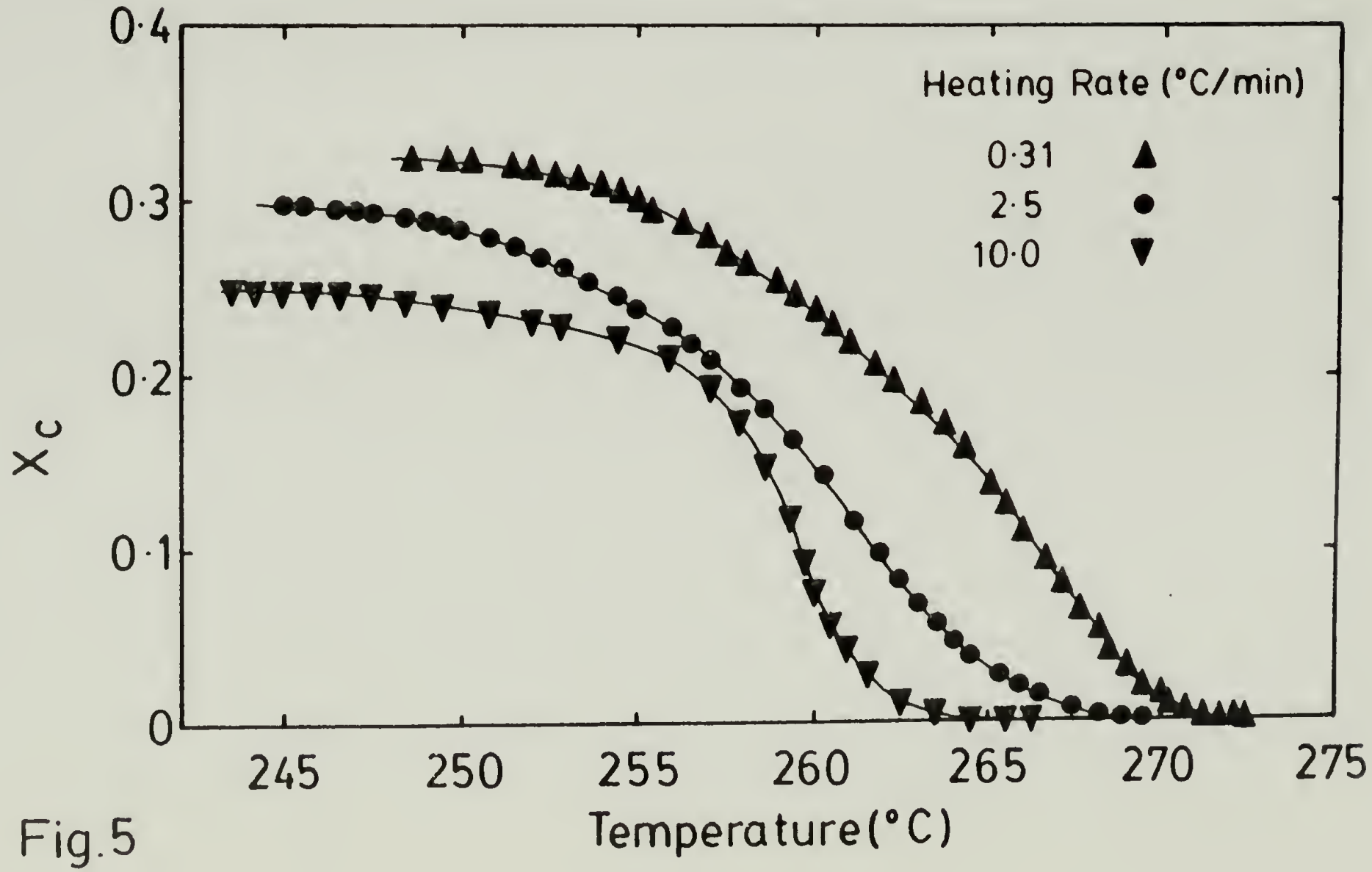

Fig.5

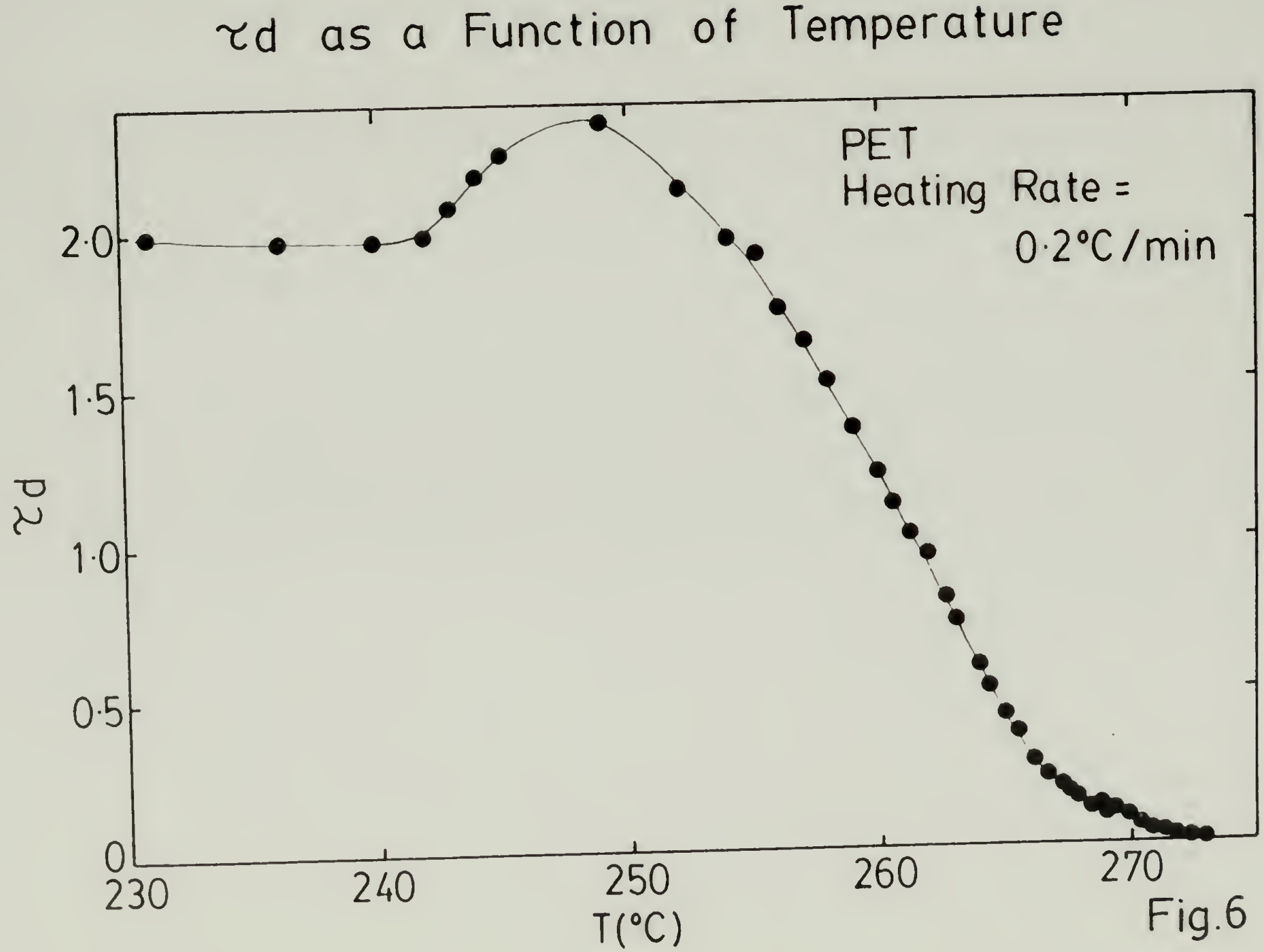
τd as a Function of Temperature
PET
Heating Rate =
0·2°C/min
τd
2·0
1·5
1·0
0·5
0
230
240
250
260
270
T(°C)

Fig.6

τd as a Function of Temperature

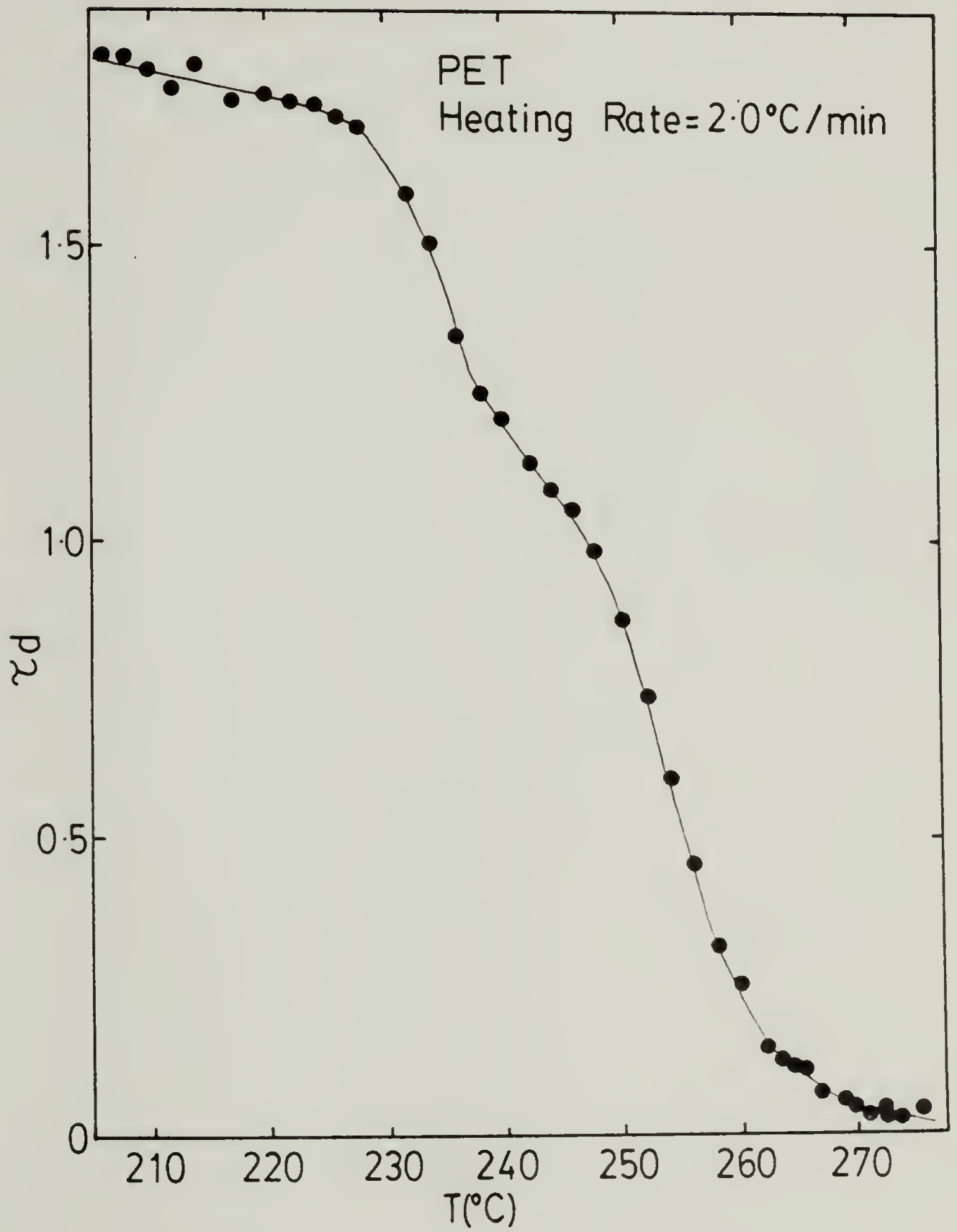

Fig. 7

PHOTOGRAPHIC MELTING STUDIES OF POLYETHYLENE TEREPHTHALATE

Fig.8a

HEATING RATE = 0·2 DEG/MIN

1°

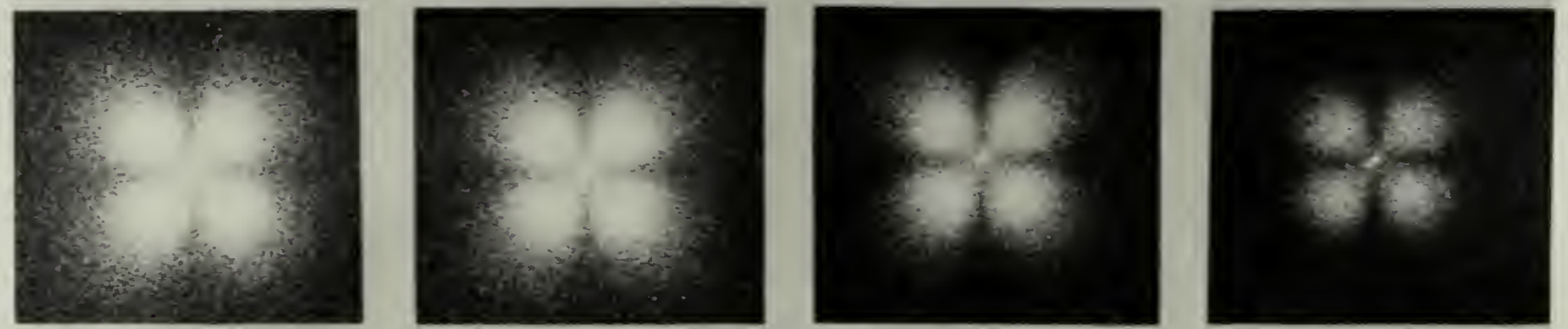

(a) T= 240·9°C (b) T=250·6°C (c) T= 255·0°C (d) T= 258·9°C

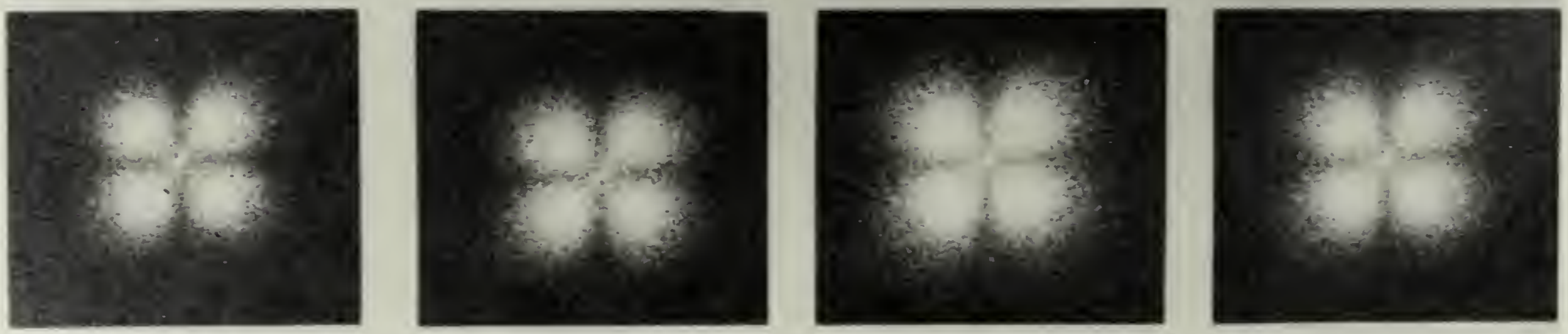

(e) T = 259·4°C (f) T = 259·7°C (g) T=262·1°C (h) T= 267·1°C

Fig.8b PHOTOGRAPHIC MELTING STUDIES OF POLYETHYLENE TEREPHTHALATE

HEATING RATE=0·2DEG/MIN (continued)

1°

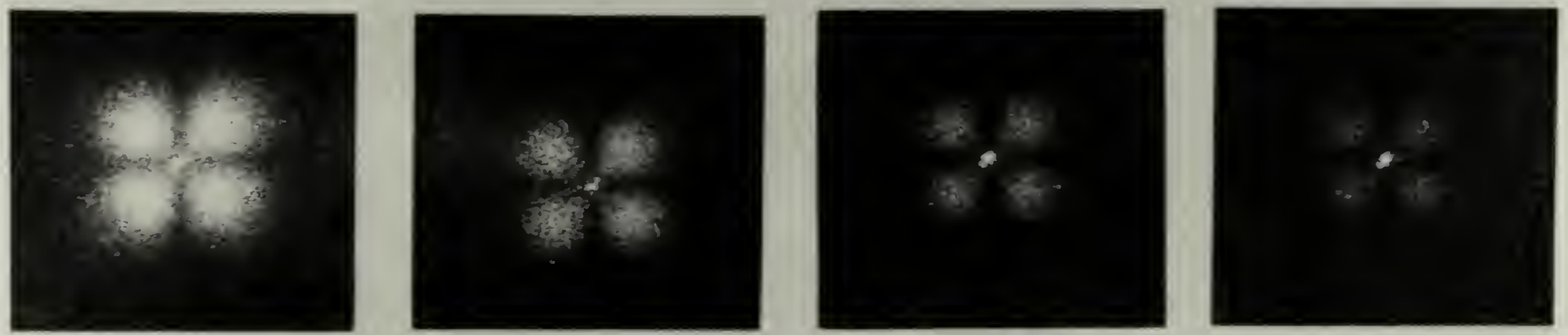

(i) T=268·0°C (j) T=269·0°C (k) T=269·4°C (l) T=269·6°C

(m) T=269·8°C (n) T=269·9°C (o) T=270·0°C (p) T=270·3°C

Fig.9

PHOTOGRAPHIC MELTING STUDIES OF POLYETHYLENE TEREPHTHALATE

HEATING RATE = 2·0 DEG/MIN

1°

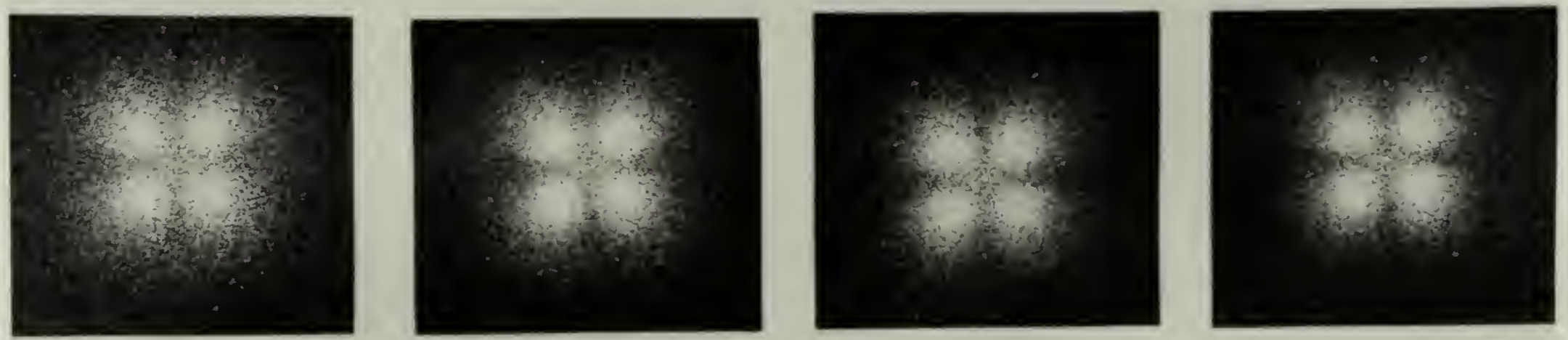

(a) T = 245·1°C (b) T = 254·6°C (c) T = 256·8°C (d) T = 258·9°C

(e) T = 260·0°C (f) T = 261·0°C (g) T = 262·5°C (h) T = 263·8°C

Melting Data of Poly(ethylene terephthalate) by Light Scattering

(Heating Rate=0·2°C/min)

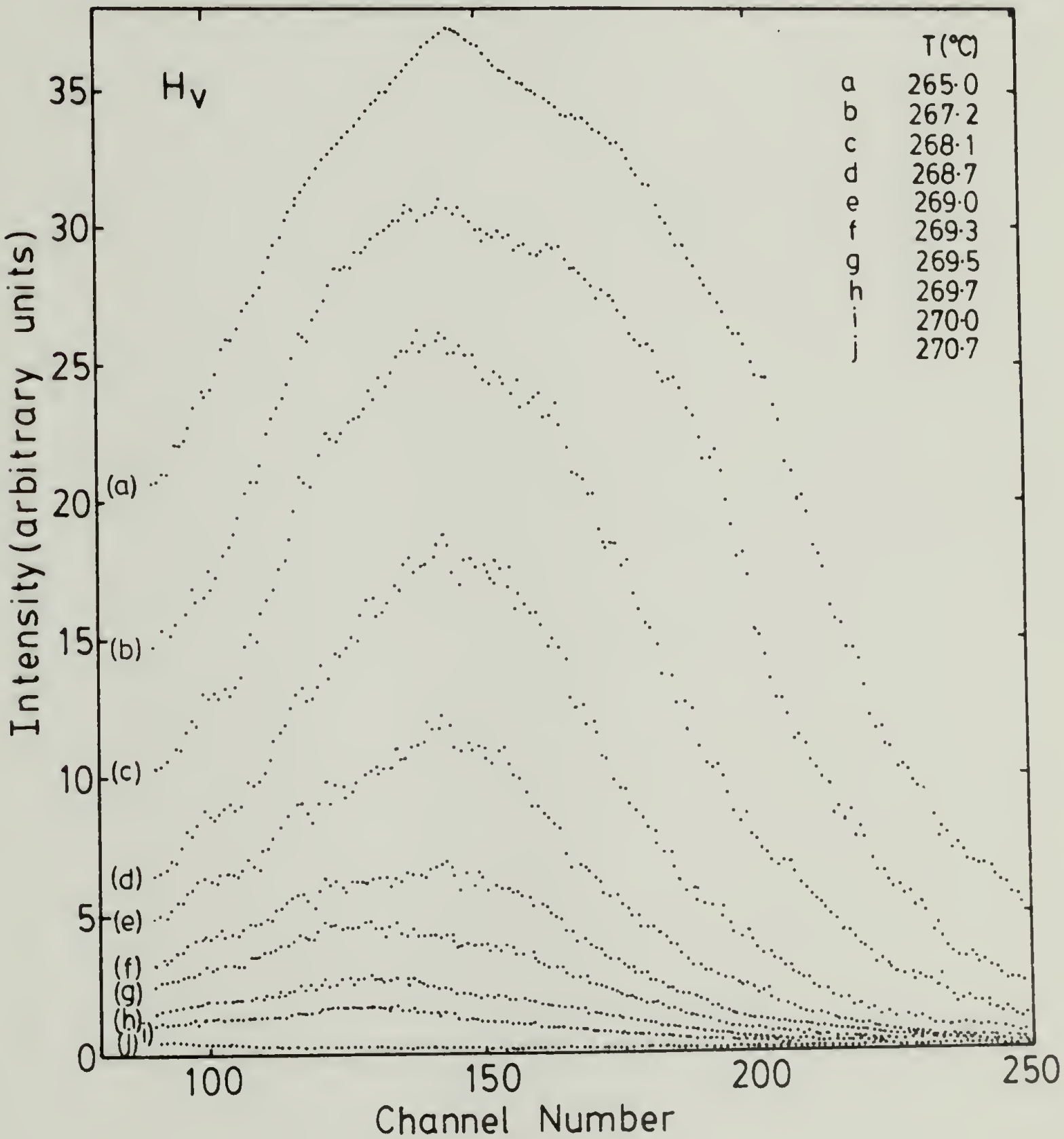

Fig.10

Magnitude of H_V Scattering Peak as a function of Temperature

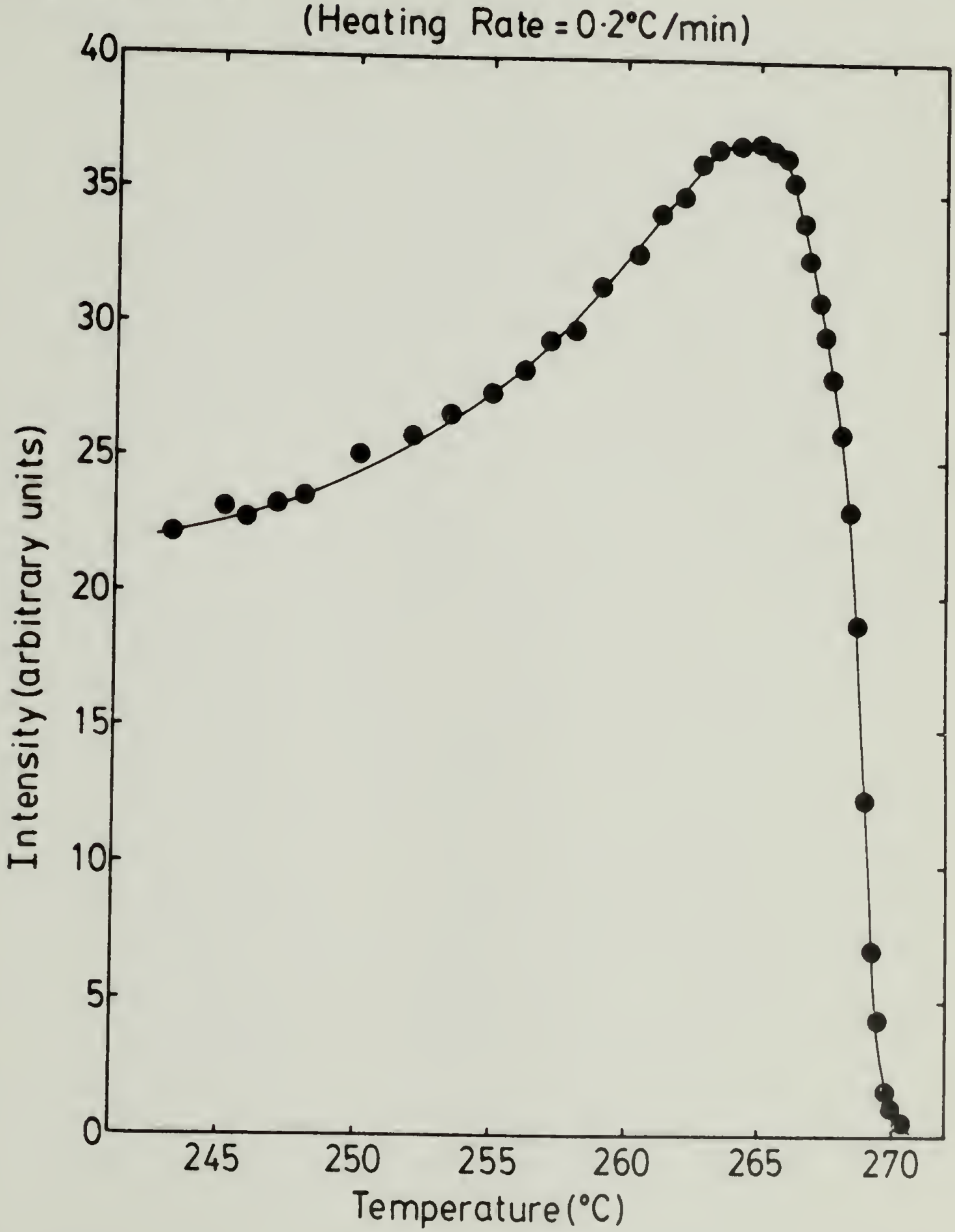

Fig.11

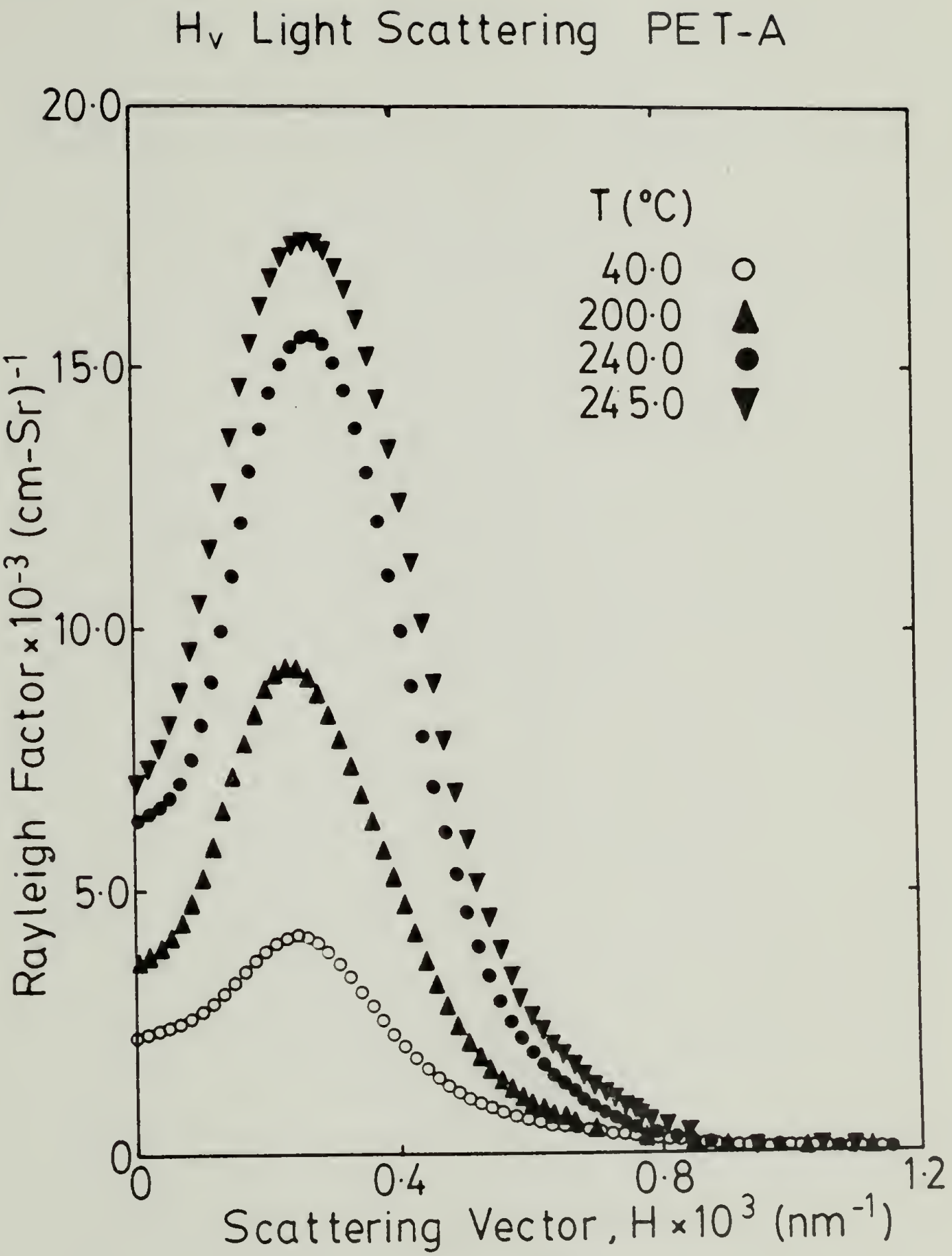
Hv Light Scattering PET-A
20·0
15·0
10·0
5·0
0
Rayleigh Factor ×10-3 (cm-Sr)-1
T (°C)
40·0
200·0
240·0
245·0
0
0·4
0·8
1·2
Scattering Vector, H ×10³ (nm⁻¹)

Fig.12

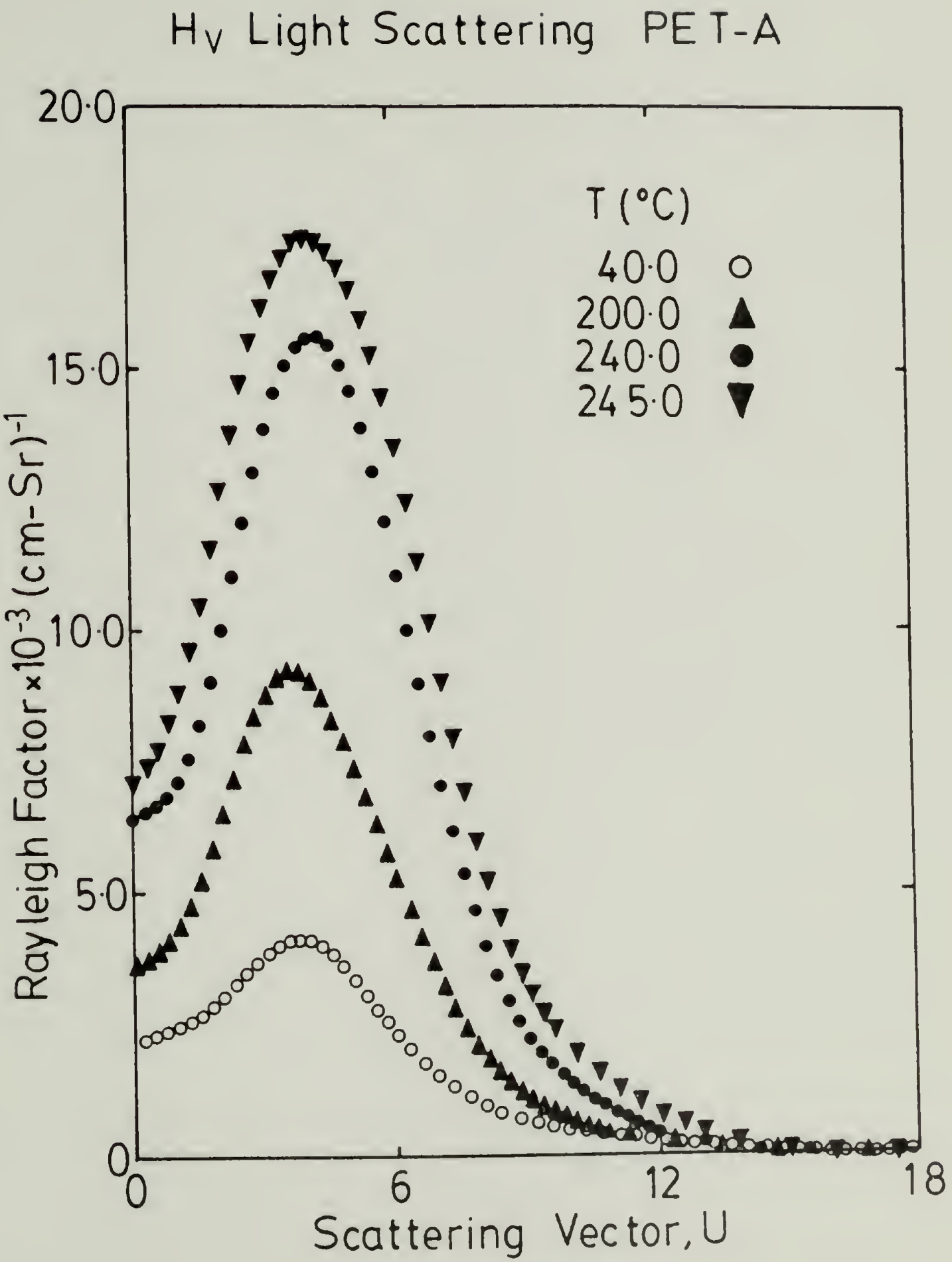
Hv Light Scattering PET-A
T (°C)
40·0
200·0
240·0
245·0
20·0
15·0
10·0
5·0
0
Rayleigh Factor ×10-3 (cm-Sr)-1
0
6
12
18
Scattering Vector, U

Fig.13

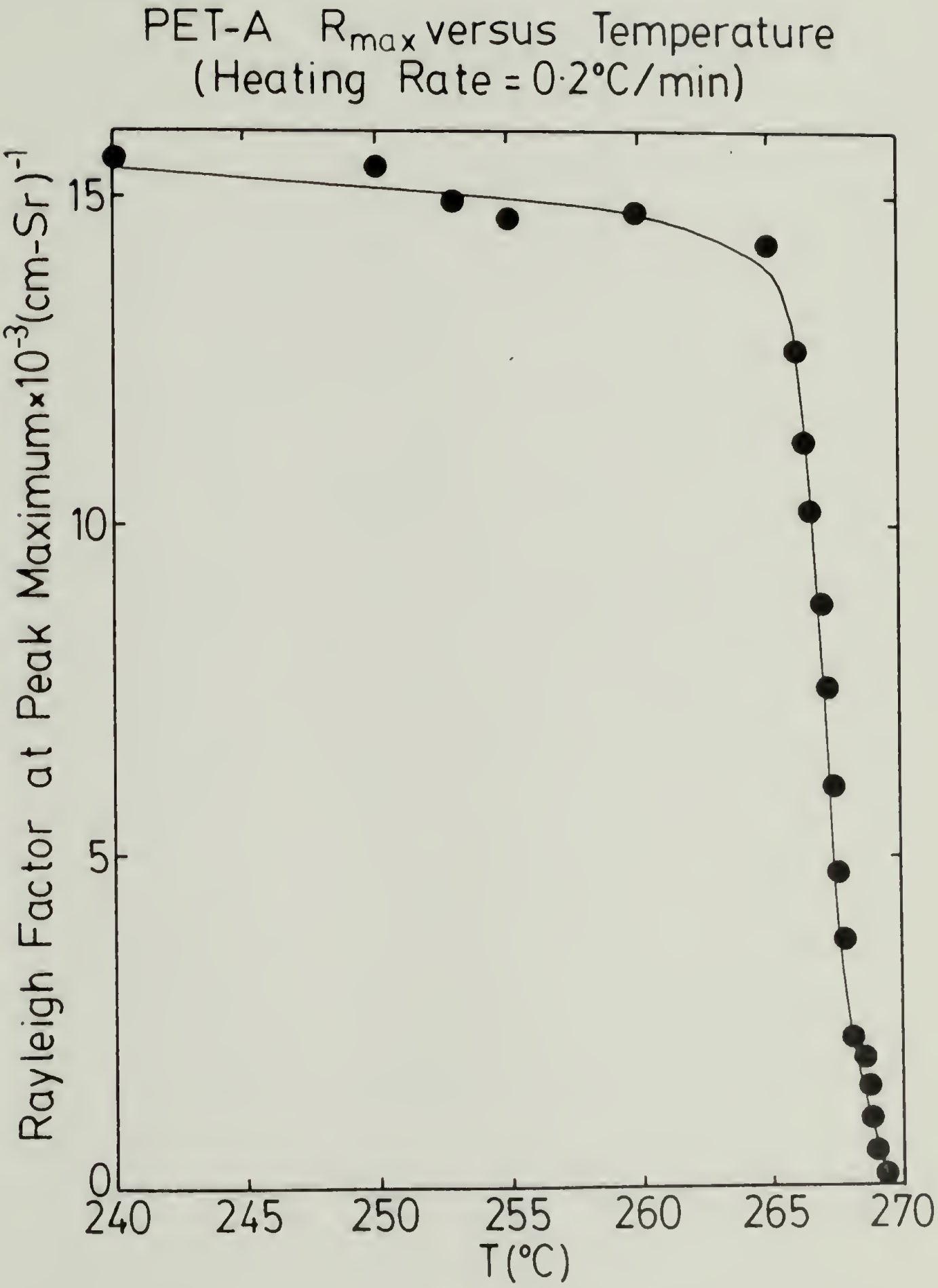
PET-A R_{max} versus Temperature
(Heating Rate = 0·2°C/min)
Rayleigh Factor at Peak Maximum ×10⁻³(cm-Sr)⁻¹
15
10
5
0
240
245
250
255
260
265
270
T(°C)

Fig.14

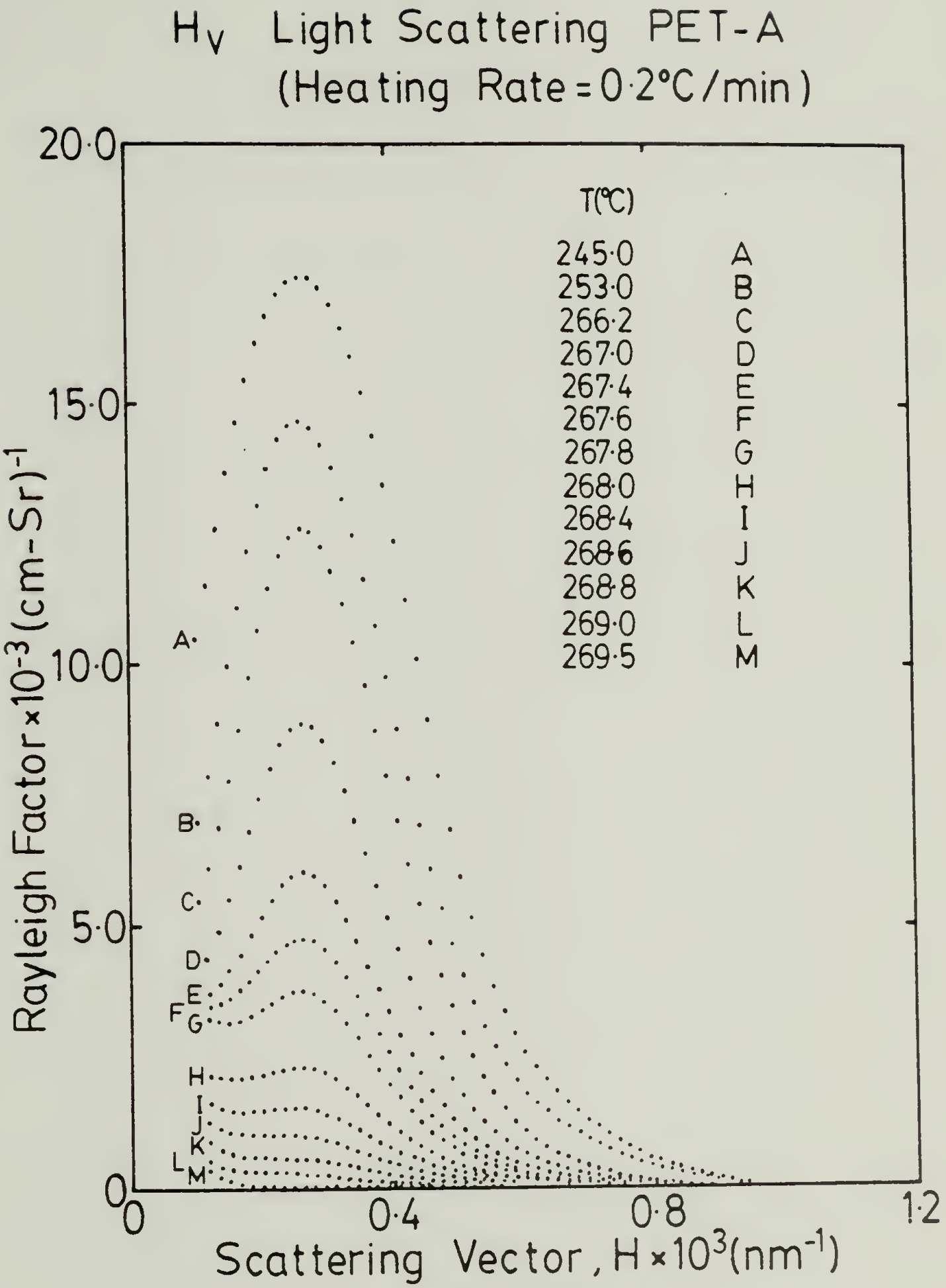
H_V Light Scattering PET-A
(Heating Rate = 0·2°C/min)
T(°C)
245·0 A
253·0 B
266·2 C
267·0 D
267·4 E
267·6 F
267·8 G
268·0 H
268·4 I
268·6 J
268·8 K
269·0 L
269·5 M
Rayleigh Factor ×10⁻³ (cm-Sr)⁻¹
20·0
15·0
10·0
5·0
0
0·4
0·8
1·2
Scattering Vector, H ×10³(nm⁻¹)

Fig.15

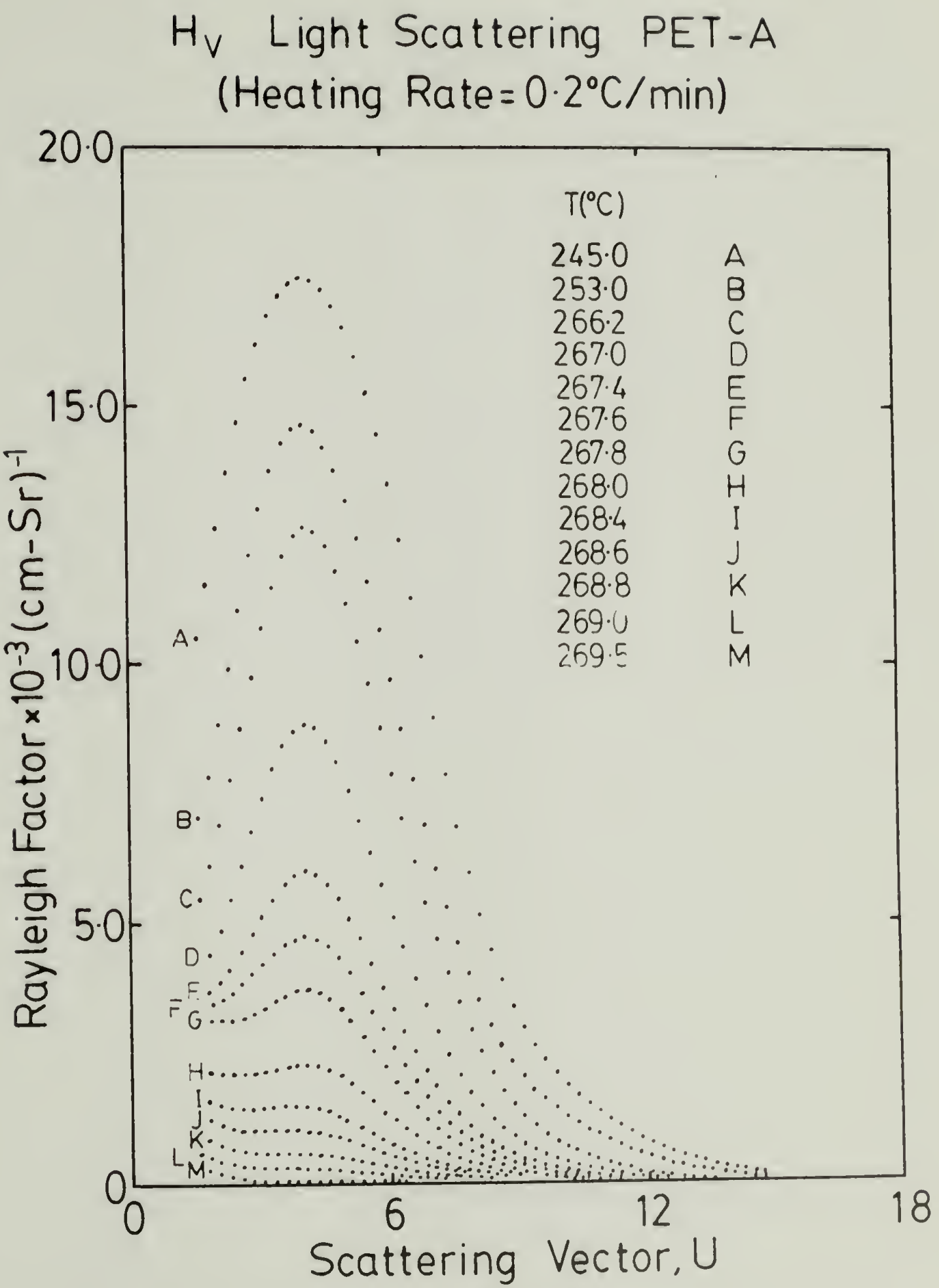
H_V Light Scattering PET-A
(Heating Rate = 0·2°C/min)
T(°C)
245·0 A
253·0 B
266·2 C
267·0 D
267·4 E
267·6 F
267·8 G
268·0 H
268·4 I
268·6 J
268·8 K
269·0 L
269·5 M
Rayleigh Factor ×10⁻³ (cm-Sr)⁻¹
20·0
15·0
10·0
5·0
0
0
6
12
18
Scattering Vector, U

Fig.16

PET-A R_S versus Temperature
(Heating Rate = 0·2°C/min)

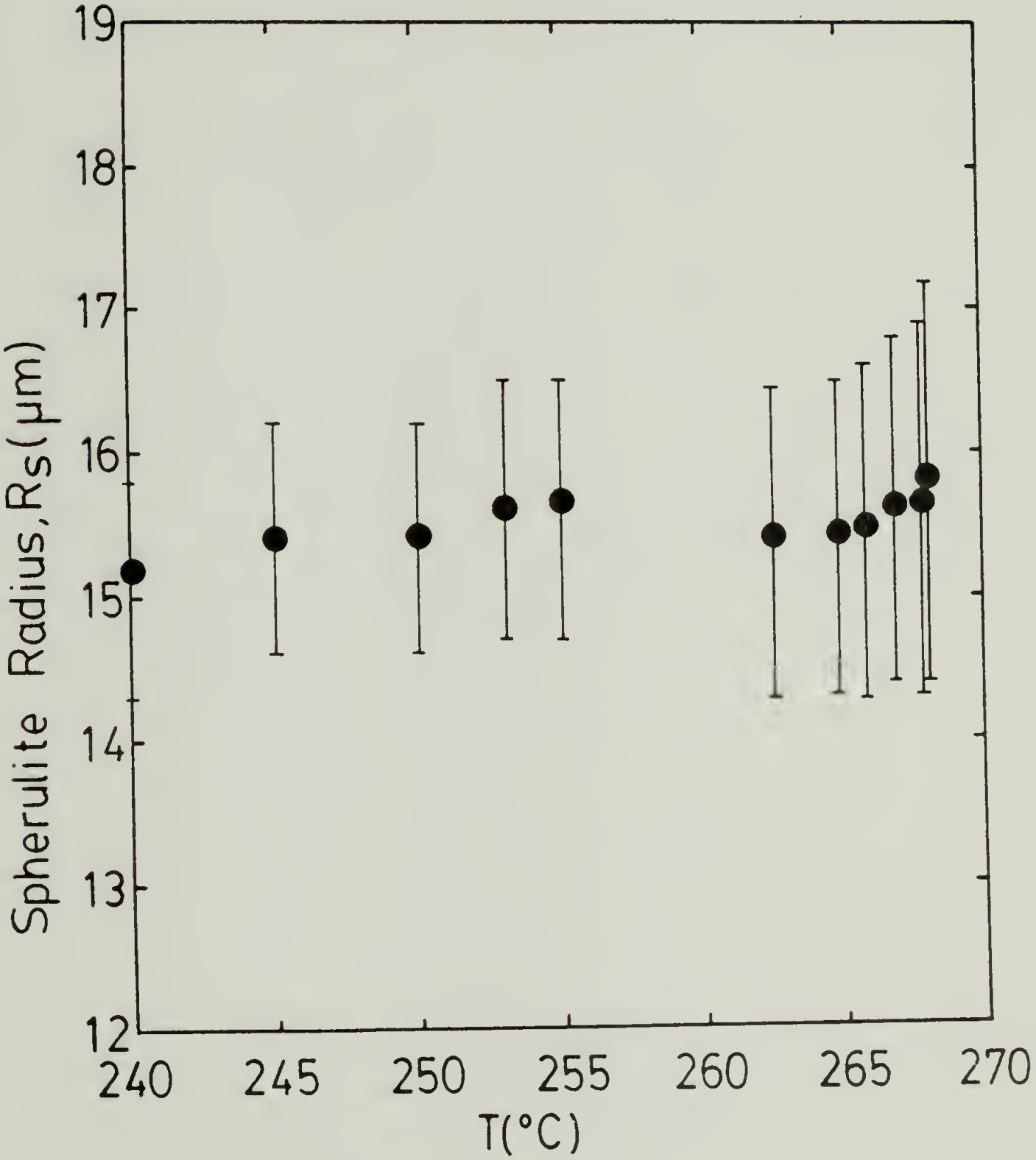

Fig.17

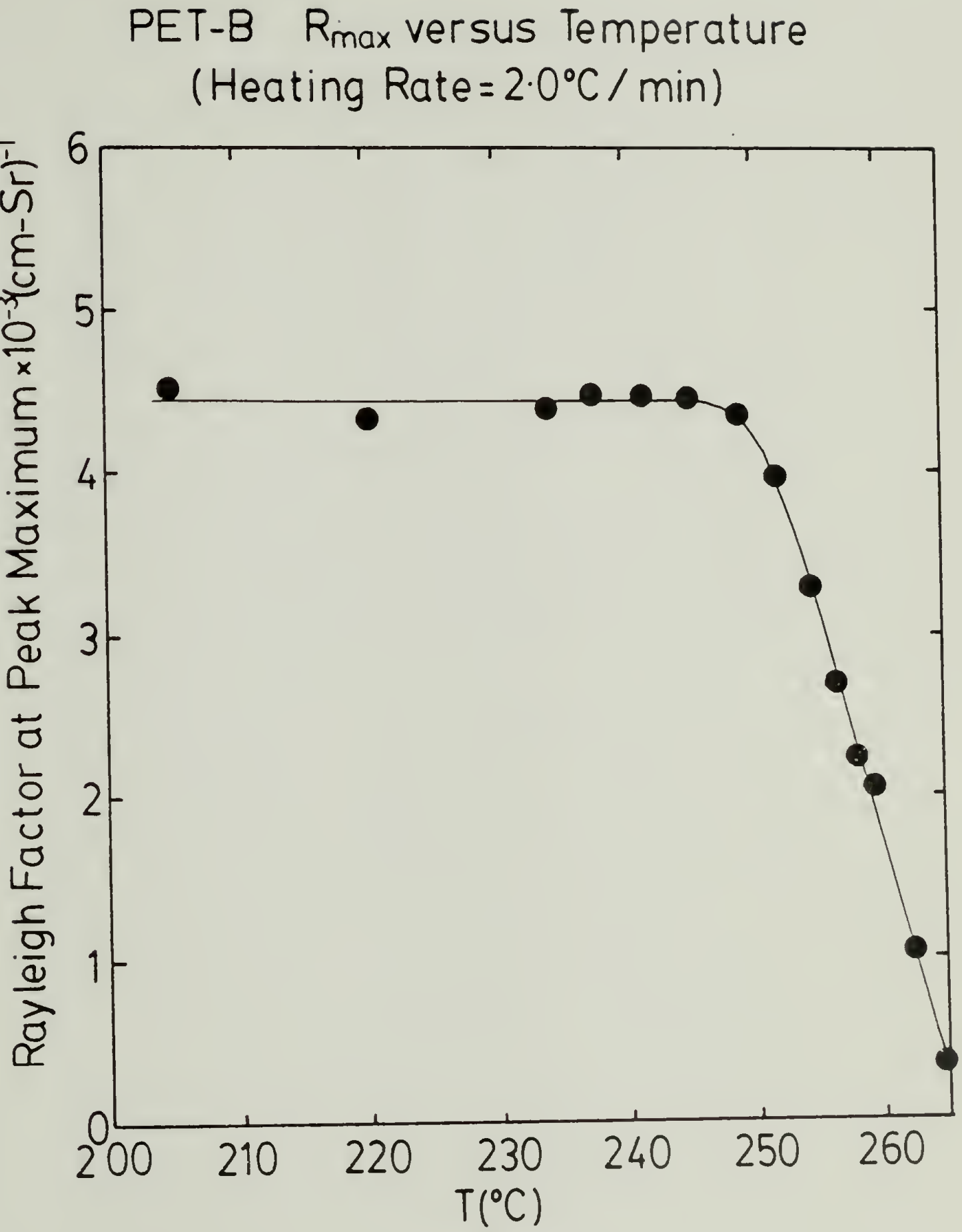
PET-B R_{max} versus Temperature
(Heating Rate = 2·0°C / min)
Rayleigh Factor at Peak Maximum ×10⁻³(cm-Sr)⁻¹
0
1
2
3
4
5
6
200
210
220
230
240
250
260
T(°C)

Fig.18

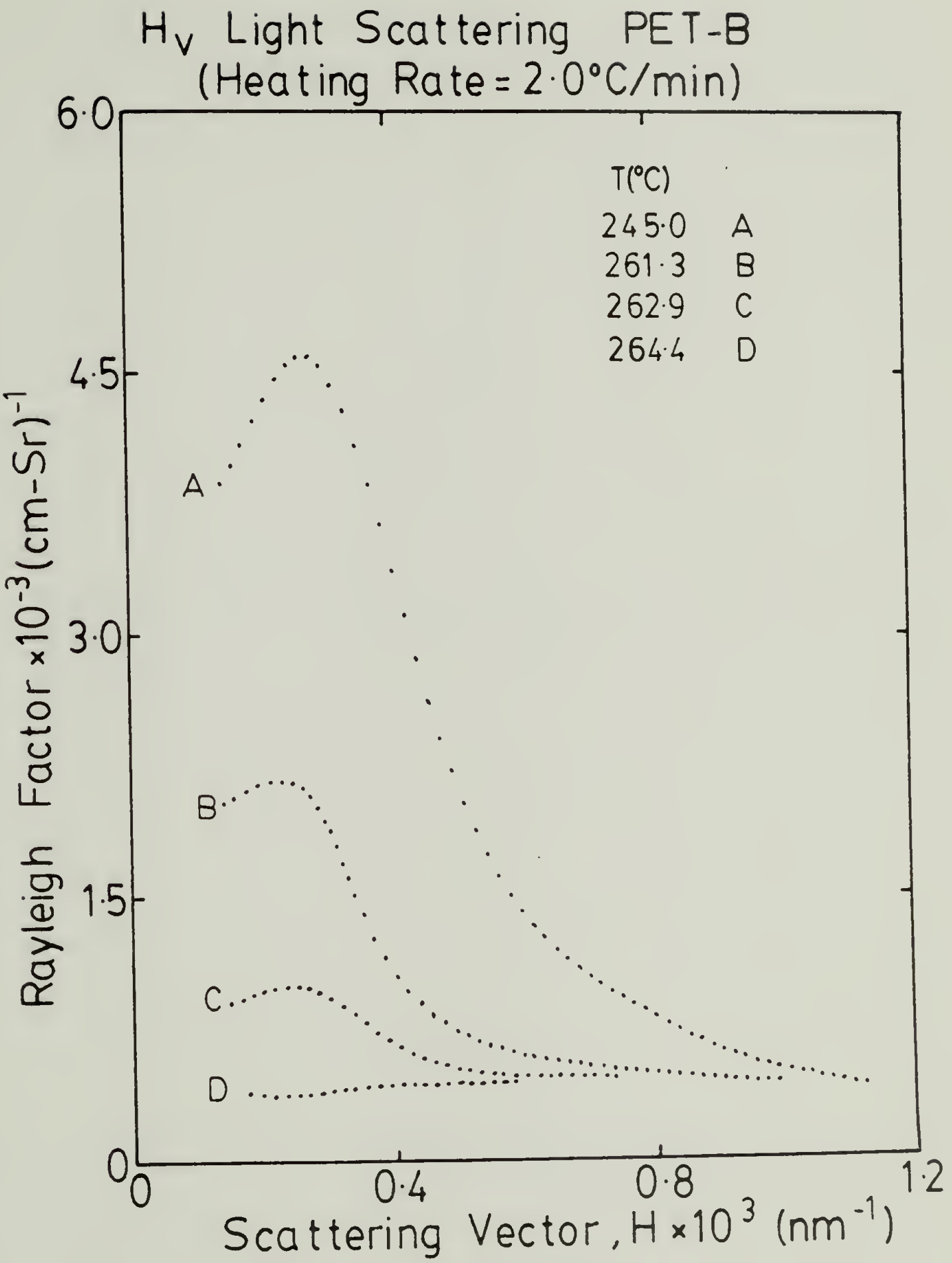
H_v Light Scattering PET-B
(Heating Rate = 2·0°C/min)
T(°C)
245·0 A
261·3 B
262·9 C
264·4 D
A
B
C
D
6·0
4·5
3·0
1·5
0
0
0·4
0·8
1·2
Rayleigh Factor ×10⁻³(cm-Sr)⁻¹
Scattering Vector, H ×10³ (nm⁻¹)

Fig.19

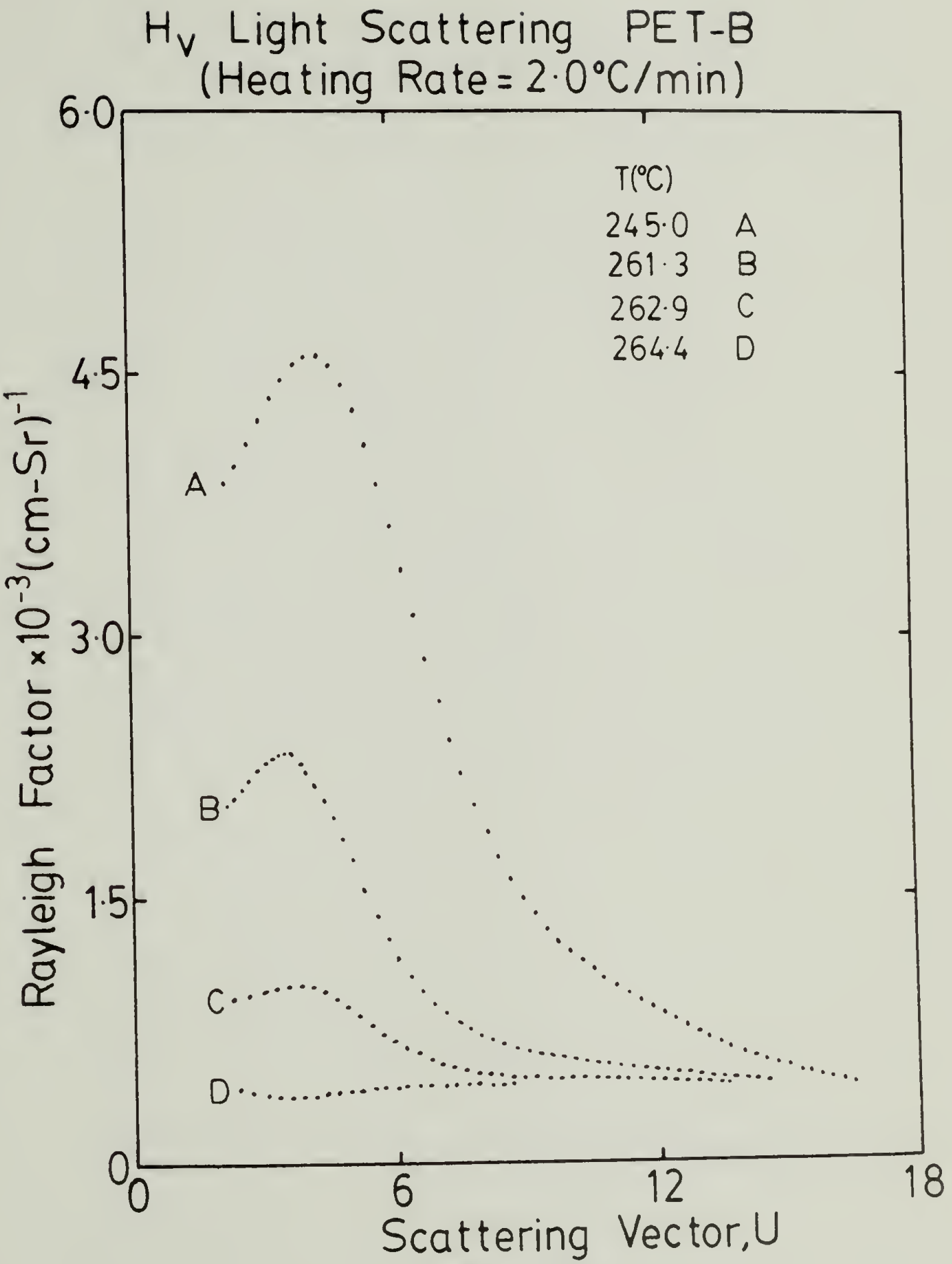
H_v Light Scattering PET-B
(Heating Rate = 2·0°C/min)
T(°C)
245·0 A
261·3 B
262·9 C
264·4 D
A
B
C
D
6·0
4·5
3·0
1·5
0
0
6
12
18
Rayleigh Factor ×10⁻³(cm-Sr)⁻¹
Scattering Vector, U

Fig. 20

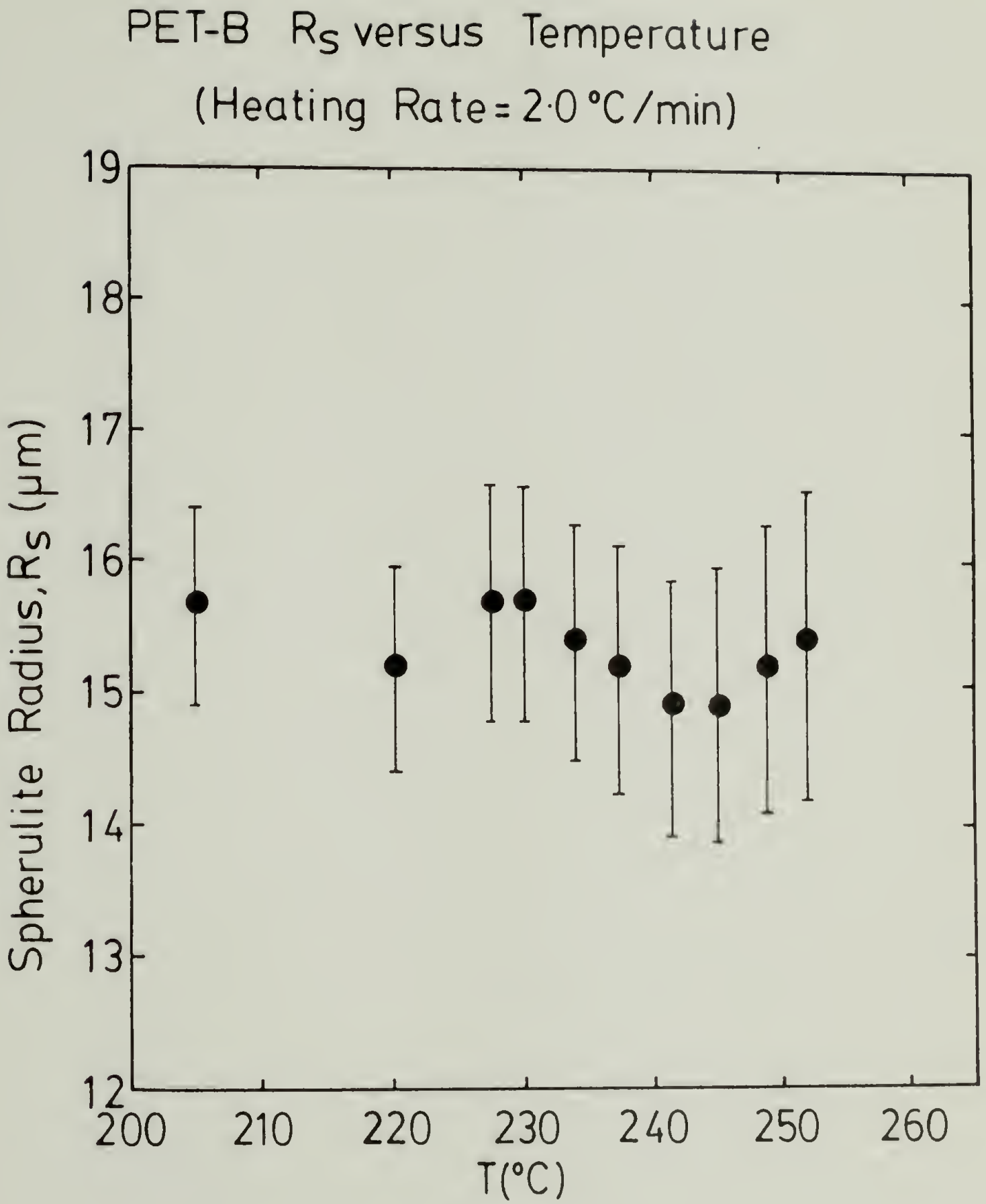
PET-B R_S versus Temperature
(Heating Rate = 2·0 °C/min)
Spherulite Radius, R_S (μm)
19
18
17
16
15
14
13
12
200
210
220
230
240
250
260
T(°C)

Fig. 21

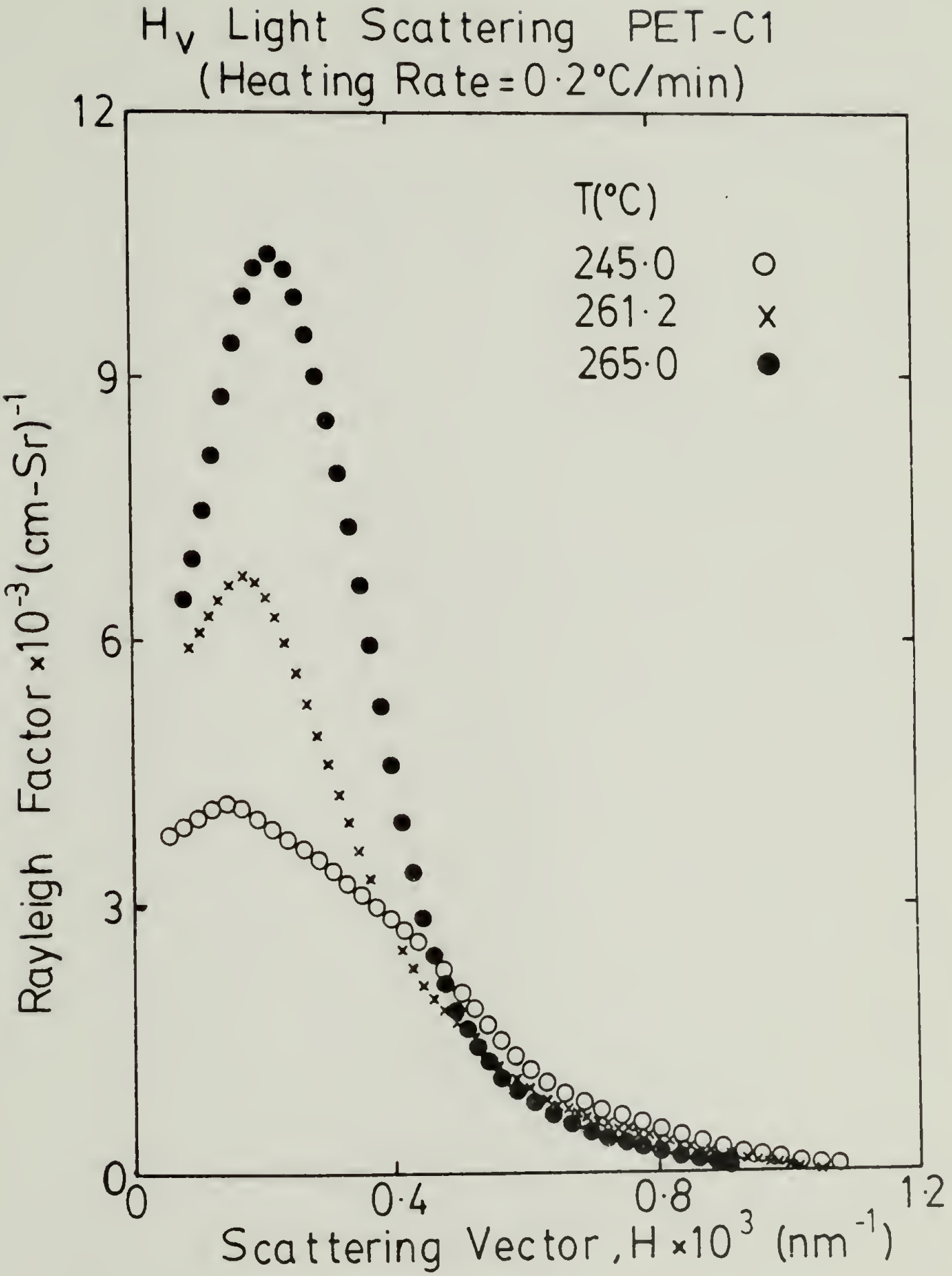
H_v Light Scattering PET-C1
(Heating Rate = 0·2°C/min)
T(°C)
245·0
261·2
265·0
Rayleigh Factor ×10⁻³ (cm-Sr)⁻¹
12
9
6
3
0
0
0·4
0·8
1·2
Scattering Vector, H ×10³ (nm⁻¹)

Fig. 22

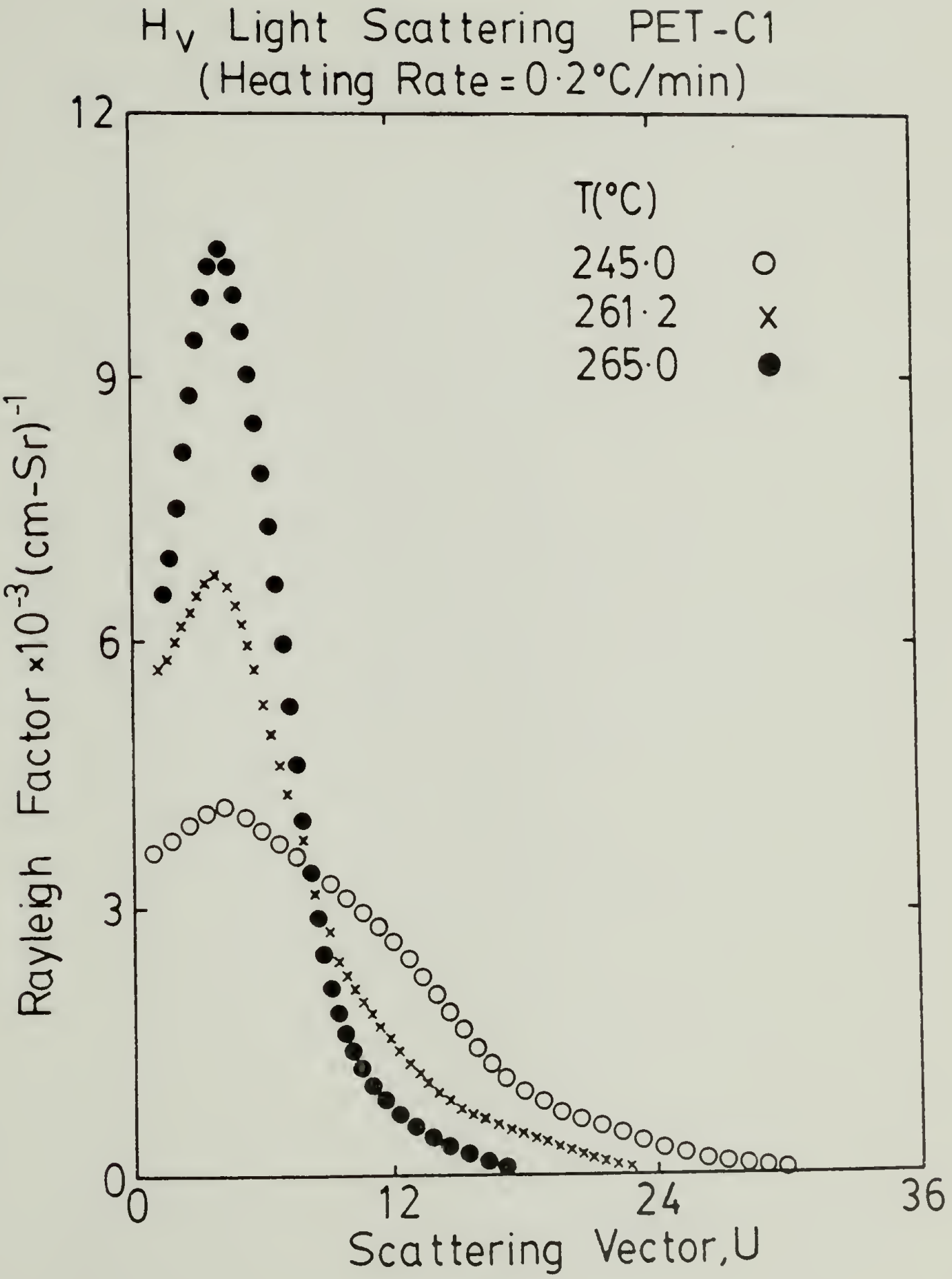
H_v Light Scattering PET-C1
(Heating Rate = 0·2°C/min)
T(°C)
245·0
261·2
265·0
Rayleigh Factor ×10⁻³(cm-Sr)⁻¹
12
9
6
3
0
0
12
24
36
Scattering Vector, U

Fig.23

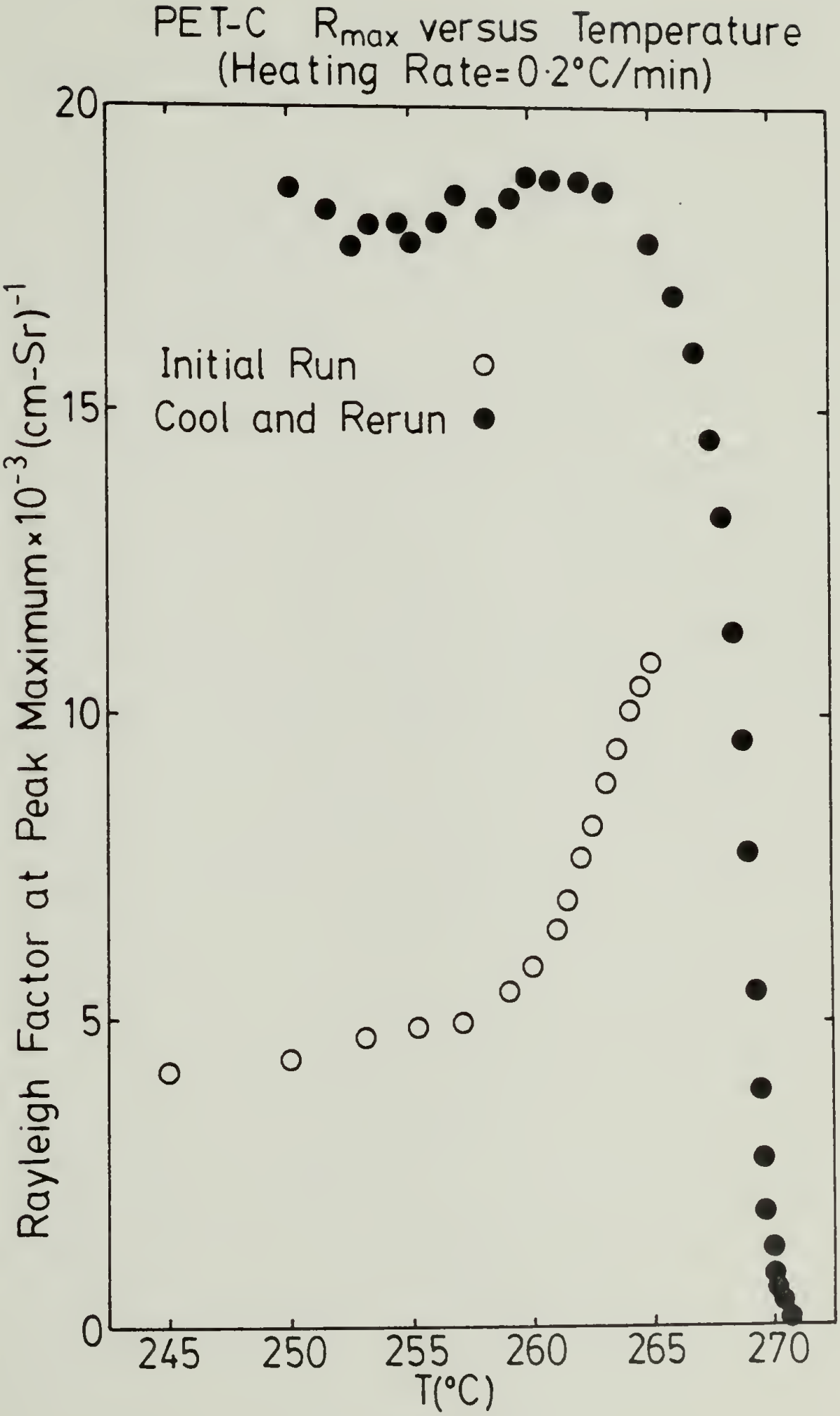
PET-C R_{max} versus Temperature
(Heating Rate=0·2°C/min)
Initial Run
Cool and Rerun
Rayleigh Factor at Peak Maximum $\times 10^{-3}$ (cm-Sr)$^{-1}$
20
15
10
5
0
245
250
255
260
265
270
T(°C)

Fig. 24

PET-C R_s versus Temperature
(Heating Rate = 0·2°C/min)

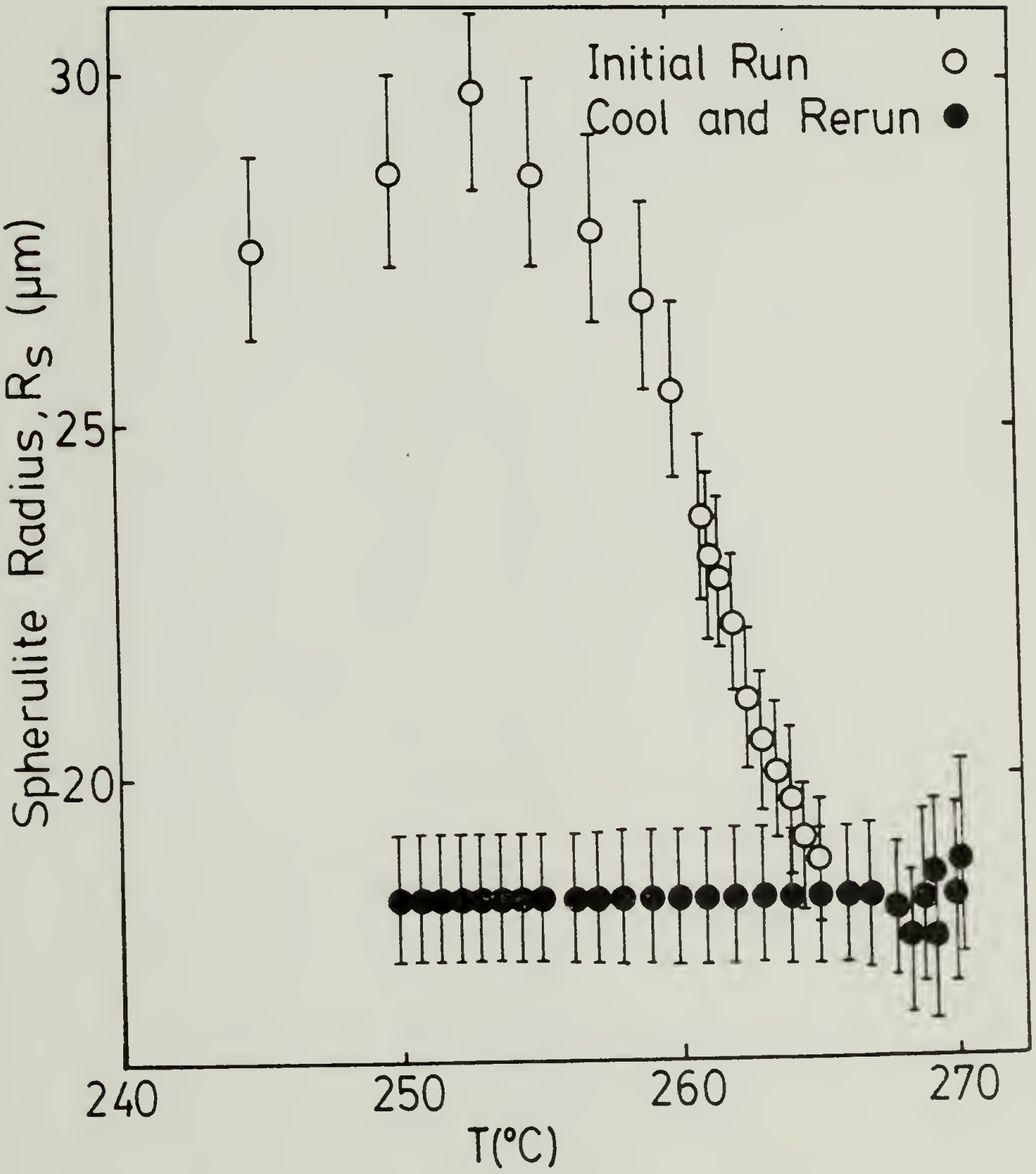

Fig. 25

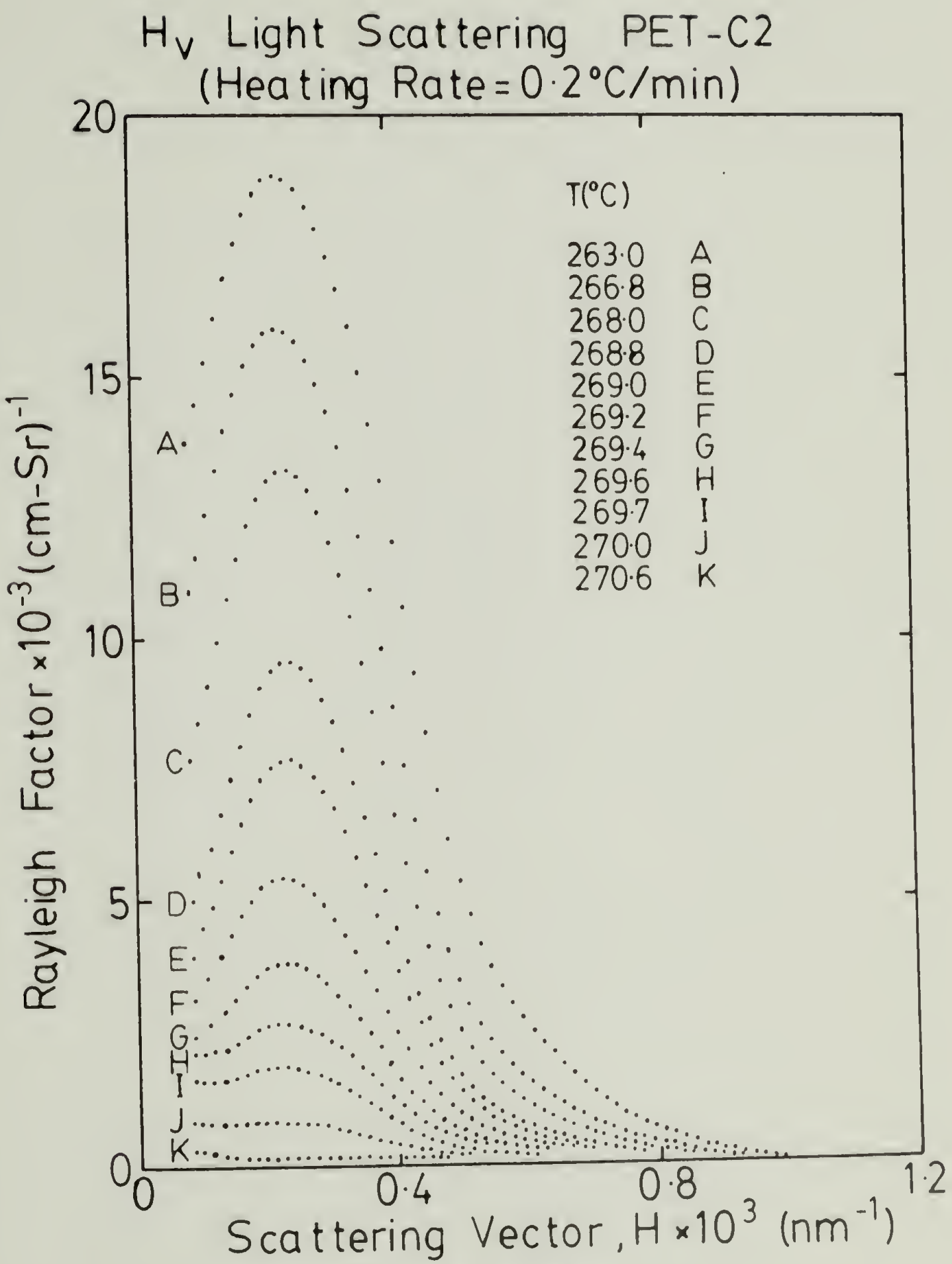
H_v Light Scattering PET-C2
(Heating Rate = 0·2°C/min)
T(°C)
263·0 A
266·8 B
268·0 C
268·8 D
269·0 E
269·2 F
269·4 G
269·6 H
269·7 I
270·0 J
270·6 K
Rayleigh Factor ×10⁻³(cm-Sr)⁻¹
Scattering Vector, H ×10³ (nm⁻¹)
0
5
10
15
20
0·4
0·8
1·2

Fig. 26

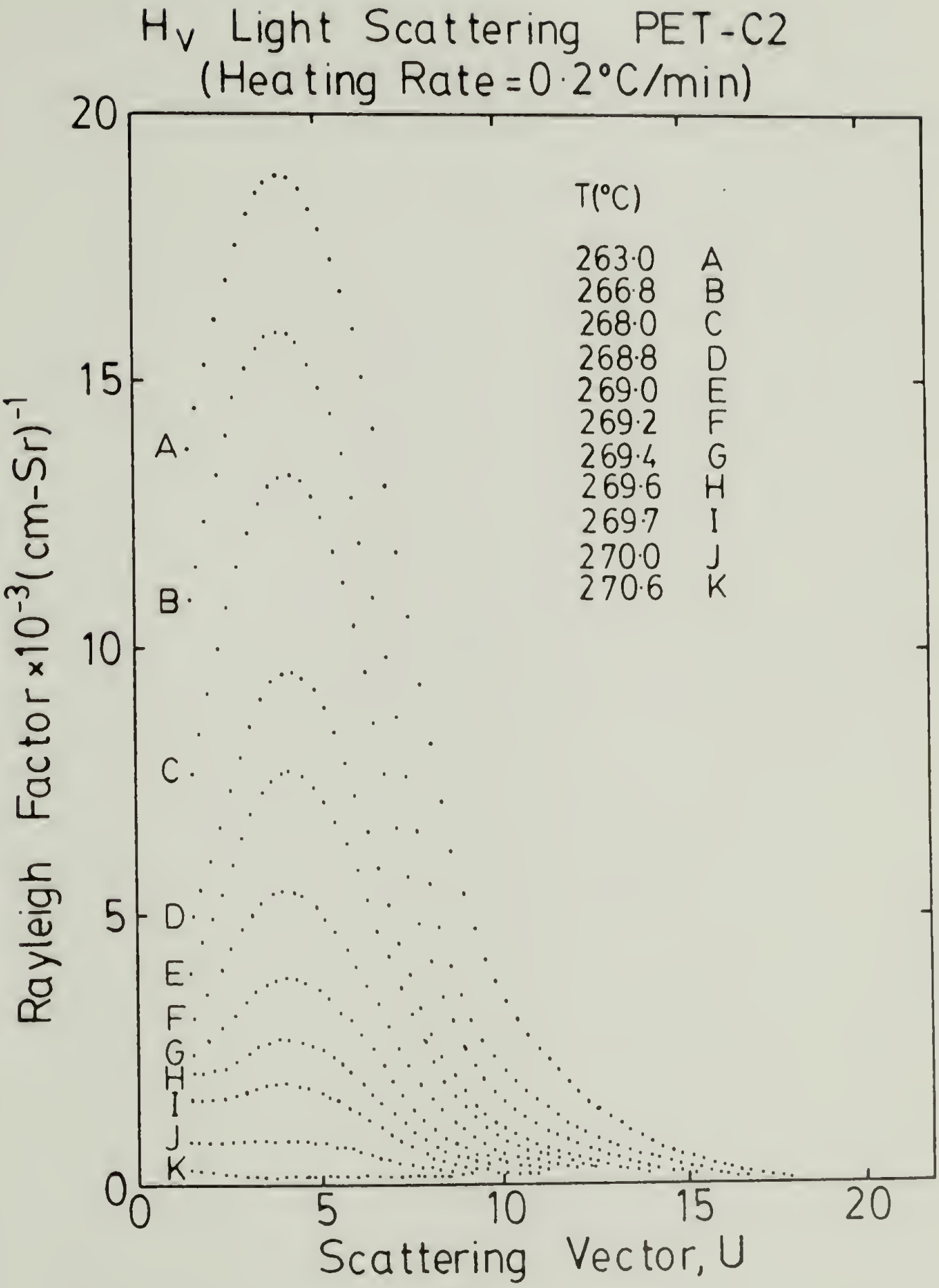
Hv Light Scattering PET-C2
(Heating Rate=0·2°C/min)
T(°C)
263·0 A
266·8 B
268·0 C
268·8 D
269·0 E
269·2 F
269·4 G
269·6 H
269·7 I
270·0 J
270·6 K
Rayleigh Factor ×10⁻³(cm-Sr)⁻¹
Scattering Vector, U
0
5
10
15
20

Fig. 27

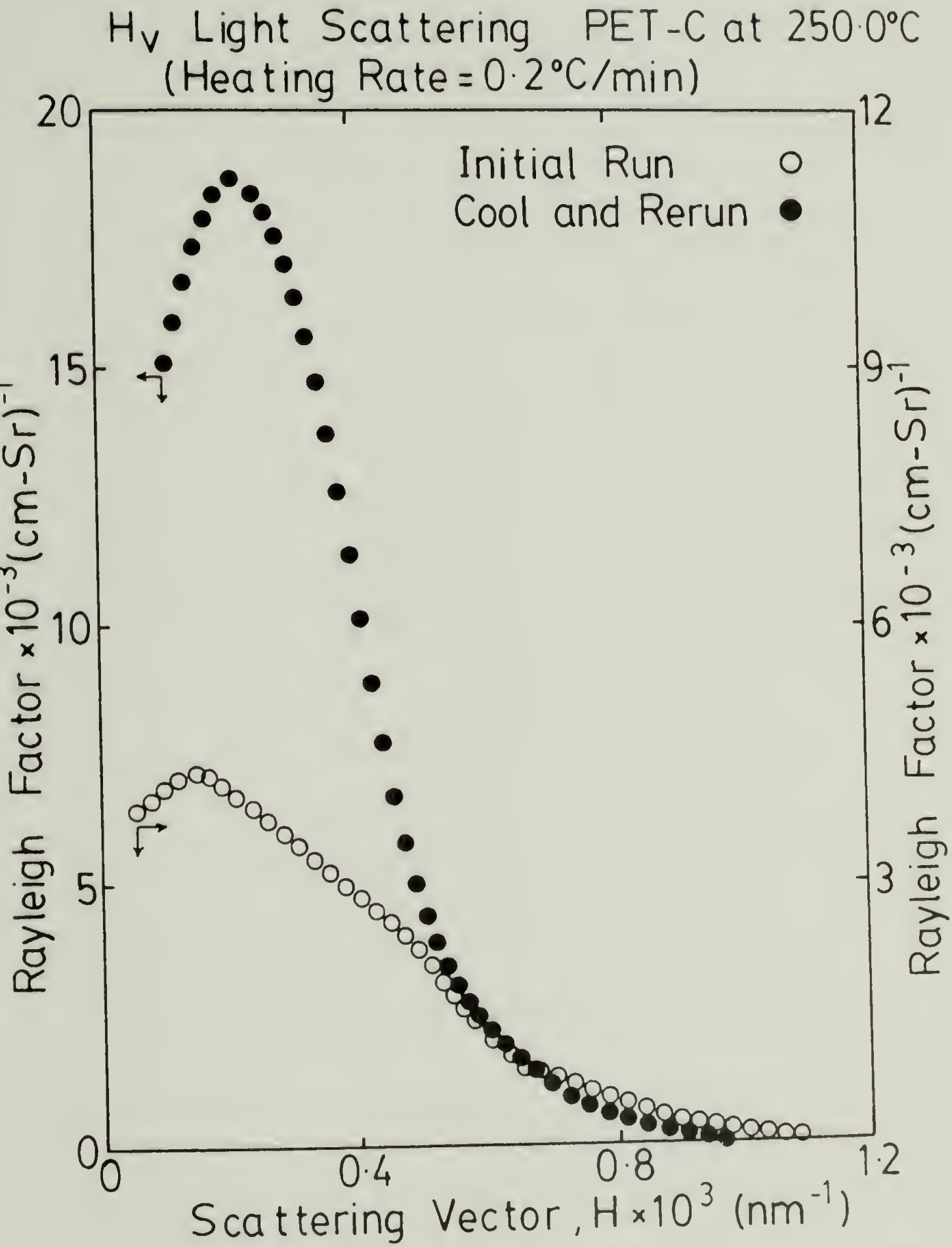
H_v Light Scattering PET-C at 250·0°C
(Heating Rate = 0·2°C/min)
Initial Run
Cool and Rerun
Rayleigh Factor ×10⁻³(cm-Sr)⁻¹
Rayleigh Factor ×10⁻³(cm-Sr)⁻¹
Scattering Vector, H ×10³ (nm⁻¹)
0
5
10
15
20
3
6
9
12
0·4
0·8
1·2

Fig. 28

Correction for Multiple Scattering

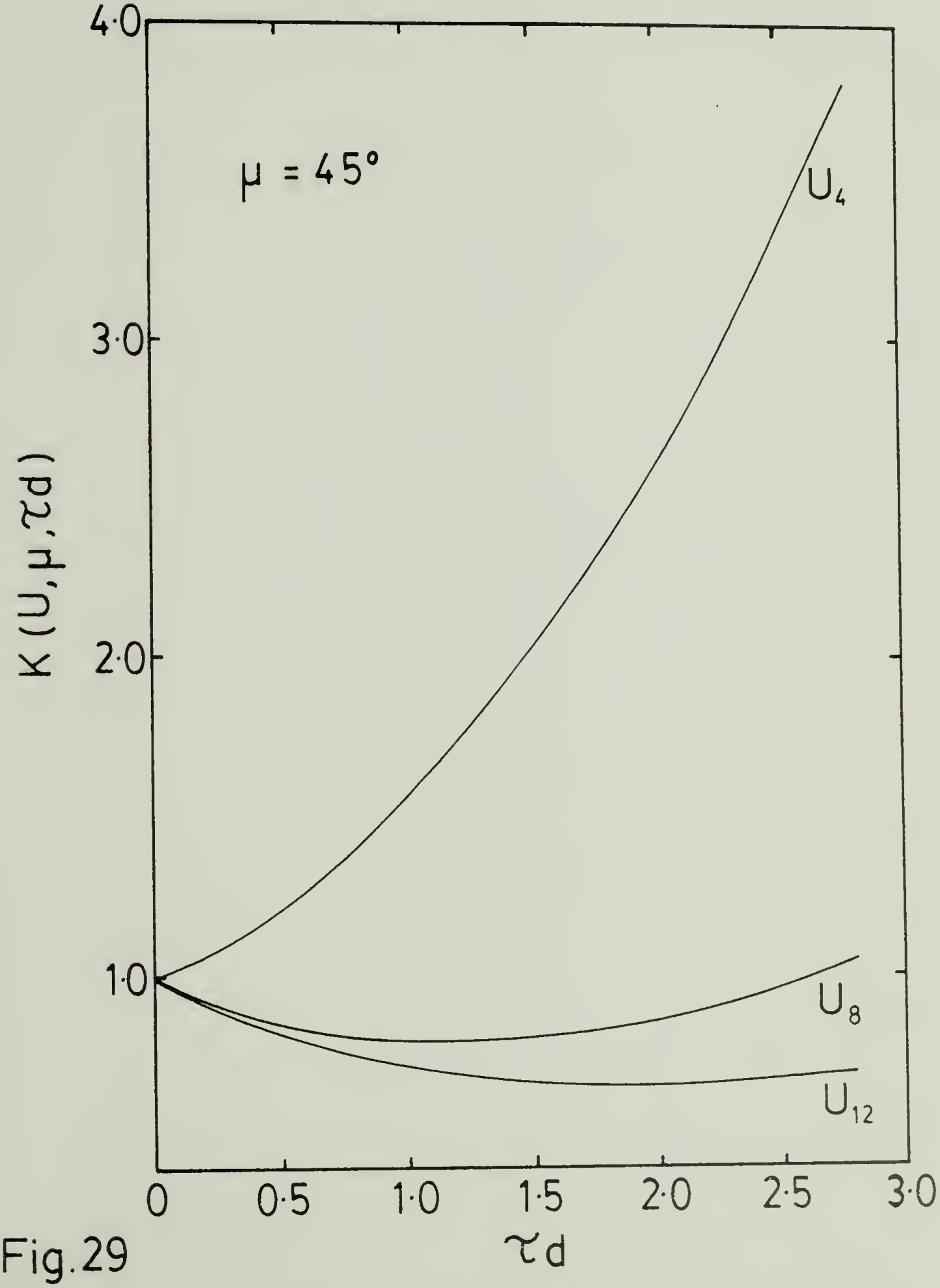

Fig.29

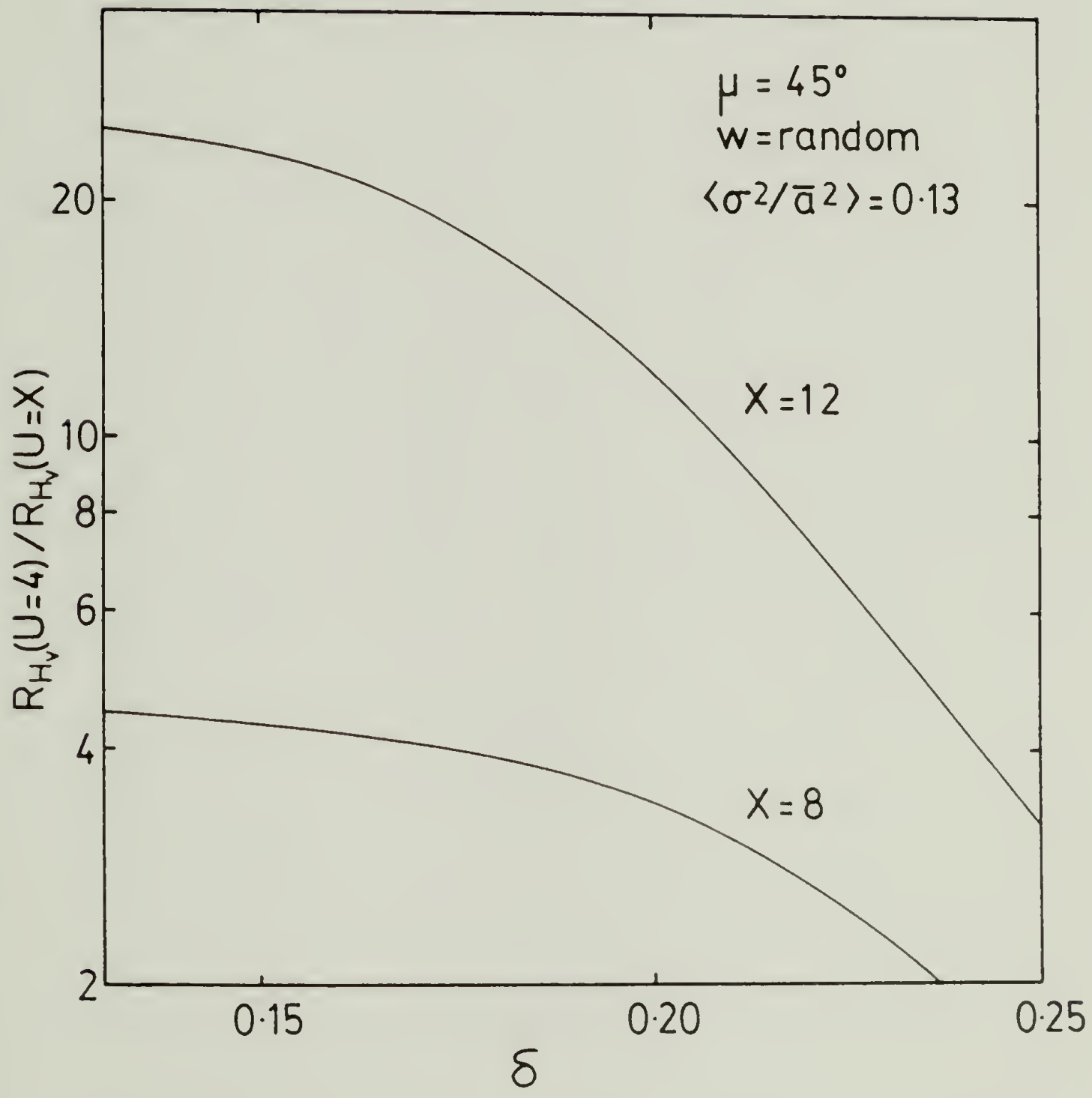
Disorder Parameter, δ
μ = 45°
w = random
⟨σ²/ā²⟩ = 0·13
X = 12
X = 8
R_Hv(U=4)/R_Hv(U=X)
20
10
8
6
4
2
0·15
0·20
0·25
δ

Fig. 30

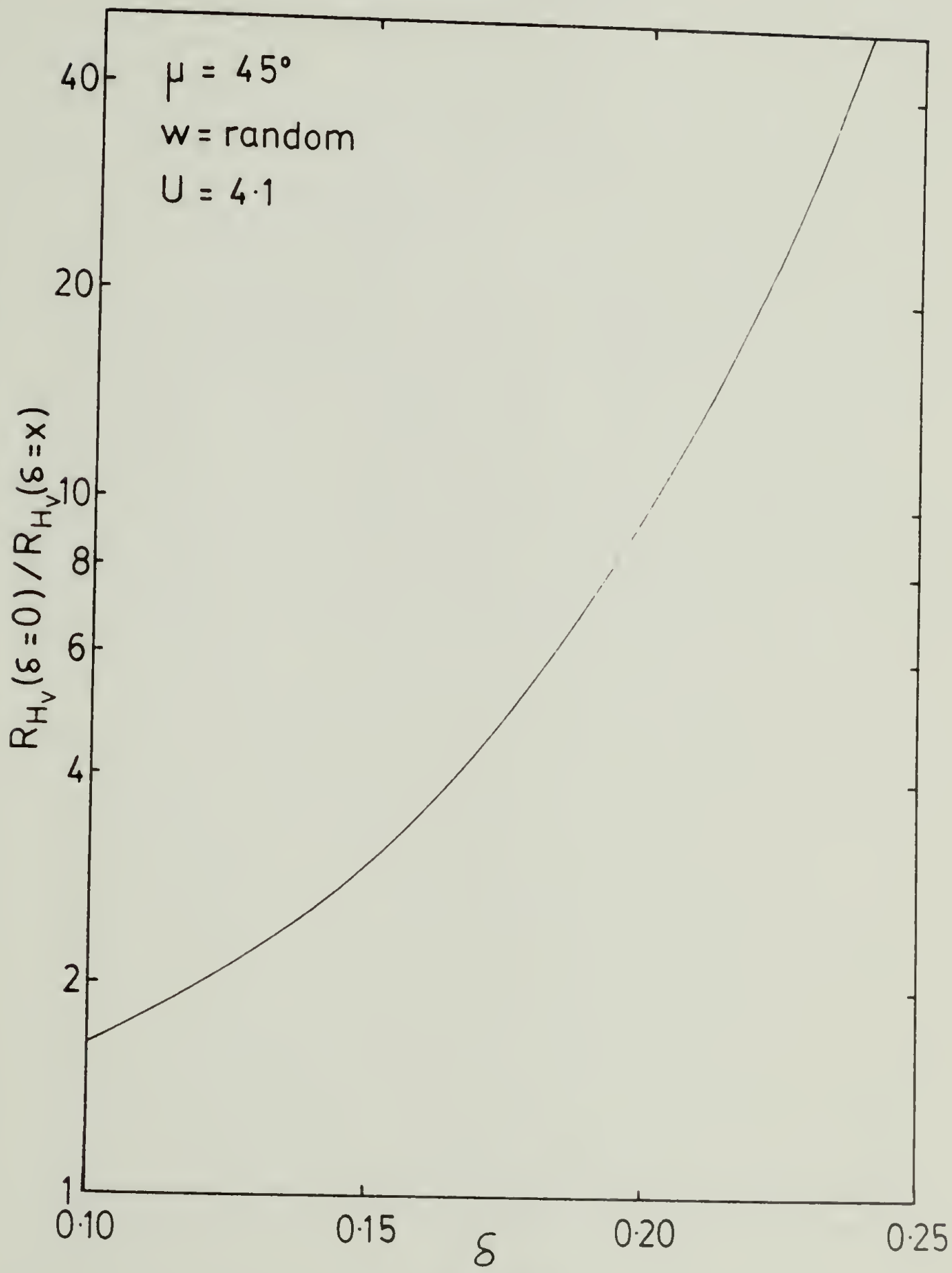
Correction for Disorder
μ = 45°
w = random
U = 4·1
40
20
10
8
6
4
2
1
$R_{H_V}(\delta=0)/R_{H_V}(\delta=x)$
0·10
0·15
0·20
0·25
δ

Fig.31

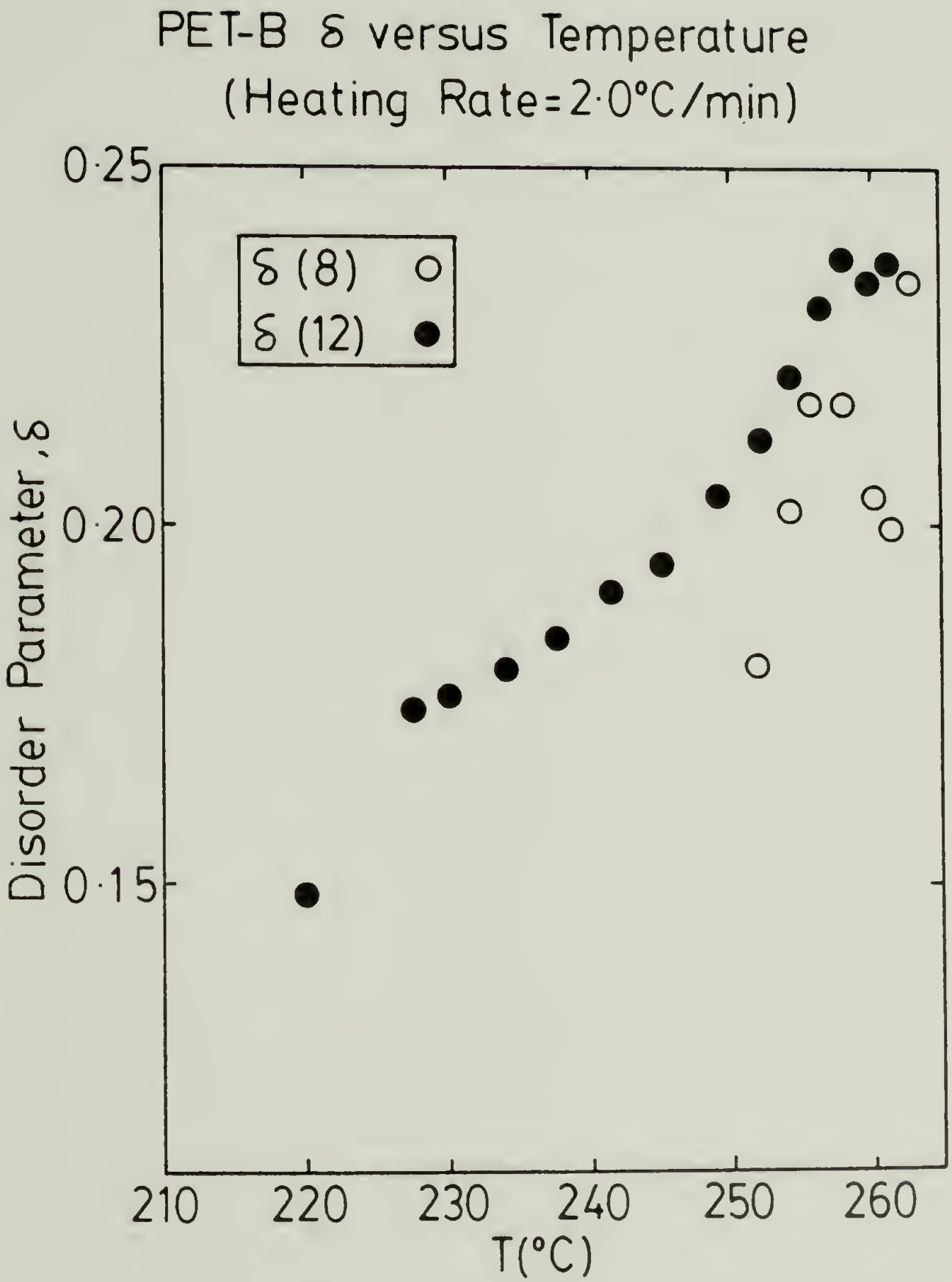
PET-B δ versus Temperature
(Heating Rate=2·0°C/min)
δ (8)
δ (12)
Disorder Parameter, δ
0·25
0·20
0·15
210
220
230
240
250
260
T(°C)

Fig.32

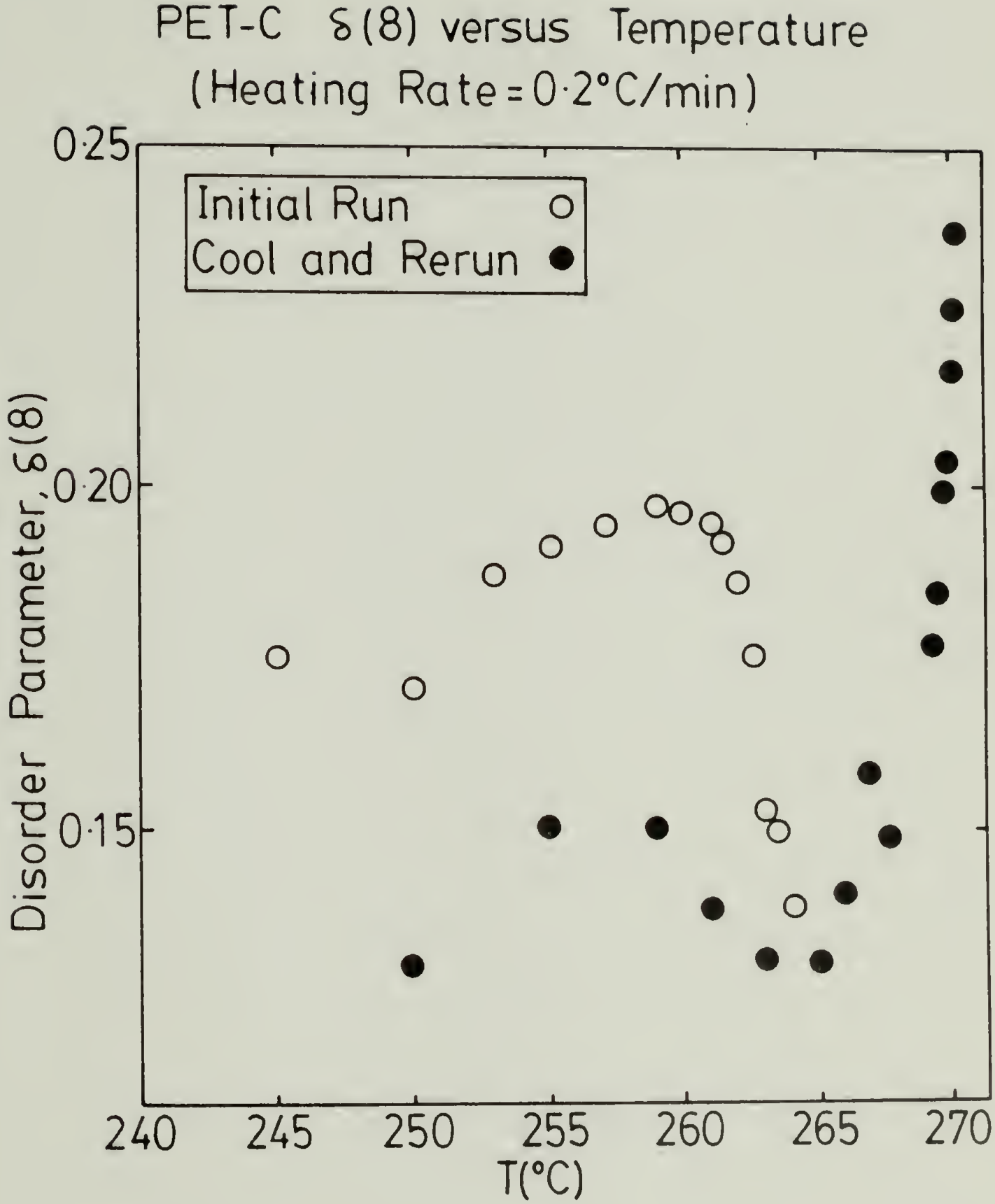
PET-C δ(8) versus Temperature
(Heating Rate = 0·2°C/min)
Initial Run
Cool and Rerun
Disorder Parameter, δ(8)
0·25
0·20
0·15
240
245
250
255
260
265
270
T(°C)

Fig. 33

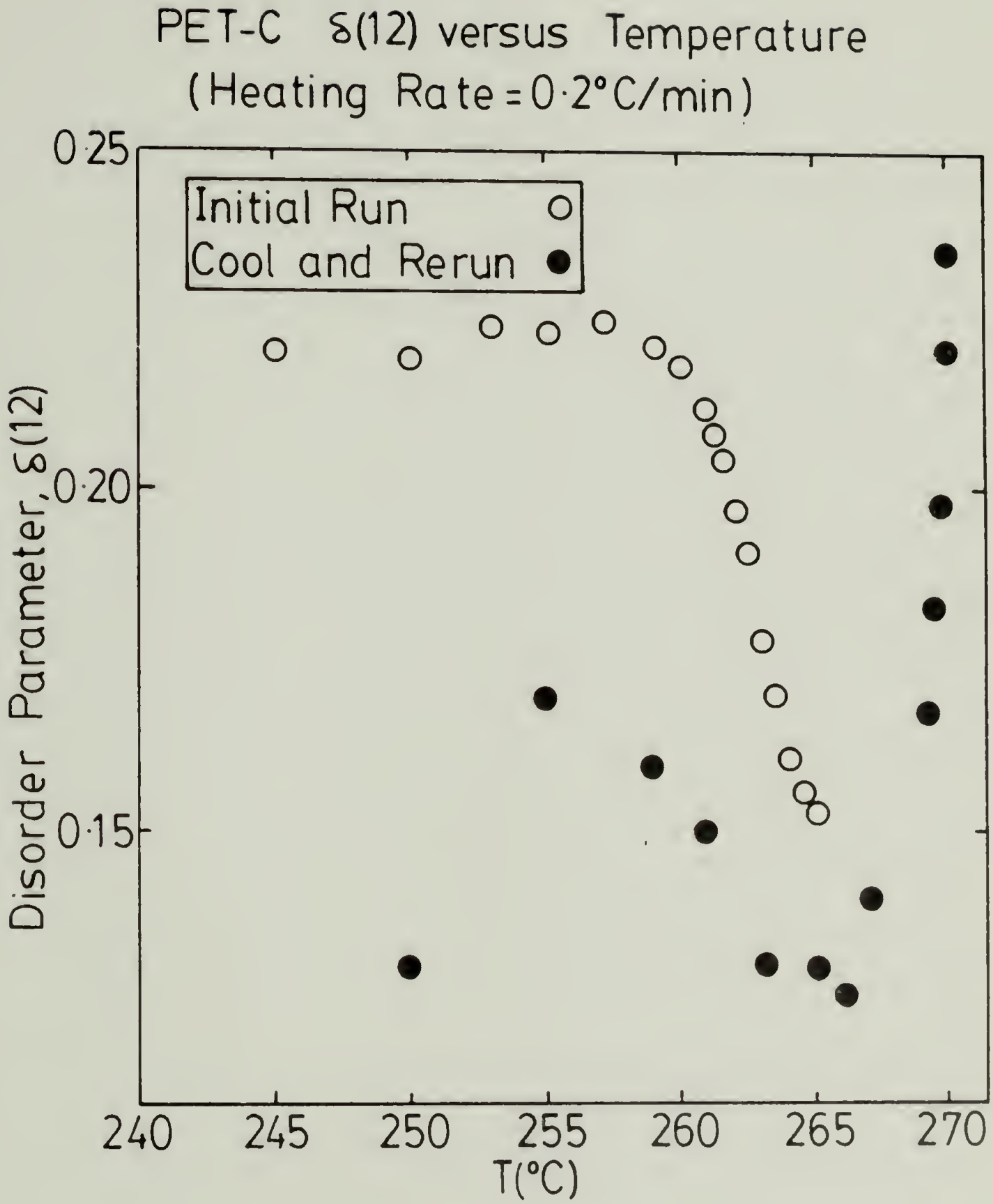
PET-C δ(12) versus Temperature
(Heating Rate = 0·2°C/min)
Initial Run
Cool and Rerun
Disorder Parameter, δ(12)
0·25
0·20
0·15
240
245
250
255
260
265
270
T(°C)

Fig. 34

$\Delta_c / \Delta_c^\circ$ versus δ

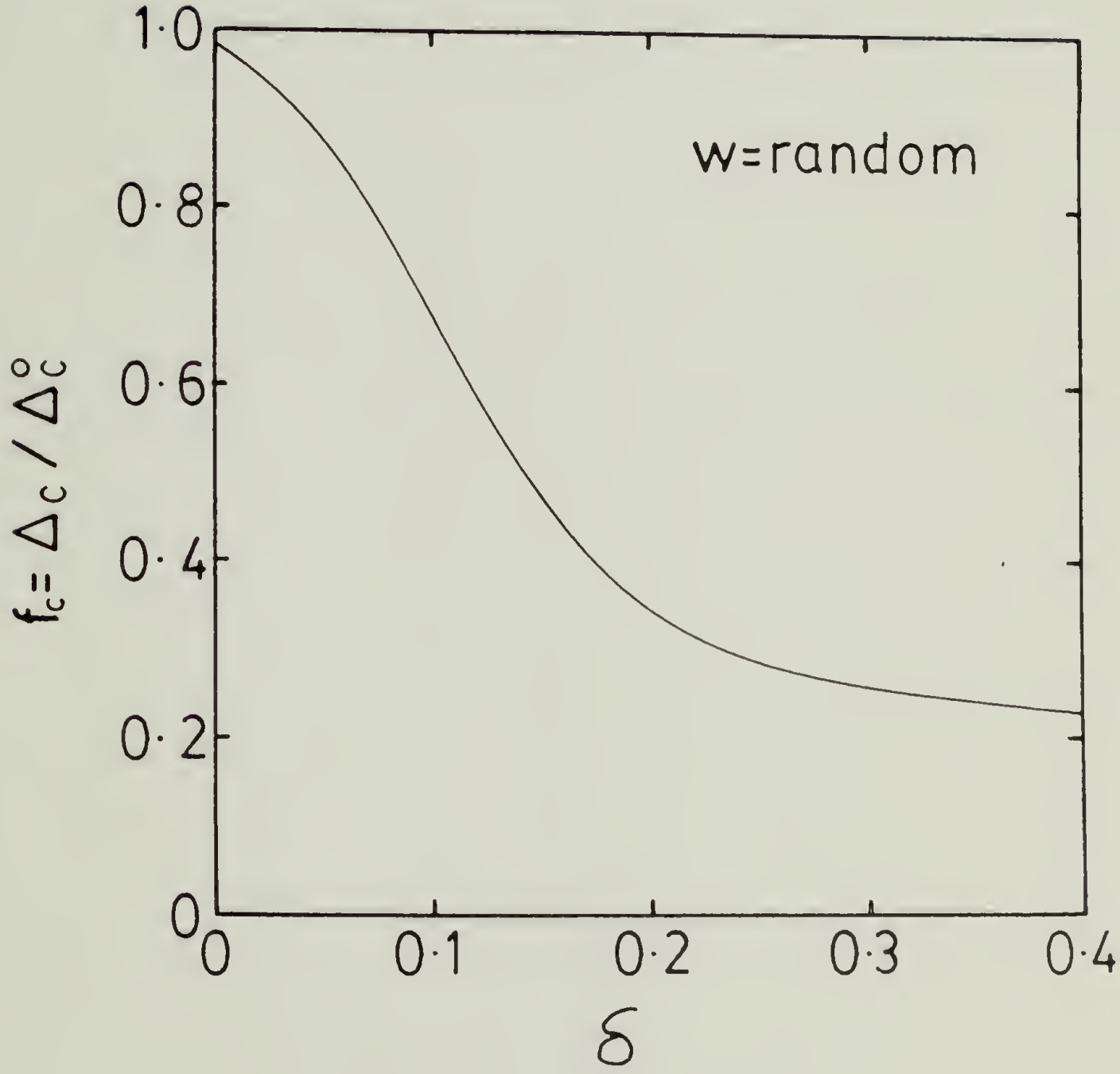

Fig. 35

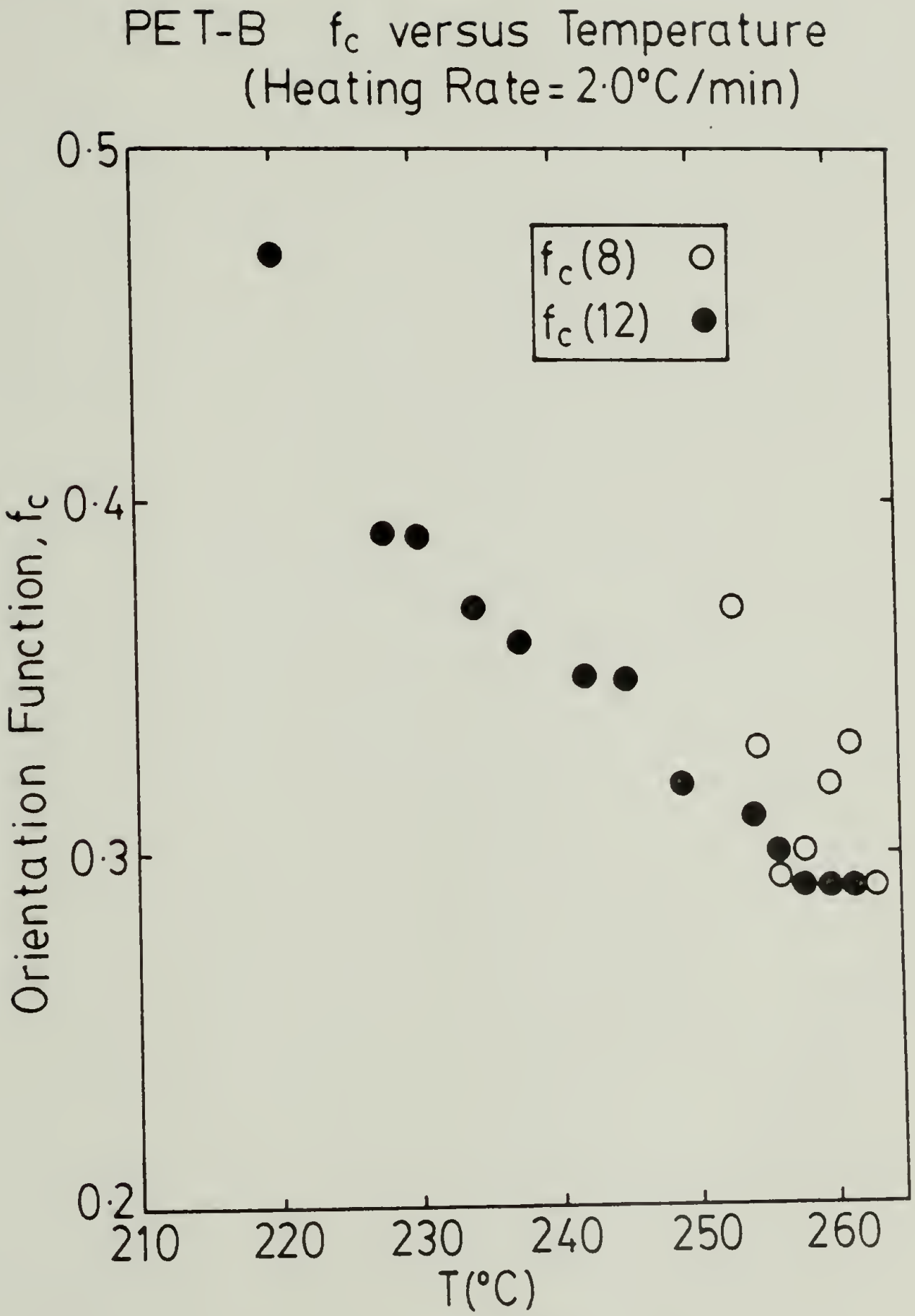
PET-B f_c versus Temperature
(Heating Rate = 2·0°C/min)
f_c(8)
f_c(12)
Orientation Function, f_c
0·5
0·4
0·3
0·2
210
220
230
240
250
260
T(°C)

Fig. 36

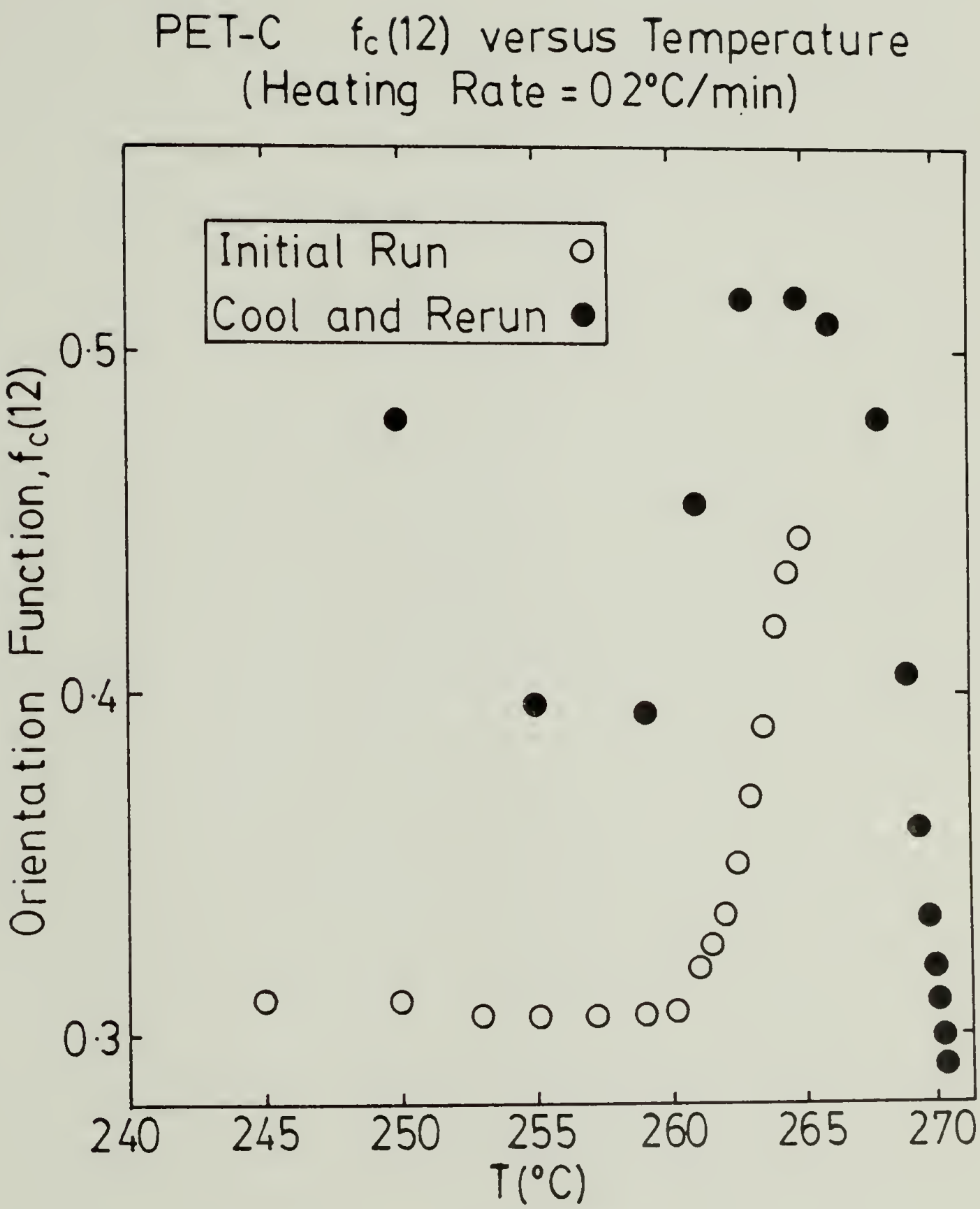
PET-C $f_c(12)$ versus Temperature
(Heating Rate = 0.2°C/min)
Initial Run
Cool and Rerun
Orientation Function, $f_c(12)$
0.5
0.4
0.3
240
245
250
255
260
265
270
T(°C)

Fig. 37

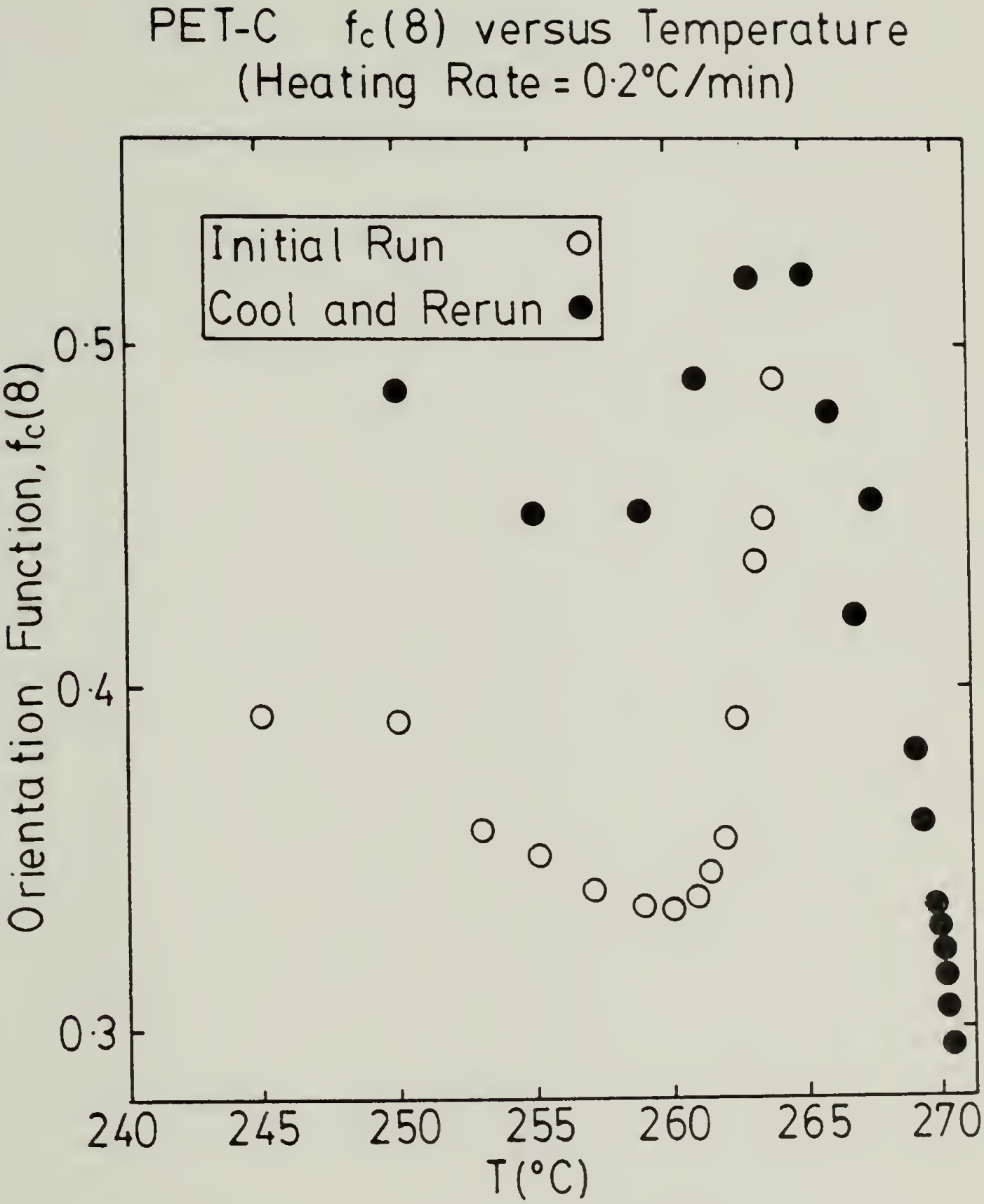
PET-C $f_c(8)$ versus Temperature
(Heating Rate = 0·2°C/min)
Initial Run
Cool and Rerun
Orientation Function, $f_c(8)$
0·5
0·4
0·3
240
245
250
255
260
265
270
T(°C)

Fig.38

R[U=4·1, μ = 45°] for PET-B at 2·0°C/min

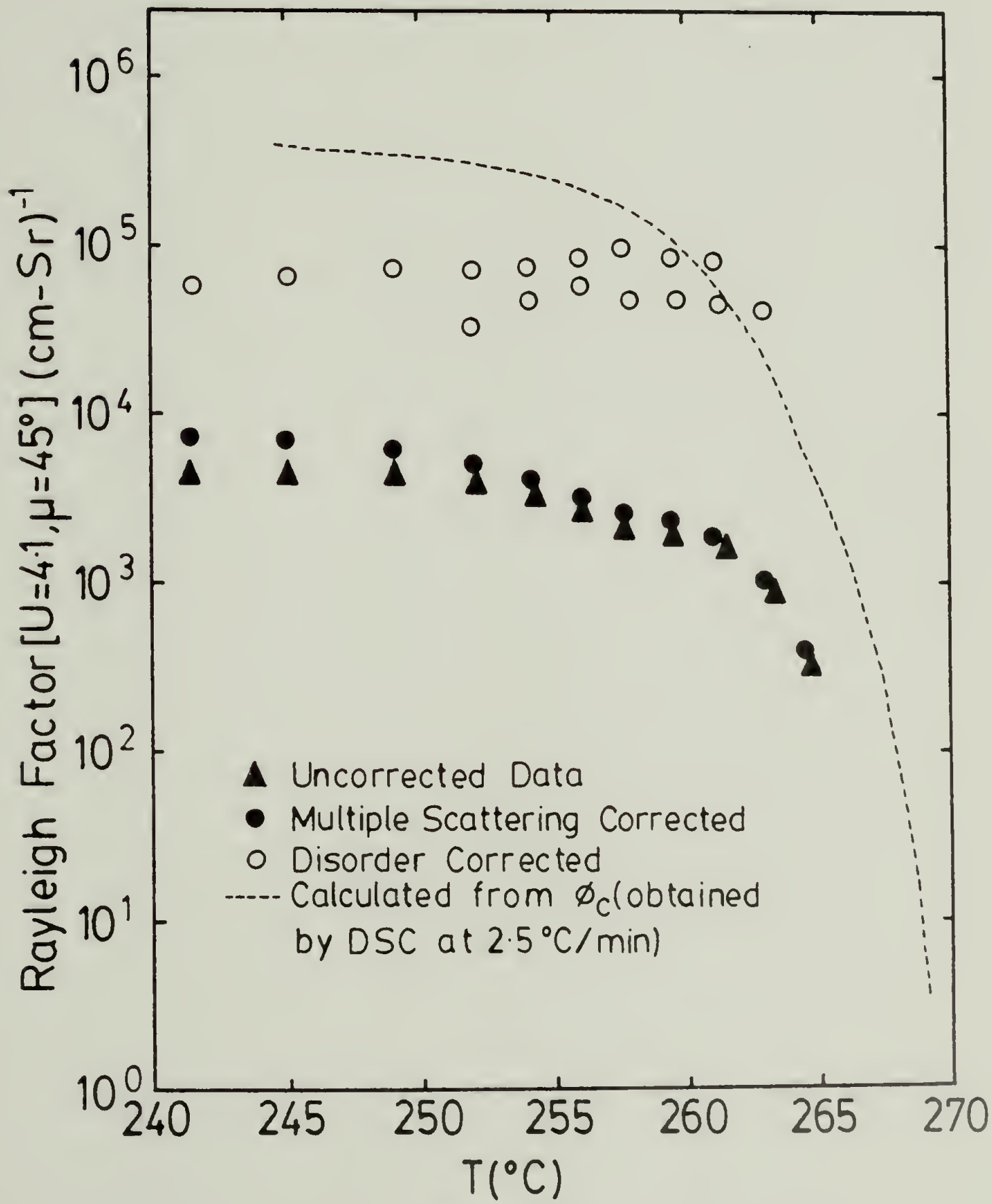

Fig. 39

R[U=4·1, μ = 45°] for PET-C2 at 0·2°C/min

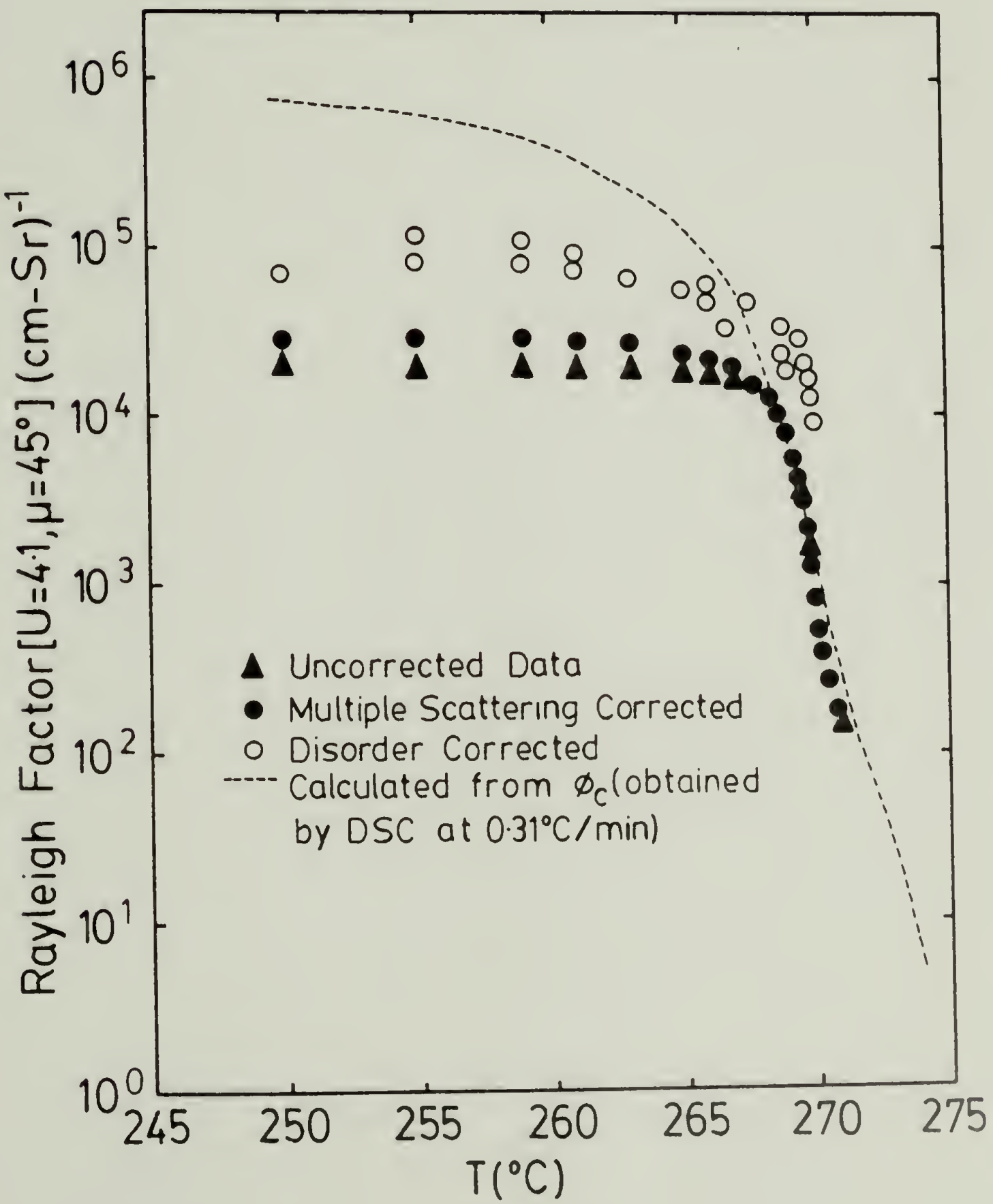

Fig. 40

APPENDIX

This Appendix contains computer programs OMA and GRAFCAL.

FILE GRAFCAL

```
      PROGRAM GRAFCAL(INPUT,OUTPUT,TAPE69,TAPE1)
      DIMENSION X1(500),Y1(500)
      DIMENSION IXAXIS(3)
      DIMENSION ILABEL(3)
      DIMENSION IYAXIS(3),ITITLE(3)
      CALL PLOTS(10)
      CALL PLOT(0.0,-11.,-3)
      CALL PLOT(1.5,1.5,-3)
      CALL FACTOR(0.8)
      READ(1,*)N,RS
      READ(69,70)(X1(I),Y1(I),I=1,N)
   70 FORMAT(12X,E12.4,24X,E12.4)
      DO 5 J=1,2
      IF(J.EQ.2)READ(1,*)N,RS
   10 DO 11 I=1,N
      IF(J.EQ.1)X1(I)=X1(I)*1000.
      IF(J.EQ.1)Y1(I)=Y1(I)/1000.
      IF(J.EQ.2)X1(I)=X1(I)*RS/1000.
   11 CONTINUE
      READ(1,*)XMIN,DELX,XLEN,YMIN,DELY,YLEN
    2 FORMAT(3A10)
      READ(1,2)IXAXIS
      READ(1,2)IYAXIS
      READ(1,2)ITITLE
      XTITLE=XLEN-4.5
      YTITLE=YLEN-0.5
      CALL SYMBOL(XTITLE,YTITLE,0.14,ITITLE,0.,30)
      XLEN=-XLEN
      CALL AXS(0.,YLEN,XLEN,2.,0.)
      YLEN=-YLEN
      CALL AXS(0.,0.,YLEN,2.,90.)
      XLEN=-XLEN
      CALL AXS(0.,0.,XLEN,2.,0.)
      CALL AXS(XLEN,0.,YLEN,2.,90.)
      READ(1,2)ILABEL
      YTITLE=YTITLE-0.50
      X1(N+1)=XMIN
      X1(N+2)=DELX
      Y1(N+1)=YMIN
      Y1(N+2)=DELY
      CALL SYMBOL(XTITLE,YTITLE,.14,ILABEL,0.,30)
      CALL LINE(X1,Y1,N,1,-4,3)
      XY=-0.20
      XT=XMIN
      DO 6 L=1,4
      CALL NUMBER(XY,-0.25,0.14,XT,0.,2)
      XT=XT+2.*DELX
      XY=XY+2
    6 CONTINUE
      YT=YMIN
      YY=-0.20
      DO 7 L=1,5
      CALL NUMBER(-0.25,YY,0.14,YT,90.0,2)
      YT=YT+2.*DELY
      YY=YY+2.
    7 CONTINUE
      CALL SYMBOL(-0.60,1.50,0.21,IYAXIS,90.0,30)
      CALL SYMBOL(0.25,-0.60,0.21,IXAXIS,0.0,30)
      DS=10./.8
      IF(J.EQ.1)CALL PLOT(DS,0.0,-3)
    5 CONTINUE
      CALL PLOT(DS,0.0,999)
      END
```

```
      PROGRAM CMA(INPUT,OUTPUT,TAPE1,TAPE2,TAPE3,TAPE4)
      COMMON/ABLOCK/A(500),T(3,500),MI(3),MF(3),JUNT
      COMMON/BBLOCK/ICODE(3),I(110),S(550)
      COMMON/CBLOCK/KZERO,KONE,XT,R,PO,TAUD,BINT,WAVO,PI,WS
      COMMON/DBLOCK/BACK(3),NUM
      DIMENSION ISAMP(6)
******   THIS PROGRAM CALCULATES RAYLEIGH FACTORS FOR
******DATA TAKEN WITH THE OPTICAL MULTICHANNEL ANALYZER.
******DATA ARE CORRECTED FOR REFRACTION,TURBIDITY(MULTIPLE
******SCATTERING), AND CHANNEL SENSITIVITY.THE PROGRAM IS
******RUN IN BATCH MODE.GET THE DATA FILES,COMPILE THE
******PROGRAM AND USE THE LGO COMMAND(E.G. LGO(,,SEIS,MAINB,SAM)
******)SEIS CONTAINS THE SENSITIVITY SCAN,MAINB THE MAIN BEAM
******SCAN AND SAM THE SAMPLE DATA FOLLOWED BY THE SAMPLE SCAN.
******A(I)=SCATTERING ANGLE   T(J,I)=SEIS,MAINB,SAM
******MI(J),MF(J)ARE INITIAL AND FINAL CHANNEL # OF SCANS.
******KZERO AND KONE ARE CHANNEL# OF ZERO AND 1ST ORDER DIFFRACTIONS
******XT=DISTANCE BETWEEN DIFFRACTIONS,BINT=TOTAL MAINBEAM INTENSITY
******R=SAMPLE-FILM DISTANCE  WAVO=WAVELENGTH RI=REFRACTIVE INDEX
******WS=SLIT WIDTH  FF=FILTER FACTOR  AAT=ANALYZER ATTENUATION
******RULING=#LINES/INCH OF GRATING  D=THICKNESS
******TAUD=TURBIDITY(1/IN) BEAMCYC AND SAMCYC ARE # CYCLES PER SCAN
****** JEFF KOBERSTEIN,2/15/78
      READ(3,1)(ISAMP(I),I=1,6)
    1 FORMAT(6A10)
      PI=3.14159
      PRINT 322
  322 FORMAT(*DO YOU WANT INSTRUCTIONS?*)
      READ 323,INST
  323 FORMAT(1A3)
      IF(INST.EQ.3HYES)PRINT 2
    2 FORMAT(*ENTER VALUES OF MAIN BEAM CHANNEL, 1ST ORDER DIFFRACTION
     +/*CHANNEL,DISTANCE BETWEEN ZERO*
     +/*AND 1ST ORDER DIFFRACTIONS(INCHES),AND FILTER FACTOR.*)
      READ *,KZERO,KONE,XT,FF
      IF(INST.EQ.3HYES)PRINT 3
    3 FORMAT(*ENTER SLIT WIDTH(INCHES),ANALYZER ATTENUATION FACTOR,
     +AND WAVELENGTH(CM)*)
      READ *,WS,AAT,WAVO
      IF(INST.EQ.3HYES)PRINT 4
    4 FORMAT(*ENTER GRATING(LINES/INCH),MAIN BEAM CYCLES, SAMPLE*
     +/*CYCLES,REFRACTIVE INDEX,TURBIDITY(1/IN),AND THICKNESS(INCH)*)
      READ *,RULING,BEAMCYC,SAMCYC,RI,TAUD,D
      IF(INST.EQ.3HYES)PRINT 5
    5 FORMAT(*ENTER CONSTANT VALUE TO BE ADDED TO SENSITIVITY  SCAN*
     +/*MAIN BEAM SCAN, AND SAMPLE SCAN,AND 0*)
      READ *,(BACK(I),I=1,3),0
      IF(INST.EQ.3HYES)PRINT 6
    6 FORMAT(*DO YOU WANT TO SMOOTH SAMPLE ?*)
      JSMC=2
      READ 323,IJSMO
      IF(IJSMC.EQ.3HYES)JSMO=1
      IF(JSMC.EQ.1)PRINT 35
   35 FORMAT(*ENTER NUMBER OF SMOOTHS*)
```

```
      IF(JSMC.EQ.1)READ 36,IDM
   36 FORMAT(I3)
      IF(IJST.EQ.3HYES)PRINT 7
    7 FORMAT(*DO YOU WANT TO INTEGRATE MAINBEAM INTENSITY?*)
      REAL 323,IINT
      IF(IINT.EQ.3HYES)JINT=1
      IF(JINT.NE.1)PRINT 37
   37 FORMAT(*ENTER INTEGRATED MAINBEAM INTENSITY*)
      IF(JINT.NE.1)READ *,EINT
      KZERO=KZERO+1$KONE=KONE+1
      AG=VALC*FULING/(2.54*(10.**7))
      AGDATE=ASIN(AG)
      R=XT/TAN(AGDATE)
      TALT=-ALOG(TALD)
      CALL READFIL
      CALL CONSENS
      IF(JSMO.EQ.1)CALL SMOOTH
      IF(JINT.EQ.1)CALL MAINBEM
      PC=EINT*FF*AAT*D*2.54*SAMCYC/BEAMCYC
      CALL ANGCOR
      PRINT 11
   11 FORMAT(//)
      PRINT 1,(ISAMP(I),I=1,4)
      KF=IABS(KZERO-MF(3))
      KI=IABS(KZERO-MI(3))
      MMI=MI(3) $MMF=KZERO-1
      IF(KI.LT.KF)MMI=KZERO+1$IF(KI.LT.KF)MMF=MF(3)
      PRINT 10
      DO 9 I=MMI,MMF
      II=I
      IF(KF.LT.KI)II=MMF+1-I
      T2=T(1,II)**2$T4=T2**2
      PRINT(4,8)A(II),T(1,II),T2,T4,T(2,II),T(3,II)
    8 FORMAT(6E12.4)
    9 CONTINUE
   10 FORMAT(//,5X,5HTHETA,6X,7HH(1/MM),7X,4HH**2,7X,4HH**4,4X,
     +16HH(1/(CF*CM)),3X,5HF*(H**4))
      END
      SUBROUTINE READFIL
      COMMON/ABLOCK/A(500),T(3,500),MI(3),MF(3),JINT
      COMMON/BBLOCK/ICODE(3),N(110),S(550)
      COMMON/DBLOCK/BACK(3),IDM
******THIS SUBROUTINE READS THE DATA FORMAT FILES ELIMINATING
******ALL BLANKS IN THE FILE AND SEQUENCING IT ACCORDING
******TO CHANNEL NUMBER.
      DO 4 J=1,3
      DO 2 I=1,550,5
      IF(ECF(J).NE.0)GO TO 2
      II=I+4
      I3=II/5
      READ(J,1) ICODE(J),N(I3),(S(I2),I2=I,II)
    1 FORMAT(A1,2X,I3,2X,F5.0,4(3X,F5.0))
      LF=II
    2 CONTINUE
```

```
      M=N(I)+1
      MI(J)=M
      DO 3 L=1,LF
      IF(ABS(S(L)).LT.1.)GO TO 3
      T(J,M)=S(L)+BACK(J)
      MF(J)=M
      M=M+1
    3 CONTINUE
      DO 5 I2=1,550
      S(I2)=0.
    5 CONTINUE
    4 CONTINUE
      RETURN
      END
      SUBROUTINE CORSEIS
      COMMON/ABLOCK/A(500),T(3,500),MI(3),MF(3),JINT
******THIS SUBROUTINE CORRECTS DATA FOR CHANEL SEISITIVITY
      VM=0.
      MMI=MI(1) $MMF=MF(1)
      DO 1 I=50,450
      IF(T(1,I).GT.VM)VM=T(1,I)
    1 CONTINUE
      DO 2 I=1,500
      T(1,I)=T(1,I)/VM
    2 CONTINUE
      DO 4 J=2,3
      IF(J.EQ.2.AND.JINT.NE.1)GO TO 4
      MMI=MI(J) $MMF=MF(J)
      DO 3 I=MMI,MMF
      T(J,I)=T(J,I)/T(1,I)
    3 CONTINUE
    4 CONTINUE
      RETURN
      END
      SUBROUTINE S100TH
      COMMON/ABLOCK/A(500),T(3,500),MI(3),MF(3),JINT
      COMMON/BBLOCK/BACK(3),NU1
******THIS SUBROUTINE S100THS THE SAMPLE SCAN
      N=MI(3)+2
      N1=MF(3)-3
      DO 3 M=1,NU1
      B0=T(3,N-2)/10.
      B1=2.*T(3,N-1)/10.
      DO 2 I=N,N1
      B2=4.*T(3,I)/10.
      B3=2.*T(3,I+1)/10.
      B4=T(3,I+2)/10.
      T(3,I)=B0+B1+B2+B3+B4
      B0=B1/2. $B1=B2/2.
    2 CONTINUE
    3 CONTINUE
      RETURN
      END
```

```
      SUBROUTINE ANGCOR
      COMMON/ABLOCK
                      @     COMMON/ABLOCK/A(500),T(3,500),MI(3),MF(3),JINT
      COMMON/CBLOCK/KZERO,KONE,XT,R,PO,TAUD,BINT,WAVO,RI,WS
******THIS SUBROUTINE CORREDTS FOR REFRACTION AND MULTIPLE SCA-
******TTERING AND CALCULATES RAYLEIGH FACTORS
      F=XT/(R*IABS(KZERO-KONE))
      ITF=IABS(KZERO-MF(3))
      IT=IABS(KZERO-MI(3))
      MMI=KZERO+1$MMF=MF(3)
      IF(ITF.LT.IT)MMI=MI(3)$IF(ITF.LT.IT)MMF=KZERO-1
******CALCULATION OF ANGLE(RADIANS)AND REFRACTION CORRECTION
      DO 1 I=MMI,MMF
      L=IABS(I-KZERO)
      A(I)=ATAN(F*L)
      A(I)=ASIN(SIN(A(I))/RI)
    1 CONTINUE
      DO 2 I=MMI,MMF
      L=I-KZERO
******CALCULATION OF SOLID ANGLE
      DX2=F*R*(L+.5)
      DX1=F*R*(L-.5)
      D2=SQRT(.25*(WS**2)+DX2**2+R**2)
      D1=SQRT(.25*(WS**2)+DX1**2+R**2)
      F4=2.*(ATAN((DX2*WS)/(2.*R*D2))-ATAN((DX1*WS)/(2.*R*D1)))
      F4=ABS(F4)
******MULTIPLE SCATTERING CORRECTION
      IF(A(I).LT..000001)F2=1.
      IF(A(I).LT..000001)GO TO 333
      A1=-1./ABS(COS(A(I)))
      X1=TAUD*(1.+A1)
      X2=EXP(TAUD*A1)-EXP(-TAUD)
      F2=X2/X1
  333 T(2,I)=T(3,I)/(F4*PO*F2)
      T(2,I)=T(2,I)-0
******CALCULATION OF SCATTERING VECTOR H
      T(1,I)=4.*3.14159*SIN(A(I)/2.)/WAVO
      T(3,I)=(T(1,I)**4)*T(2,I)
      A(I)=A(I)*360./(6.2832)
    2 CONTINUE
    3 CONTINUE
      RETURN
      END
      SUBROUTINE MAINBEM
      COMMON/ABLOCK/A(500),T(3,500),MI(3),MF(3),JINT
      COMMON/CBLOCK/KZERO,KONE,XT,R,PO,TAUD,BINT,WAVO,RI,WS
      BINT=0.
      MMI=MI(2)$MMF=MF(2)
      DO 2 I=MMI,MMF
      BINT=BINT+T(2,I)
    2 CONTINUE
      RETURN
      END
```